MICROFABRICATED CONTINUOUS FLOW SEPARATION AND MANIPULATION SYSTEMS FOR HUMAN WHOLE BLOOD

A Dissertation
Presented to
The Academic Faculty

By

Young Do Jung

In Partial Fulfillment
Of the Requirements for the Degree
Doctor of Philosophy in the
School of Electrical and Computer Engineering

Georgia Institute of Technology

May 2010

MICROFABRICATED CONTINUOUS FLOW SEPARATION AND MANIPULATION SYSTEMS FOR HUMAN WHOLE BLOOD

Approved By:

Dr. A. Bruno Frazier, Advisor
School of Electrical and Computer Engineering
Georgia Institute of Technology

Dr. Mark G. Allen
School of Electrical and Computer Engineering
Georgia Institute of Technology

Dr. Robert J. Butera
School of Electrical and Computer Engineering
Georgia Institute of Technology

Dr. Peter J. Hesketh
School of Mechanical Engineering
Georgia Institute of Technology

Dr. John A. Buck
School of Electrical and Computer Engineering
Georgia Institute of Technology

Date Approved: March 30, 2010

ACKNOWLEDGEMEMT

As a PhD graduate student, I have encountered with numerous opportunities and obstacles, and I could not have succeeded without a tremendous amount of support. First, I would like to express my sincere thanks to my thesis advisor, Professor A. Bruno Frazier, for giving me the opportunity to work on the BioMEMS projects, for providing me with the guidance, constructive feedback, and support over the past five years, and for the long hours that he has spent editing this thesis.

I would like to thank Professor Robert J. Butera for his valuable advice, who served as Chairman of the committee for the thesis proposal. I would also like to thank the members of my dissertation defense committee, Professor Mark G. Allen, Professor John A. Buck, and Professor Peter J. Hesketh.

I also need to recognize the members of the Microinstrumentation Research Lab (both past and present) at the Georgia Institute of Technology. Specifically, I would like to thank Dr. Ki-Ho Han for spending hours working with me when I first joined the group and for all of his additional guidance and encouragement after he left the group. Also, special thanks should be given to Dr. Yoonsu Choi for his advice and insight in overcoming various problems in the fabrication process.

I am also thankful to Dr. Dongsheng Wang from Emory University for providing me the help on the biological side of my project. I want to thank the Microsensor and Microactuator group here at the Georgia Institute of Technology, especially Dr. Chang-Hyeon Ji. Additionally, I would like to thank Gary Spinner, and the entire Microelectronics Research Center Cleanroom staff for all of their assistance and for making the MiRC Cleanroom a great place to work.

I would also like to acknowledge the National Institutes of Health for their support of my research and the Kwanjeong Educational Foundation for the financial support. There were also numerous academic administrators, professors, staff members, and other students from the Georgia Institute of Technology that contributed the insightful guidance, support, and direction necessary for me to complete my degree.

Finally, I am eternally grateful for the love and support of my friends and family. I am lucky to have been able to form such great friendships here in Atlanta, 7,000 miles from my hometown, and I thank them for being there for me throughout this experience. I want to say how fortunate I feel about my family. They are the biggest and best support group and cheering section I can imagine. This would have been impossible without them.

TABLE OF CONTENTS

LIST OF TABLES

LIST OF FIGURES

SUMMARY

The objective of the research in this dissertation is to develop microsystem based separation technologies for whole cell cancer analysis using human whole blood as the input sample. This research work is carried out with two different approaches; one based on a miniaturized cascade magnetophoresis system and a second based on dielectrophoresis. The miniaturized systems can be fabricated using MEMS technologies combined with plastic fabrication techniques.

The design, fabrication, packaging, and characterization of several versions of the magnetophoresis and dielectrophoresis microsystems for whole cell cancer analysis in human whole blood sample are presented. Each microsystem consists of five elements that are essential for the successful separation and / or manipulation of cells. Those essential components include microfluidic channels, inlet / outlet ports, ferromagnetic structures and / or comb-shaped electrodes, a microfluidic interface, and system packaging. For the operation of each microsystem, a blood or tumor cell sample is introduced into a device through a tubing and an SLA-based interface. In the magnetophoresis system, the RBCs or the magnetic cells in the sample experience a strong magnetophoretic force under a non-uniform magnetic field created by external permanent magnets and electroplated ferromagnetic structures. This allows the RBCs to be separated from the nucleated blood cells or the tagged cells to be separated from the non-magnetic cells. In the dielectrophoresis system, cells with different dielectric properties experience either positive or negative dielectrophoretic force under a non-uniform electric field created by an external AC signal and comb-

shaped electrodes and move from their original positions in a laminar flow pattern to different positions.

The first magnetophoresis microsystem, the six-stage cascade paramagnetic mode magnetophoretic separation system, was designed and has successfully shown high throughput RBC separation from a human whole blood sample. The second magnetophoresis microsystem was developed for the isolation of malignant cancer cells from benign tumor cells and has successfully separated malignant tumor cells tagged with magnetic nanoparticles based on their surface expression level of a specific protein from benign tumor cells. Additionally, in an effort to improve the throughput of RBC removal from a non diluted whole blood sample, a magnetophoresis system with 40 separation stages is proposed and designed. Two dielectrophoresis systems were developed; one dielectrophoresis system tested its switching and separation capability based on the native dielectric properties of different cell types, while the other investigated the frequency response of different cell types by measuring their crossover frequencies in a medium with different conductivity. Additionally, an integrated cascade system contains magnetophoresis and dielectrophoresis components is proposed and designed.

CHAPTER 1

INTRODUCTION

1.1 Origin and History of the Problem

1.1.1 Origin of the Problem

According to the American Cancer Society, cancer accounted for 559,888 deaths in the United States in 2006 and is estimated to be 292,540 deaths for men and 259,800 for women in 2009. This makes cancer the second largest cause of US mortality only surpassed by heart disease [1]. The overall cancer incident rate per capita has been declining since peaking in early 1990s as a result of cancer prevention efforts such as comprehensive tobacco control programs, increased individual and community watch for obesity, increased physical activity, and better nutrition, as well as increased awareness of the relationship between ultraviolet radiation and skin cancer [2]. However, as a result of aging and growth in the US population, the total number of cancer deaths set a record high in 2006 [3]. One research study using computer simulations found that the lifetime probability of developing cancer is 1 in 2 for men and 1 in 3 for women [4].

Early detection of cancer through regular screening tests provides a better chance of successful cancer treatment for patients and has contributed to the decline in the cancer related death rate [2]. Moreover treating patients with cancer in the early stages would cost much less and help reducing the overall health care cost for the individual as well as for the community. However, regular screening tests using conventional cancer detection methods are not readily available for everyone because

of the limited resources. In rural areas, medical experts and facilities for the tests are not easily accessible. Even in urban areas with ample medical resources, the cost associated with cancer screening deters many people from having regular screening tests [2].

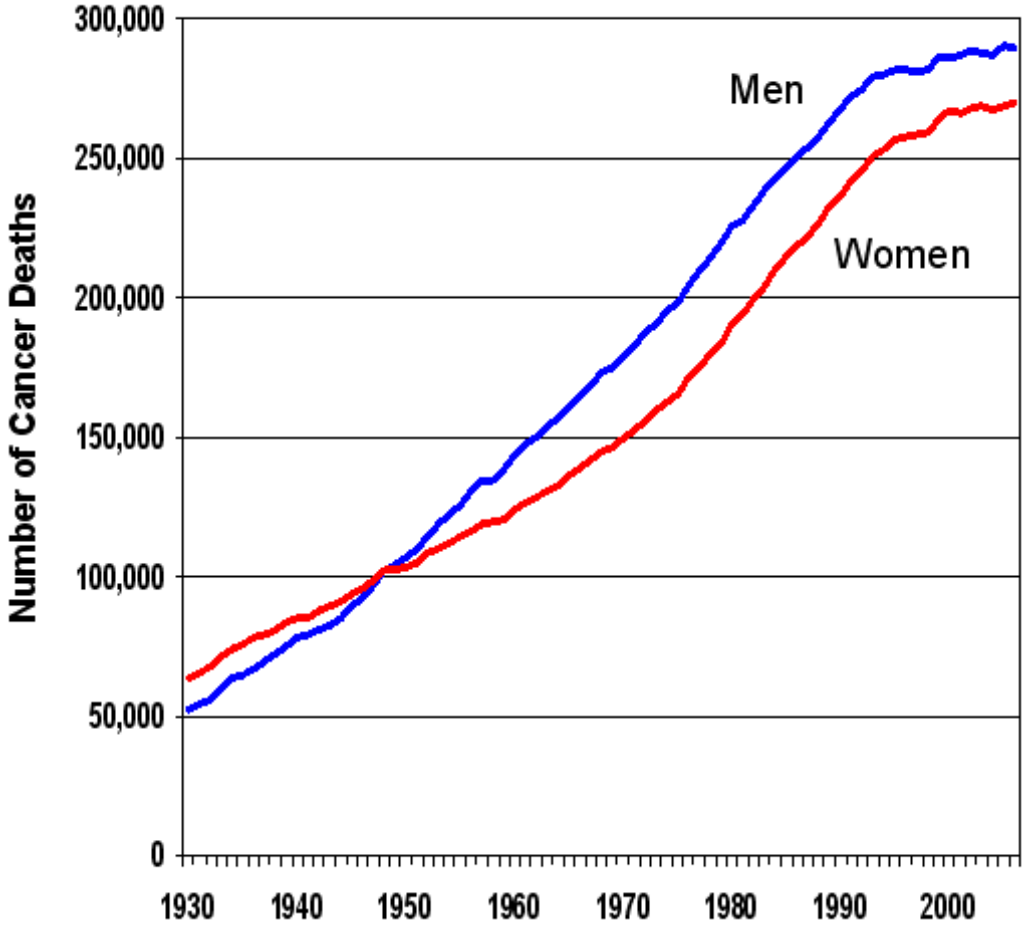

Figure 1.1. Trends in the number of cancer deaths among men and women, US, 1930-2006. ***(Graph from [3]).***

1.1.1.1 Conventional Cancer Analysis Technologies

Currently, there are several clinical cancer screening methods available for different types of cancers. For example, breast cancer is screened by a regular

clinical breast exam and/or a mammogram. Cervical cancer is detected using a Pap test to find abnormal cells from the tissue. Screening for colorectal cancer is conducted using a fecal occult blood test or a colonoscopy. Screening for lung cancer requires a chest x-ray and/or a sputum cytology test. In screening for prostate cancer, a digital rectal exam or a blood test to detect the prostate-specific antigen is usually performed [5].

Once cancer or suspected cancer is found through simple screening methods, more detailed analytic tests are followed for accessing tumor progression, heterogeneity, and the effect of drug therapy.

Conventional non-cell based analytic tools are classified into two sub categories, the analysis of DNA/RNA and the analysis of proteins in tumor samples and blood from cancer patients. These analyses are conducted to find the differences in the level of DNA damage or genomic alterations in a patient's tumor sample and/or blood sample compared to healthy individuals. Typical procedures for DNA/RNA analysis include PCR / sequencing, and Comet Assay™ for DNA damage assessment [6]. For protein analyses [7], there are several techniques such as a Western Blot [8], enzyme-linked immunosorbent assay (ELISA) [9], immunohistochemistry (IHC) [10], surface-enhanced laser desorption/ionization (SELDI) [11], and matrix-assisted laser desorption/ionization (MALDI) time of flight mass spectrometry (TOF-MS) [12].

1.1.1.2 MicroSystem-Based Cancer Analysis Technologies

Miniaturization of these analytic tools has various advantages such as a shorter analysis time, a smaller sample size, less reagent volume required for analysis, and especially an integrated understanding of the biological system by studying

multiple components simultaneously [13, 14]. Microfluidic based PCR chips have been developed by a number of groups, which enable cost and time savings with smaller volume and faster thermocycling rates [15, 16]. Chip based mass spectrometry has been demonstrated by several groups as well [17, 18]. Also, microarray technologies have been applied to detect and analyze a protein or multiple protein interaction in a single experiment [19~22].

1.1.1.3 Whole Cell Based Cancer Analysis Technologies

Cell based cancer analysis is another important analytic methods in detecting cancer and monitoring the stages of cancer progression. Determining the density of circulating tumor cells (CTCs) in blood is a good example of cell based cancer analysis. CTCs are known to be the tumor cells in blood derived from the clones in primary tumors. CTCs can be found in patients even before a primary tumor is detected with conventional clinical screening methods. Thus detecting CTCs in blood can be used as an early detection methodology for cancer. Moreover, the density of CTCs in blood has been shown to directly correlate with the progression of cancer so that determining the level of CTCs in blood can be helpful in characterizing genetic and immunophenotypic changes with tumor progression [23].

One of the most widely used macroscale cell analysis systems is fluorescence activated cell sorting (FACS) based on immuno-fluorescence. FACS was invented in the late 1960s by Bonner et al. and commercial machines became available in the early 1970s [24]. Currently, more than 30,000 FACS instruments are used in thousands of laboratories throughout the world [25]. For cell separation with FACS, the cells are stained with fluorescent dyes through specific antibody-antigen bonding

chemistries and confined to a column of liquid. The cell suspension is injected through a small nozzle and the liquid stream is exposed to excitation laser beams.

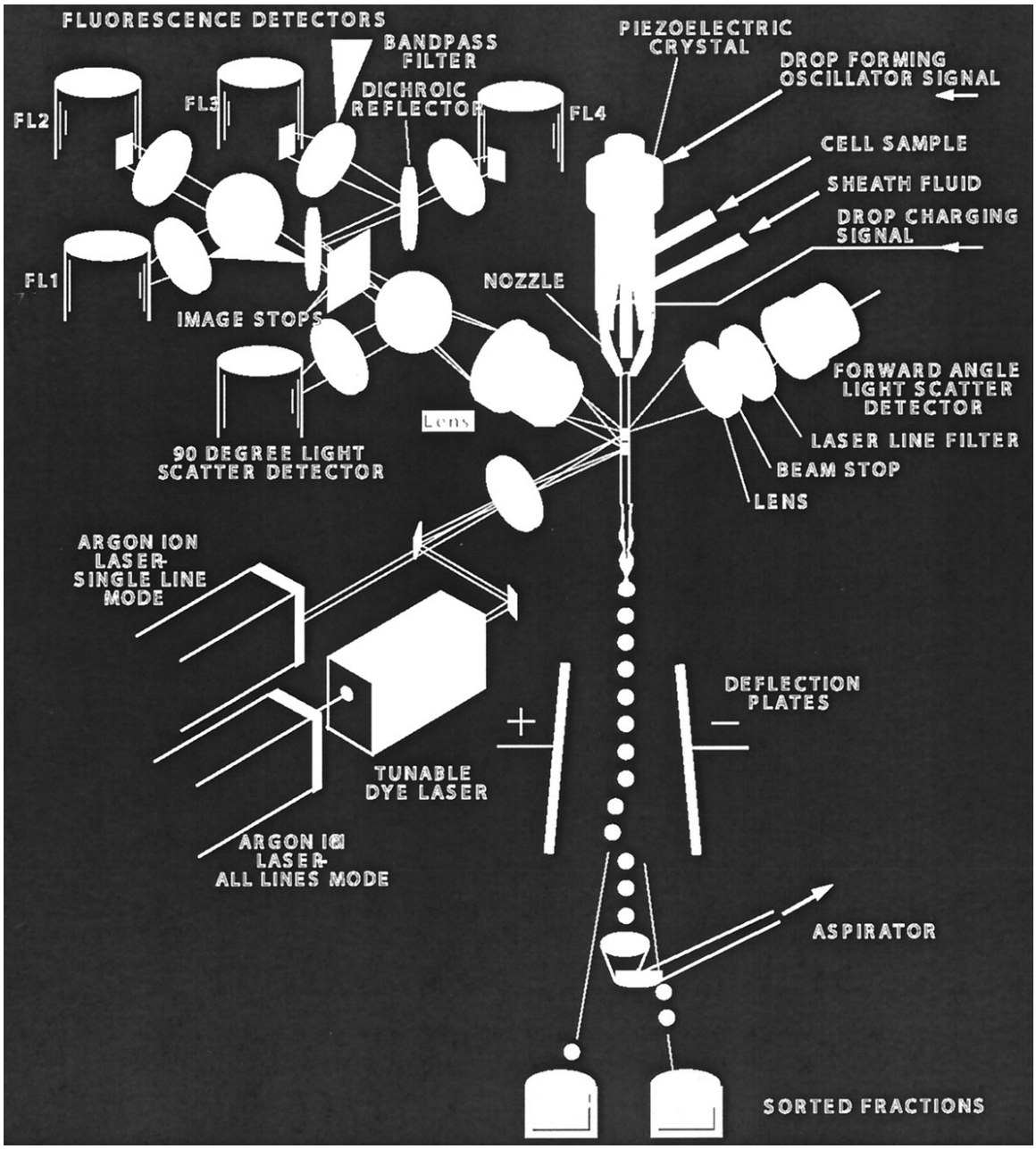

Figure 1.2. Diagram of modern three-laser FACS with multiple detectors. ***(Image from [25]).***

The stained cells in the stream emits a fluorescent pulses during laser beam illumination. A Photodetector detects and analyzes the emitted light and generates a charging pulse. The charging pulse induces a charge in the stream while the droplets that contain targeted cells break off from the stream. Finally, the charged droplets are deflected and separated in an electrostatic field. Recent advances in fluorescent dye techniques enable FACS to separate more than 10 different types of cells simultaneously [25]. Although FACS can separate biological cells efficiently with high accuracy, high equipment and operation costs, the requirement of trained personnel to operate the system and long preparation time for labeling samples hinder macroscale FACS from being suitable for clinical point-of-care devices [26, 27].

Density gradient centrifugation is a cheaper and easier-to-operate alternative for cell separation. In batch density gradient separations, the mixture of diverse cells is layered on top of a density gradient in a tube and the tube is subjected to centrifugation. The different types of cells pass through the density gradient at different rates depending on their sizes and shapes and appear as distinct bands in the gradient. Recently Ito et al. have demonstrated a continuous flow density gradient separation using a centrifuge bowl with a single circular channel [28].

In continuous flow density gradient separation, a set of different density media is continuously introduced through five outer inlets, while the sample suspension is injected through one inner inlet. Centrifugal force combined with drag force distributes the cells into corresponding density layers and the distributed cells are separated into six different outlets [28, 29]. For precise sub-classification of cells, the media's density gradient should be close to that of the different target cells. Although

density gradient centrifugation is a simple and cheap option for cell separation, it requires recovery of the separated cells from the density gradient media. Microenvironment alteration around the cells during the recovery process is an issue in the extraction of target cells from the cell mixture in their initial state.

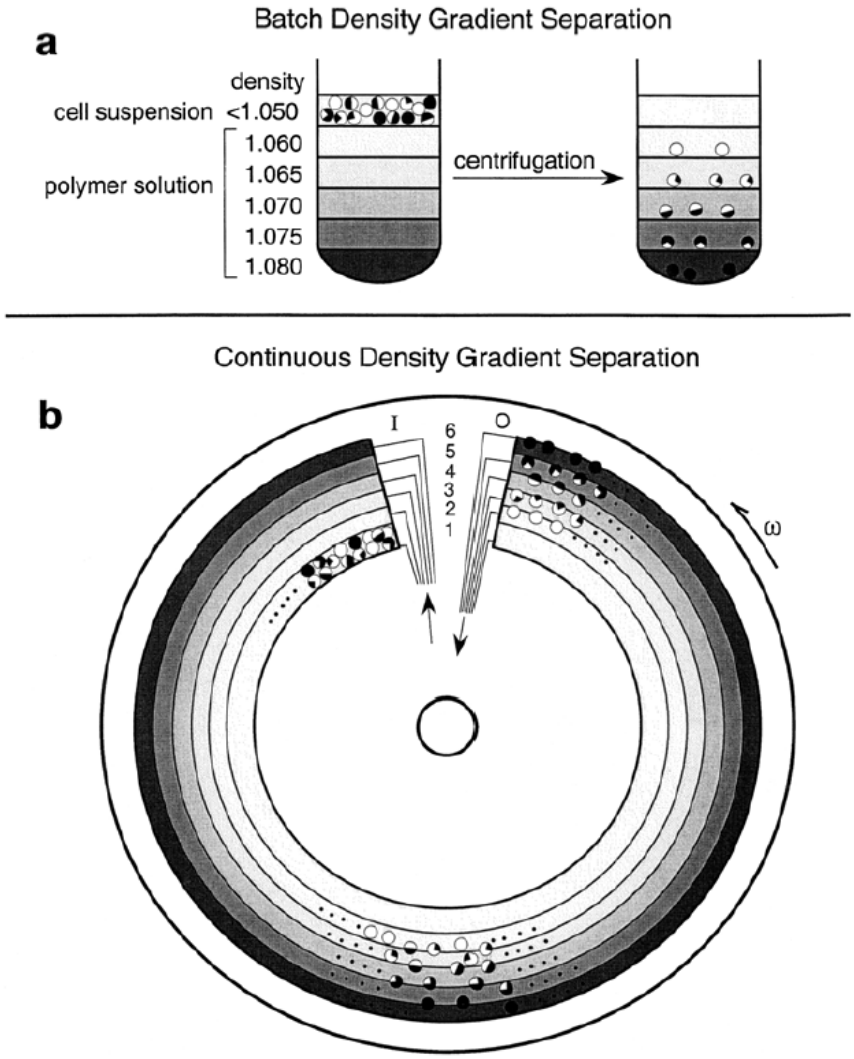

Figure 1.3. Whole cell separation using centrifugation: batch density gradient separation and continuous density gradient separation. ***(Image from [28]).***

Filtration through micro-pores is another easily accessible option in separating cells using their size differences, but clogging issues during the separation process

make this only suitable for a batch type separation system. Tangential flow filtration enables continuous separation of mixed particles through precise control of trans-membrane pressures and feed flow rates [30].

Magnetically-activated cell separation (MACS) is another widely used macroscale cell based analysis technology using magnetophoretic force as a driving force. MACS will be covered in more detail in Chapter 2.

1.1.1.4 MicroSystem-Based Whole Cell Cancer Analysis Technologies

Microfabricated bioanalytical devices have existed for approximately 40 years and achieved several commercial and scientific successes [31]. The ability to design and control experiments using microfabricated devices has attracted attention in biological applications [32, 33]. Microfluidic cell preparation systems in particular have received much attention among researchers because of their small device size, high surface-area-to-volume ratio, high throughput, etc [34~36].

In many instances, miniaturization of cell separation systems helps increase the magnitude of generated forces, such as dielectrophoretic or magnetophoretic forces on biological cells [34]. The larger forces along with the fact that the dimensions of the separation system are comparable in size scale to the biological cells enable more effective separation of target cells. Temperature control is critical in cell experiments and high surface-area-to-volume ratio in microfabricated systems enhances heat dissipation that reduces the risk of significant temperature rise during experiments [34]. Moreover, the ability to perform biological experiments efficiently with only a small amount of complex fluids and without the need for an expert operator makes

microfluidic systems promising candidates for point-of-care devices in resource-limited situations [37~39].

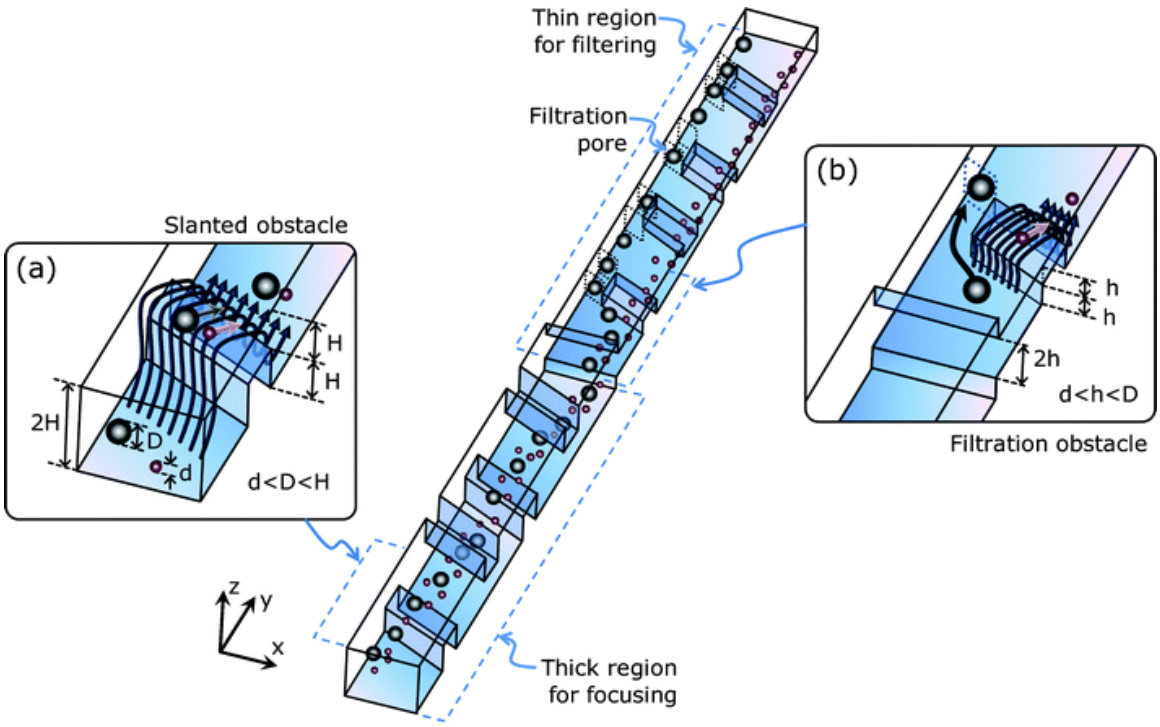

Figure 1.4. Hydrophoretic filtration by slanted obstacles and filtration obstacles. ***(Image from [41]).***

Various microfluidic separation systems have been developed utilizing diverse cell properties as the separation mechanism. Using differences in cell size and deformability, neuroblastoma tumor cell separation from whole blood was demonstrated with sieving structures with different gaps [40]. Choi et al. have shown continuous separation of white blood cells (WBCs) from red blood cells (RBCs) by hydrophoretic filtration with a microfluidic device composed of slanted obstacles and filtration obstacles [41]. A microstep device was developed to separate bacteria cells by shear-driven backward flow that avoids possible blockage of the filter by larger

cells [42]. Yamada et al. have demonstrated size-dependent separation in a microfluidic device employing effective flow manipulation based on the concept of hydrodynamic resistance in microchannels [43].

Suspended particles exposed to an ultrasonic standing wave field in microfluidic channels are affected by an acoustic radiation force and forced to move toward either pressure nodes or pressure antinodes, depending on the density and compressibility of the particles and media [44]. Continuous separation of mixed particles in a suspending media into multiple outlet fractions was demonstrated with laminar flow and acoustic standing wave forces in microfluidic channels [45~47]. Petersson et al. have shown the continuous separation of RBCs, WBCs, and platelets by free flow acoustophoresis and manipulating the density of suspending media [48].

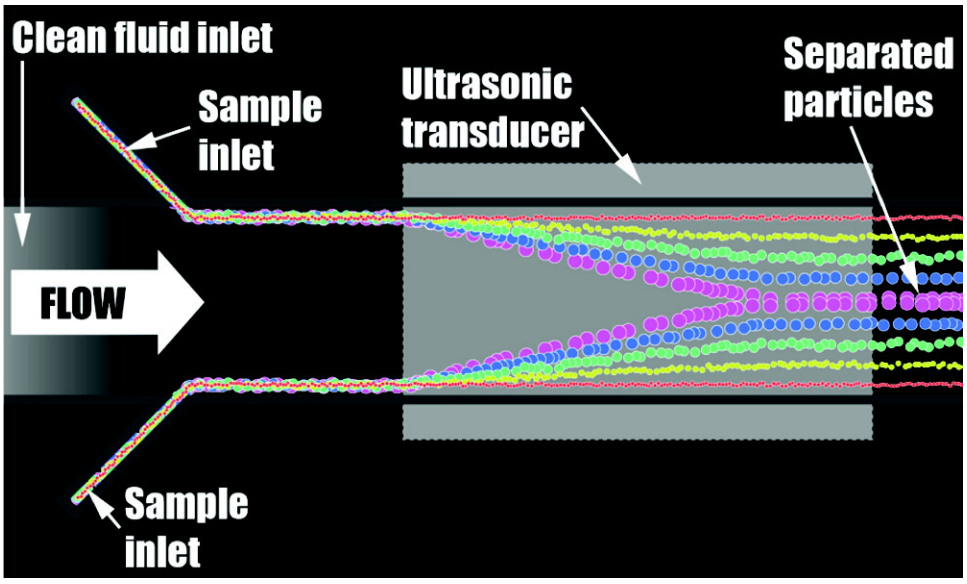

Figure 1.5. Operation principles of free flow particle separations by acoustophoresis. ***(Image from [48]).***

Microparticles or cells can be guided by optical gradient forces without any physical contact in a microfluidic channel, depending on the refractive index and the size of the particle, as well as the focusing laser power, fluid flow velocity, driving force direction, and optical lattice geometrical parameters. Various continuous flow cell manipulation systems using optical gradient forces have been demonstrated [49~54]. MacDonald et al. have demonstrated continuous fractionation of cells within a passive optical lattice, where cells experience different guiding affinity depending on their refractive index and size [55]. Applegate et al. have shown optical trapping, manipulation, and sorting of cells and colloids with diode laser bars [56].

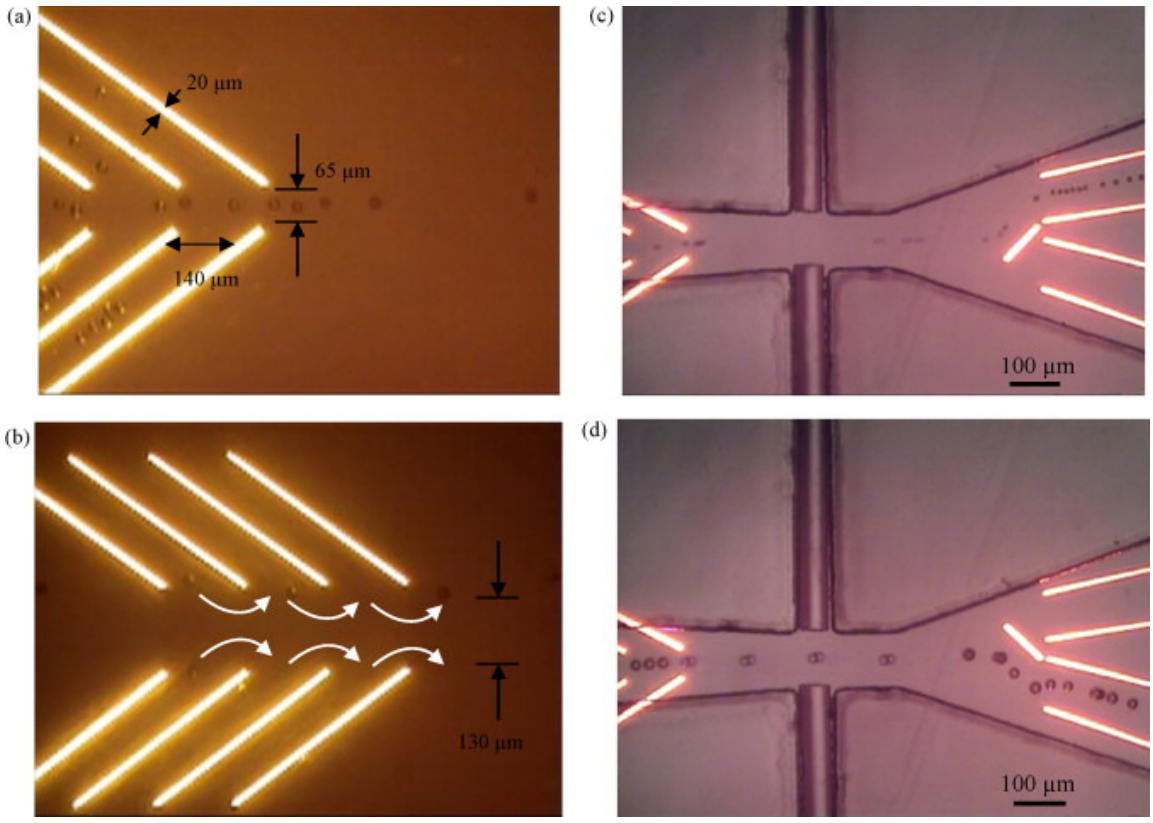

Figure 1.6. Micrograph of particle separation by optically induced flow cytometry. ***(Image from [53]).***

In presence of a high magnetic field gradient, microparticles or cells with different magnetic susceptibilities can be separated by magnetophoresis. Microfluidic magnetophoresis systems will be covered in more detail in Chapter 2, 3, and 4.

Biological cells or particles with different intrinsic dielectric affinity can be separated in a non-uniform electric field by varying the frequency of an applied alternating current (AC) source. Depending on their dielectric affinity and the applied electric field frequency, some cells experience attractive force in the direction of electric field gradient and others experience repulsive force in the opposite direction of applied field gradient. Microfluidic dielectrophoresis systems will be covered more in detail in Chapter 5, 6, and 7.

One major challenge in detecting the level of targeted rare cancer cells or CTCs in blood comes from the fact that human whole blood is a heterogeneous mixture of diverse blood cells and 98 % of blood cells are RBCs whose cell density is around 5×10^9 cells per milliliter and usually the cell density of CTCs in peripheral blood ranges from 0~1 cells per milliliter, which is extremely low compared to that of RBCs. This requires extremely precise identification and separation of CTCs from whole blood samples. Another challenge arises from the characteristic of blood that it responds quickly to small changes in environment and can be easily altered during the separation and identification process. Due to these challenges, separating and monitoring the level of targeted rare cells in blood has not been quite successful with miniaturized cell analysis systems.

1.2 Objective: Develop a Continuous Flow Separation and Manipulation System for Cancer Cell Isolation from Human Whole Blood using Microfabrication Technologies

The objective of my research was to develop microsystem based separation technologies for whole cell cancer analysis using human whole blood as the input sample. Two different approaches have been demonstrated; one based on a miniaturized cascade magnetophoresis system and a second based on dielectrophoresis that enables efficient and novel separation of targeted rare cells from human whole blood fabricated using MEMS technologies combined with plastic fabrication techniques. Continuous flow magnetophoresis will be used as an enrichment device for separating and removing most RBCs from a human whole blood sample, while concentrating targeted rare cells and other nucleated blood cells. Integrated, continuous flow dielectrophoresis will be demonstrated as an isolation device for separating targeted rare cells from other nucleated cells and residual RBCs.

The research was organized into three specific aims. Furthermore, each specific aim was divided into a series of sub-aims. Three specific aims with the corresponding sub-aims are as follows.

Specific Aim #1: Develop a microfluidic separation system using magnetophoresis to separate blood cells and targeted rare cells.

Subaim 1.1: Develop a cascade type continuous flow magnetophoretic microseparator for blood cell separation in diluted blood without magnetic tagging.

Subaim 1.2: Develop a magnetophoretic microseparator for specific cancer cells depending on the expression level of proteins on the cell surface.

Subaim 1.3: Develop a continuous flow magnetophoretic microseparator for blood cell separation in whole blood without magnetic tagging.

Specific Aim #2: Develop a microfluidic separation system using dielectrophoresis to separate blood cells and targeted rare cells.

Subaim 2.1: Characterize the dielectrophoretic responses of blood and head/neck cancer cells in the buffer solution with different conductivity.

Subaim 2.2: Develop a continuous dielectrophoretic microsystem for blood cells manipulation and separation.

Subaim 2.3: Develop a continuous dielectrophoretic microsystem for head/neck cancer cells separation.

Specific Aim #3: Develop microfluidic interfaces and packages for improved sample introduction and stable experiments.

Subaim 3.1: Develop microfluidic interfaces for each microsystem using plastic fabrication techniques for interconnecting the macro world with the microfluidic devices.

Subaim 3.2: Develop system level packages for each microsystem using plastic fabrication technique for reliable experiments.

Specific Aim #4: Integrate magnetophoretic and dielectrophoretic microsystems into a single microfluidic system for rare cell separation from human whole blood.

1.3 Overview of the Thesis and What Each Chapter Entails

Chapter 1 of this dissertation includes the origin and history of the problems in rare cell separation from human whole blood for detecting and monitoring cancer. The research objectives are also presented in Chapter 1. Chapter 2 presents the details of magnetophoresis systems including the theoretical background, design consideration, and two applications using the magnetophoretic microsystem. Chapter 3 presents the development of the magnetophoresis microsystem for blood cell separation using their native magnetic properties. A six stage cascade magnetophoretic microsystem was developed and characterization results are presented in Chapter 3. The application of magnetophoresis microsystem for cancer cell separation based on the surface expression level of target proteins is presented in Chapter 4. A three stage cascade microfluidic device is developed and characterization results along with sample preparation steps are presented in Chapter 4. Chapter 5 describes in detail about the dielectrophoretic separation systems with their theoretical and historical background, and brief introduction of their applications for blood and cancer cells separation. Chapter 6 presents the development of the dielectrophoresis microsystem for blood cell stream manipulation and separation using their native dielectric properties. The application of a dielectrophoresis microsystem for cancer cell separation and characterization is presented in Chapter 7. Finally Chapter 8 describes the development of proposed forty stage whole blood separator and integrated microfluidic system of magnetophoresis and dielectrophoresis for target rare cell separation from human whole blood. Chapter 9 summarizes the overall research results and describes future works.

CHAPTER 2

MAGNETOPHORESIS SYSTEM

2.1 Introduction

Magnetic force has been utilized over thousands of years and uses can be found from small refrigerator magnets to huge power plant generators. If focused on the application of magnetic force to the separation of particles, high gradient magnetic field separation (HGMS) has been shown to be an effective method for removal of metals or radioactive particles from waste fluids and gases in macro scale industrial applications [57, 58].

The magnetophoretic force experienced by a particle suspended in a fluid arises from a change in the magnetic energy in the system. Magnetic energy density in a linear isotropic medium is expressed as $\frac{1}{2}HB$, where H and B represent a magnetic field intensity and magnetic flux density respectively, and the magnetic energy in a suspending fluid with a susceptibility of χ_F enclosed in a volume V_P can be presented as:

$$\frac{1}{2}HB_F V_P = \frac{1}{2}\mu_F V_P H^2, \text{ where } B_F = \mu_F H \text{ and } \mu_F = \mu_O(1+\chi_F). \quad (2.1)$$

If a particle with a volume V_P and susceptibility of χ_P is placed inside the fluid, the energy increment U of the system by replacing the fluid with the particle is given as:

$$U = \frac{1}{2}HB_P V_P - \frac{1}{2}HB_F V_P = \frac{1}{2}(\mu_P - \mu_F)V_P H^2 = \frac{1}{2}\mu_O(\chi_P - \chi_F)V_P H^2. \quad (2.2)$$

The magnetic force associated with this magnetic energy change can be calculated by taking ∇U and can be written as:

$$\vec{F}_m = \frac{1}{2}\mu_O \chi V_P \nabla(H^2), \text{ where } \chi = \chi_P - \chi_F . \quad (2.3)$$

From Equation 2.3, magnetic force can be viewed as a product of χV_P, which represents physical properties of a target particle and $\nabla(H^2)$, which reflects the magnetic field properties surrounding a particle. Effective separation of weakly magnetic particles that show small differences in magnetic susceptibility from the suspending fluid requires a considerable increase either in the magnitude of magnetic field intensity, H, which usually can be achieved by using more powerful external magnetic source or in the magnitude of ∇H [59].

A uniform external magnetic field generated by an external permanent magnet becomes inhomogeneous around ferromagnetic structures because of the appearance of magnetic polarity on the ferromagnetic wires. A resultant, magnetic field gradient is created near the ferromagnetic structures. The magnetic field gradient reaches a maximum if ferromagnetic structures are placed in a way such that the axis of wires is always perpendicular to the direction of external magnetic field. High gradient magnetic field separation, HGMS, uses this magnetic field gradient and is a powerful method in the separation of micron-sized, weakly magnetic particles.

Various HGMS systems have been demonstrated for biological applications, such as the purification of proteins [60], the extraction of synthesized organic compounds from water [61], magnetic sorting or extraction of cells [62, 63], and locally targeted drug delivery [64~66].

2.2 Macroscale Magnetophoresis Systems

One of widely used macroscale magnetophoresis separation system is magnetically activated cell separation (MACS). MACS technology was commercialized in the late 1980s by Miltenyi et al. and its enrichment capability has been shown in various studies [67~69]. For cell separation with MACS technology, target cells are labeled with superparamagnetic microbeads by antibody-antigen immunoreactions and the labeled cell suspension is placed inside a column with a ferromagnetic mesh. The column is positioned between strong permanent magnets and a high gradient magnetic field is induced on the column matrix so that target cells labeled with magnetic microbeads are retained in the column by magnetophoretic force, while the unlabeled cells are eluted by a buffer solution.

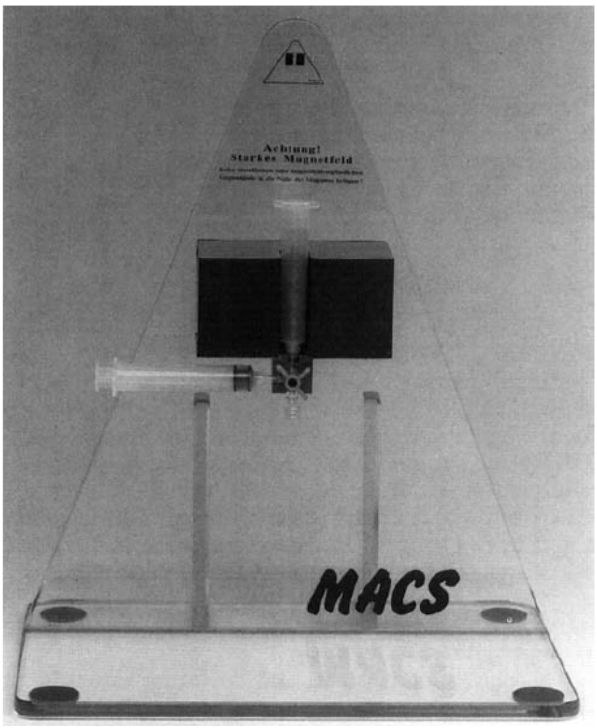

Figure 2.1. Magnetically Activated Cell Sorting (MACS) system. ***(Picture from [72]).***

Commercially available magnetic microbeads for current MACS technology are composed of a biodegradable matrix; thus the additional detachment process needed to remove the microbeads from the target cells after the separation process becomes unnecessary. Although MACS technology provides a gentle and fast enrichment method in cell preparation with simpler operational procedures than FACS, it still requires a discontinuous sample preparation step for labeling the samples with magnetic beads and removing the microbeads from the cell media after the separation [70~74].

It has been reported that in whole blood, deoxyhemoglobin RBCs have a much higher magnetic susceptibility than other biological cells and can be treated as paramagnetic particles, while WBCs or other nucleated cells behave like diamagnetic particles [75]. Using their native magnetic properties, RBCs, WBCs, and other rare circulating cells in human whole blood can be separated using high magnetic flux gradients [76~78].

Takayasu et al. have developed a macroscale continuous magnetic separator and demonstrated the separation of blood components from whole blood based on HGMS and a gas-permeable membrane with nitrogen gas [79]. The magnetic separator has 3.6 m flow length and the flow channel was made of plastic tubing and co-wound with a ferromagnetic wire on a Plexiglass tube. As a blood sample passes through the flow channel, depending on their magnetic properties, the blood components are separated into three different outlets. However, because of its macroscale size combined with the small magnetic susceptibilities of the blood components, the continuous magnetic separator required very high external magnetic

source over 2 T for the separation of blood components from whole blood continuously.

2.3 Microscale Magnetophoresis Systems

2.3.1 Brief Introduction of Magnetophoresis

Unlike macroscale systems that require a huge external magnetic field to create a high magnetic field gradient on biological cells, microfluidic magnetophoresis systems can create a high magnetic field gradient with a much smaller external magnetic field; thus small permanent magnets can be used, reducing the overall size of the whole separation system [80]. Various microfluidic magnetophoresis systems have shown the ability to separate out RBCs efficiently from whole blood samples, thus isolating nucleated cells for further analysis [77, 78, 81].

In a high gradient magnetic field, blood cells experience an attractive or repulsive magnetophoretic force depending on their native magnetic properties. The magnetic force, F_{BC}, on a blood cell derived in our previous work [82] was expressed as:

$$\vec{F}_{BC} = -\frac{2\kappa\mu_o\Delta\chi V_{BC}a^2}{r^3}[\kappa\frac{a^2}{r^2}+\cos 2\varphi]H_o^2\vec{a}_r - \frac{2\kappa\mu_o\Delta\chi V_{BC}a^2}{r^3}\sin[2\varphi]H_o^2\vec{a}_\varphi, r > a$$

$$(\kappa = \frac{\mu_w - \mu_B}{\mu_w + \mu_B}) \quad (2.4)$$

where μ_O, μ_B and μ_W are the magnetic permeabilities of the air, the buffer solution, and the ferromagnetic structures, respectively; H_O is the external magnetic field intensity; χ_{BC} and χ_B are the magnetic susceptibilities of the blood cell and the

buffer solution; $\Delta\chi(=\chi_{BC}-\chi_{B})$ is the relative magnetic susceptibility of the blood cell with respect to the buffer solution; V_{BC} is the volume of a blood cell; a is the radius of a circular ferromagnetic wire; r and φ are cylindrical coordinates for distance and angle; and $\vec{a}_r$ and $\vec{a}_\varphi$ are unit vectors for distance and angle in cylindrical coordinate, respectively.

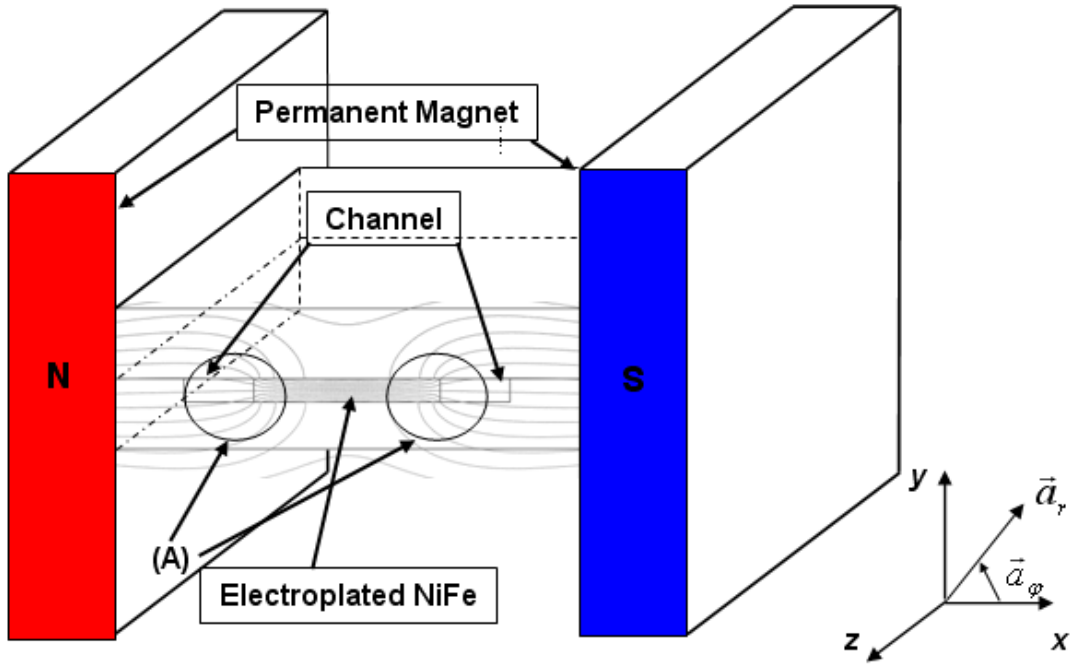

Figure 2.2. A high magnetic field gradient is generated in the region (A) around the ferromagnetic structures using permanent magnets as the field source. The RBCs are attracted toward the ferromagnetic capture structures by the paramagnetic force created by the magnetic field gradient.

From the Equation 2.4, when magnetic particles are placed on the x-axis or in the microfluidic channel as shown in Figure 2.2 ($\varphi \approx 0^{\circ}$ or 180°, $\sin 2\varphi \approx 0$, $\cos 2\varphi \approx 1$), magnetic particles whose $\Delta\chi$ is positive (paramagnetic particles) are attracted toward the ferromagnetic structures where the magnetic field

gradient becomes higher, while those that have negative $\Delta\chi$ are pushed away from the ferromagnetic structures. Deoxyhemoglobin RBCs have a positive $\Delta\chi$ in most buffer solutions, so they are attracted toward the ferromagnetic capture structures by the paramagnetic force.

2.3.2 Advantage of Magnetophoresis Compared to Other Microsystem in Manipulating Blood and Cancer Cells

2.3.2.1 Reason for Chosen as Driving Force in Proposed System

Human whole blood consists of 45 % blood cells and 55 % plasma with 98 % of the blood cells being RBCs, whose cell density is around 5×10^6 cells/μL [83]. The number of specific rare cells in the blood stream contains valuable information about the human body. For example, the density of the circulating tumor cells (CTCs) in blood has shown to directly correlate with the progression of cancer. The number of CTCs introduced daily into the blood stream from one gram of tumor tissue is about 1×10^6, but the number of epithelial cells in blood from a person without any known cancer is very low and almost never exceeds one cell per 7.5 mL of blood [23, 84, 85]. The cell density of rare cells is extremely low compared to that of normal blood cells such that separating targeted rare cells other than normal RBCs in human whole blood without any microenvironment alteration has been a challenge in the development of integrated microfluidic analysis systems using whole blood as input samples. The removal of RBCs from whole blood samples in the early stages of a blood sample preparation would greatly help downstream sub-classification, analysis, and treatment of targeted rare cells. By using magnetophoresis as a driving

force, this task can be carried out most effectively without the need for complex intercellular tagging procedures.

In the development of a magnetophoretic microseparation system, several key design and operation factors should be considered. The first consideration should be given to the relative position of the external magnetic field source and the microseparator system. From the Equation 2.4, when the microfluidic channels, which the magnetic particles are flowing through, are placed on the axis where $\varphi \approx$ 0º or 180º, ($\sin 2\varphi \approx 0$, $\cos 2\varphi \approx 1$), particles whose $\Delta\chi$ is positive (paramagnetic particles) are forced (captured) toward the dense magnetic field area (close to ferromagnetic structures), while particles that have negative $\Delta\chi$ are pushed away toward the coerce magnetic field area. This mode of operation is called as the paramagnetic capture mode (Figure 2.3 (a)).

In a complimentary mode of operation, when the microfluidic channels are placed on the axis where $\varphi \approx$ 90º or 270º, ($\sin 2\varphi \approx 1$, $\cos 2\varphi \approx 0$), diamagnetic particles are captured toward the ferromagnetic structures, while paramagnetic particles are forced away from the ferromagnetic structures. This mode of operation is called as the diamagnetic capture mode (Figure 2.3 (b)). These two operation modes can be used interchangeably in one magnetophoretic microseparator by simply changing the position of the external magnetic source around the microseparator.

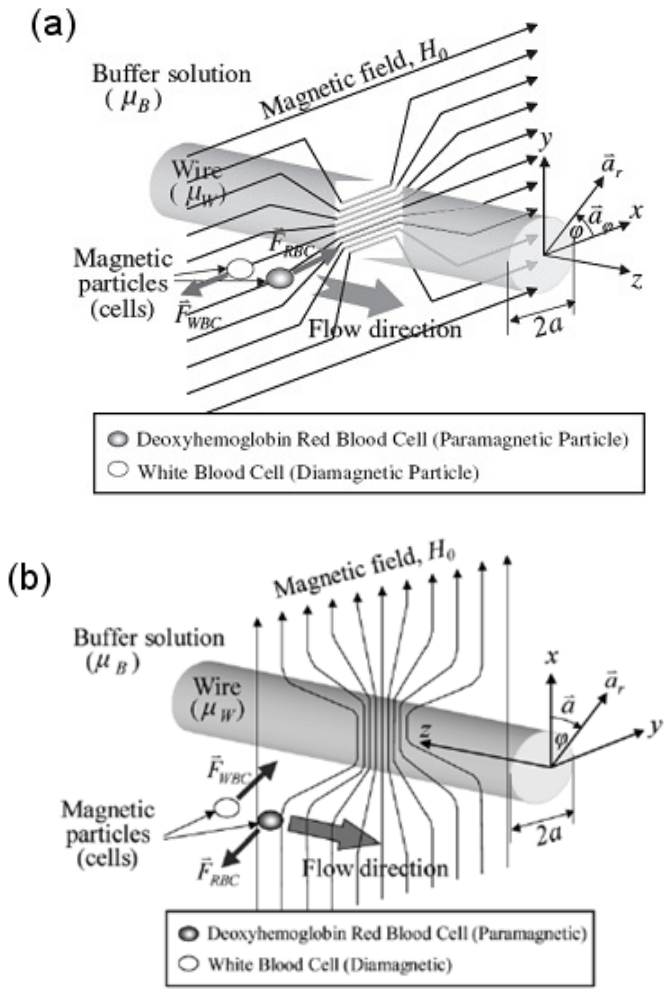

Figure 2.3. Working principle of the paramagnetic capture mode operation and the diamagnetic capture mode operation. ***(Images from [77, 86]).***

Having multiple separation stages in a microfluidic chamber can enhance separation efficiency compared to having a single wire. Previously, blood cell separations were carried out with a single stage and a three stage ferromagnetic structures and the characterization results showed that the three stage design was capable of higher throughput with improved separation efficiency. Even though increasing the number of separation stages could be helpful in terms of throughput and separation efficiency, there are restrictions in increasing the number of separation

stages. With the same external magnetic source, there is a minimum time required for capturing target cells that dictates the minimum length of each separation stage. Therefore, the overall length of the separation chamber should be increased as the number of separation stages is increased. This would result in added sample retention time, which is the time period for the input sample to travel from the inlet to the outlet of the system.

In separating targeted magnetic cells, there are two major driving forces utilized in the separation process. These two driving forces are the, magnetophoretic force created by external magnetic sources and the drag force created by the interaction of magnetically forced cells in the fluid flow. For a magnetophoresis microsystem to separate target particles continuously, the balance between the two forces should be considered carefully in designing the microsystem and the packaging. Usually, as the magnitude of a magnetophoretic force becomes greater, the required capture time for separating target cells shortens. However, the possibility of target particles being held inside the separation chamber also increases unless the drag force on the target cells becomes proportionally higher. This balance can be controlled by changing the sample flow rate, the distance between the external magnetic source and the microseparator channel, and the magnitude of external magnetic source. However, when the target cells consist of magnetic cells with similar but different levels of magnetic susceptibility, this balance control for continuous mode separation becomes extremely difficult and the separation efficiency would be lowered with continuous mode separation. For these cases, another method of operation, Hold and Release, is preferable to continuous mode separation. In the hold and release mode operation,

the target cells with a higher magnetic susceptibility are captured and held on the ferromagnetic structures in the separation channel during a 'hold phase' with the use of external magnetic sources and released into capture outlet during a 'release phase' with a small or no external magnetic source.. During the hold and release operation, other groups of targeted cell types with a lower magnetic susceptibility can be separated into a collection channel if the drag force of the other cells in the fluid is great enough to overcome the magnetophoretic forces used to 'hold' the cells with the higher magnetic susceptibility. The targeted cell types with the lower magnetic susceptibility are separated as in the continuous mode operation.

2.4 Applications of Microscale Magnetophoresis Systems

In this work, two magnetophoretic separation systems were developed and characterized. The first magnetophoretic microsystem was developed for high throughput blood cell separation. This microsystem uses a six stage cascade style paramagnetic capture mode to separate the blood cells effectively. The development and characterization of the magnetophoretic microsystem is presented in detail in Chapter 4. Another magnetophoretic microseparator system using three stage paramagnetic capture mode was developed for determining the heterogeneity of head/neck cancer cells based on the surface protein expression level of target cancer cells. This system is presented in detail in Chapter 5.

CHAPTER 3

MAGNETOPHORESIS SYSTEM APPLICATION I

(High Throughput RBC Removal from a Blood Sample)

3.1 Introduction

Human whole blood consists of 45 % blood cells and 55 % plasma with 98 % of the blood cells being RBCs with a cell density of around 5×10^6 cells/μL [83]. On the contrary, the cell density of rare cells such as CTCs is extremely low compared to that of normal blood cells; thus separating target rare cells other than normal RBCs in human whole blood without any microenvironment alteration has been a challenge in the development of integrated microfluidic analysis systems using whole blood as input samples. The removal of RBCs from whole blood samples in the early stage of a blood sample preparation would greatly help the downstream sub-classification, analysis, and treatment of target rare cells. By using magnetophoresis as a driving force, this task can be carried out most effectively without complex intercellular tagging procedures.

3.2 Magnetic Microseparation System Design

Previously proposed paramagnetic microsystems for blood cells separation [77] have shown high separation efficiency of 93.5 % for RBCs and 97.4 % for WBCs at a volumetric flow rate of 5.0 μL/hr corresponding to 2.5×10^6 cells/hr. However, the separation efficiencies decreased to 75 % and 65 % as the volumetric flow rate increased to 20 μL/hr and 30 μL/hr, which hindered its application to fast

processing of small volumes of blood sample (~ 5 μL) from the finger tip or a cotton swab, etc.

To increase the volumetric flow rate while maintaining high separation efficiency, a new magnetophoretic microseparation system design is required. The most important factor considered in the design of new magnetophoretic system was the required trapping time for the RBCs to move from position (x_1, y) to position (x_2, y), $x_1 \geq x_2$. The trapping time can be calculated as:

$$t = \frac{3\mu_O \eta (A/l)}{\Delta\chi V_{BC}(\mu_O M_S) B_O a^2} \times [(x_1^4 - x_2^4) + 2(6y^2 - Ka^2)(x_1^2 - x_2^2) +$$

$$2(K^2 a^4 + 21y^4 - 9Ka^2 y^2) \times \ln\left(\frac{x_1^2 + Ka^2 - 3y^2}{x_2^2 + Ka^2 - 3y^2}\right) + \frac{2y^6}{3y^2 - Ka^2} \ln\left(\frac{x_2^2}{x_1^2} \times \frac{x_1^2 + Ka^2 - 3y^2}{x_2^2 + Ka^2 - 3y^2}\right)\Bigg],$$

$$K = \frac{\mu_O M_S}{2B_O}$$

(3.1) [77]

where μ_O is the magnetic susceptibility of the air; η is the apparent viscosity of the blood cells in the buffer solution; A is the maximum cross-section area presented perpendicular to the velocity; l is the characteristic length of the blood cell in the direction of velocity vector; $\Delta\chi$ is the relative magnetic susceptibility of a blood cell relative to the buffer solution; V_{BC} is the volume of the blood cell; M_S is the saturation magnetization field of the rectangular wire; B_O is the external magnetic flux; and a is the radius of the circular ferromagnetic wire or half height of rectangular wire.

The first design variable considered was increasing the number of separation stages. By increasing the number of separation stages, already captured RBCs would be swept into the collection channel, giving more space for the remaining RBCs to be

attracted the ferromagnetic structures, thus increasing the separation efficiency. Thus for similar separation efficiency, the required effective trapping time can be decreased. However, the number of separation stages can not be increased indefinitely. To move RBCs from one point in the main channel to the other point where cells can be swept into collection channel, RBCs should be exposed to the lateral magnetophoretic forces for a certain amount of time (trapping time) as described in Equation 3.1. If the size of glass slide, on to which the microseparation system is fabricated, is limited, the more separation stages there are, the shorter each stage would be making the resident time shorter than the required trapping time at a specific volumetric flow rate. In this work, the total length of the main separation chamber was chosen to be 48 mm. For the unretained cells to pass through the separation chamber within 5 minutes, the average cell flow velocity should be higher than 0.16 mm/s. To achieve the volumetric flow rate of 20 μL/hr or higher with the fore-mentioned cell flow velocity, the cross sectional area of each of two main channels should be around 2×10^4 μm^2. The channel depth was chosen to be 100 μm considering the available fabrication process. The required trapping time for RBCs at 70 μm away from the ferromagnetic structures to move to 20 μm away from the wires was calculated to be 35 seconds. Considering both the trapping time and the minimum average flow rate, each separation stage should have a length of 5.6 mm or longer. The actual length of the separation stages was chosen to be 8.0 mm; thus the total number of separation stages was increased to six.

The second design option was increasing the cross sectional area of each main channel. In the previous paragraph, the microchannel depth was chosen to be 100 μm.

Moreover, to achieve a 2×10^4 μm^2 cross sectional area, the channel width should be increased up to 200 µm. However, those cells initially positioned further away from the ferromagnetic structures than 100 µm would be hard to be captured effectively. To overcome this limitation, the channel width of first separation stage was chosen to be 200 µm, but after each separation stage, the width was decreased down to 180 µm, 160 µm, 140 µm, 120 µm, 100 µm, and 100 µm by making the width of ferromagnetic structures wider at each of the subsequent stages.

Because the number of collected RBCs in the center channel is far more than that of cells in the side channel after six stages, some collected RBCs can backflow into the two outer side channels and side channel outlets by diffusion. Thus, in this work, the three outlet channels (two side outlet channels, one center outlet channel) were designed as isolated flow channels to increase the overall separation efficiency of the system.

The overall design and operational concept of six stage cascade paramagnetic mode magnetophoretic separation (PMMS) system is shown in Figure. 3.1.

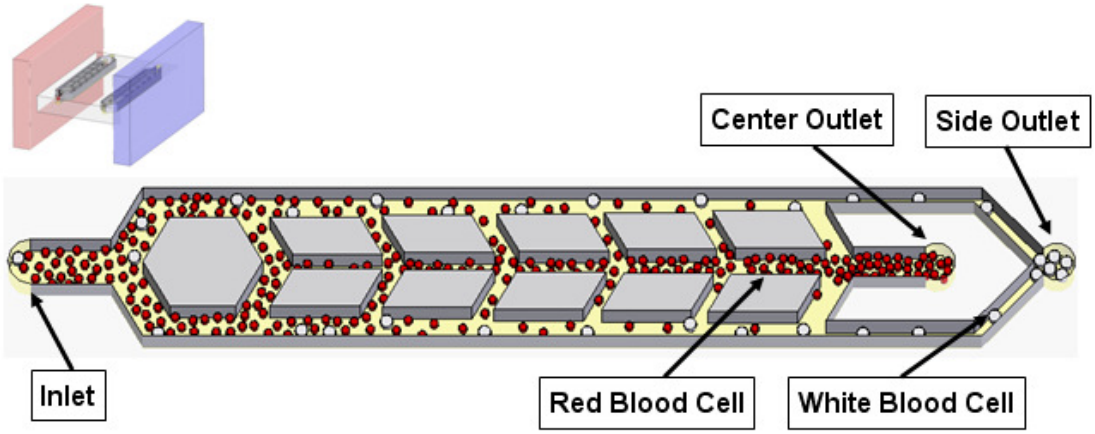

Figure 3.1. Operation of the PMMS system.

As shown in Figure 3.1, the whole blood sample entered the PMMS system and was subsequently divided into two outer microchannels flowing parallel to the ferromagnetic structures. The RBCs were attracted to the ferromagnetic structures by the force produced by the magnetic field gradient and forced into the center microchannel, while WBCs and other rare cells were forced outward and travel along the two outer channels. The fluid channel network were designed so that only the RBCs forced to the edge of the ferromagnetic capture structure were swept into the center channel, while other cells in the flow stream had a low probability of being swept into the center channel. The remaining RBCs in the outer channels were attracted and separated into the center flow channel at the subsequent separation stages. By combining six separation stages in a cascade mode, the RBC level in the outer channel was reduced stage by stage and after six separation stages, the RBCs were removed from the flow stream in the two outer channels.

The magnetophoresis system for blood cell separation requires two photolithography steps. The two mask designs for microfluidic channel and ferromagnetic structures are shown in Figure 3.2. The distance between the separation chamber and the inlet hole was increased to provide a better image of the separation chamber area during the experiments, since the microfluidic interface for the inlet required minimum spaces for bonding and those bonded area became obscure.

The mask designs were initially drawn and saved in DXF file format by Autodesk® AutoCAD and later converted into DWM format using ASM 2500W (Art Work Conversion Software, Inc., Santa Cruz, CA, USA) for the pattern generator.

The converted files were sent to Georgia Tech Microelectronics Research Center (MiRC) mask shop for the production of 5” × 5” chromium layered glass mask.

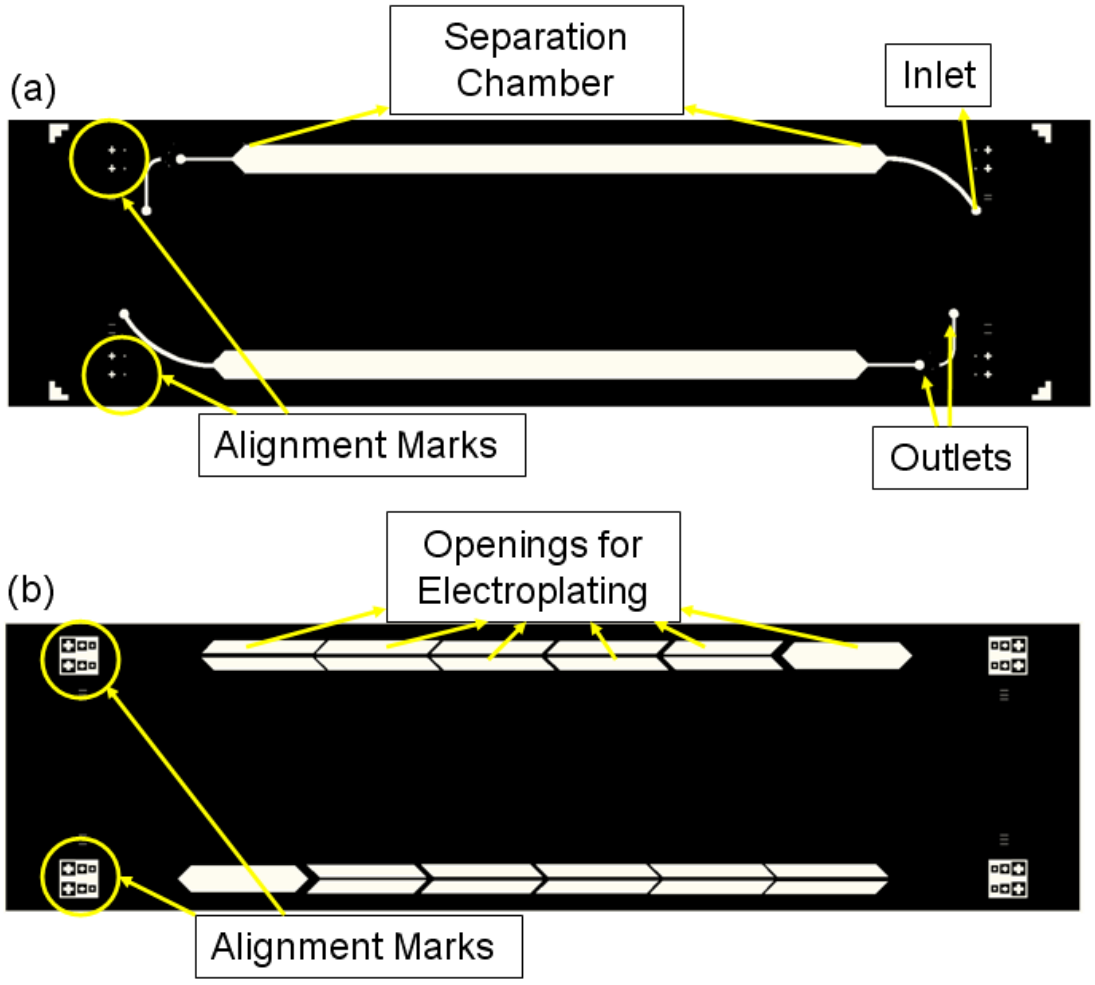

Figure 3.2. Mask design for microfluidic channel (a) and electroplated ferromagnetic structures (b).

3.3 Microsystem Interface and Package Design

The microfluidic separation system required microfluidic interfaces to introduce the blood samples into the microsystem and to collect the separated target cells, and system packaging to protect and stabilize the microsystem during experiments. For this purpose, the plastic fluid interfaces and packaging were fabricated utilizing stereolithography (SLA) technology and assembled with rubber O-rings to provide reliable fluid interconnection and sealing between the microsystem and macro experimental instruments, Figure 3.3 [87]. The cylindrical structures represent the area for holding the capillary tubing. The "[" shaped edge was to provide space for the tip holder of system packaging (to hold the microfluidic system while conducting the experiments).

A cross-sectional view of the fluid interconnection part of the designed interfaces is shown in the bottom figure of Figure 3.3. The lower O-ring was attached to the bottom part of the SLA interface to prevent the overflow of ultra violet (UV) cure adhesive resin into the inlet ports during the bonding process between the SLA parts and the glass substrates. The upper O-ring was inserted after the SLA fabrication process to hold the capillary tubing firmly in place during experiments. The capillary tubing was used to interface the macroscale fluid delivery system to the microscale separation system.

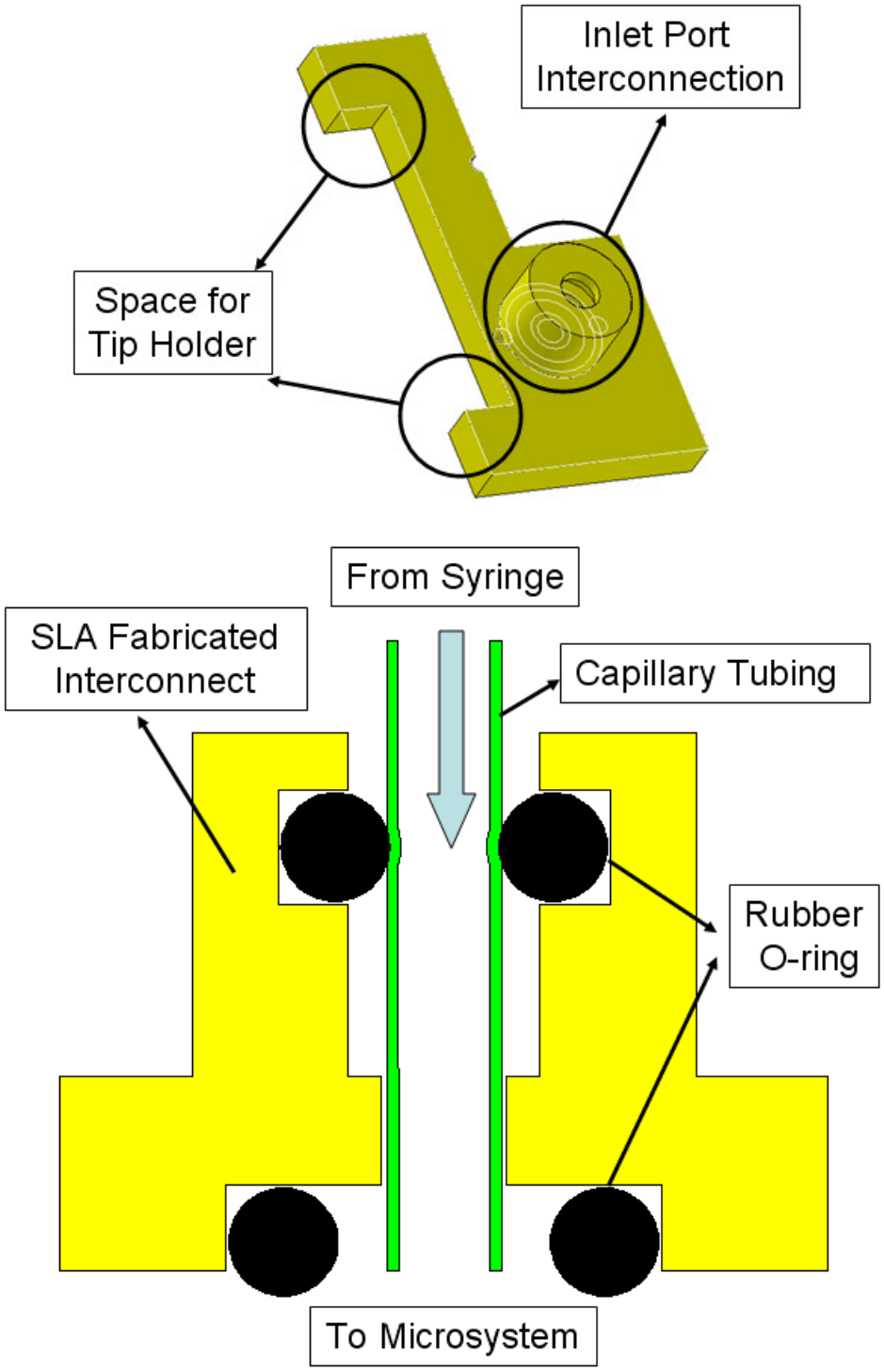

Figure 3.3. Design of the microfluidic interface (top) and a cross-sectional view of the SLA fluid interface design with rubber O-rings (bottom).

The system packaging for the magnetophoretic separation system was composed of two side pockets to hold the permanent magnets and one center stage to place and hold the assembled microsystem. The system packaging designs are shown in Figure 3.4. The system package was designed such that the permanent magnets could be positioned to create a magnetic field perpendicular to the sample flow inside the microseparator. Open cavities in the system package under the microchannel area were used to enable monitoring of the blood cell movement during separation by providing light passage from the bottom-side microscope light source.

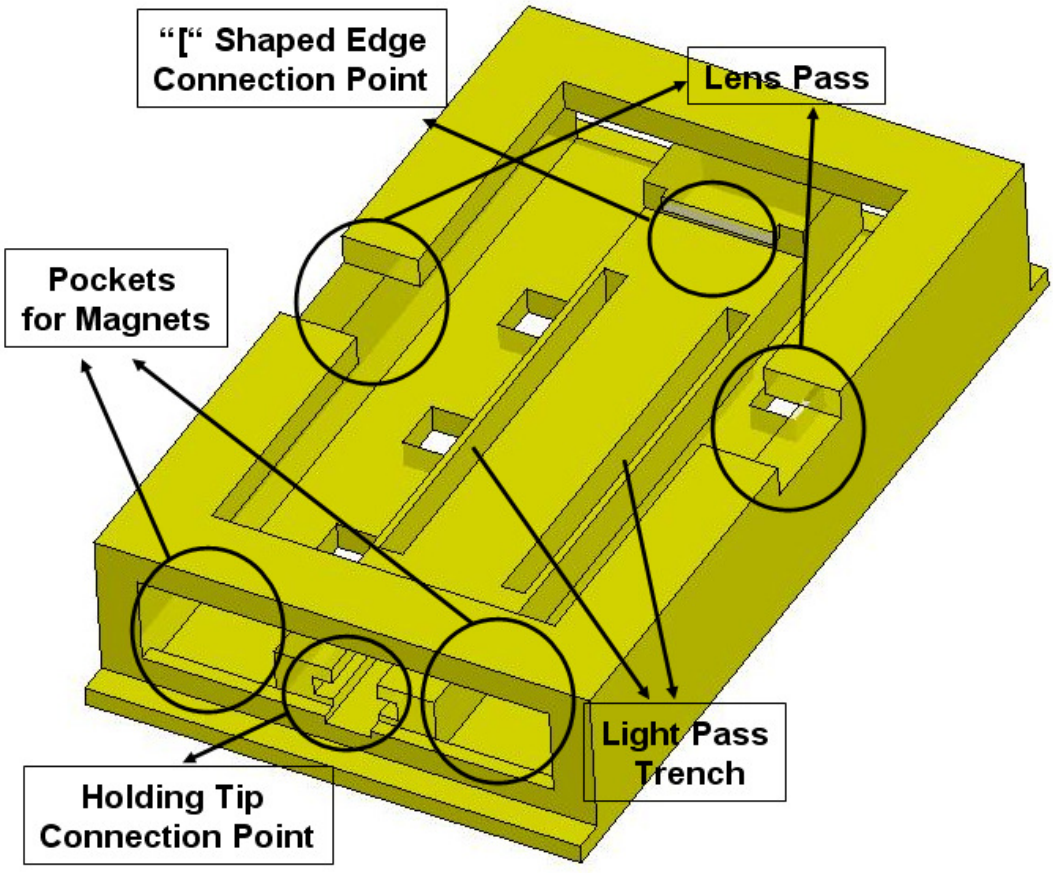

Figure 3.4. Design of the magnetophoretic separation system packaging.

The overall size of the system packaging is 105 mm × 65.0 mm × 21.5 mm (length × width × height). The width of center stage for microsystem was chosen to be 21.0 mm (1 mm larger than microfluidic chip width) and the width of side pocket was chosen to be 16.5 mm.

For the drawing of the microfluidic interface and system packaging, Solid Edge® program was used and the design was saved as STL file format which is native to the stereolithography CAD software created by 3D Systems®.

3.4 Microsystem Fabrication and Packaging

The separation channel of the PMMS system consisted of microfluidic channels, ferromagnetic structures and microfluidic interconnections. The overall fabrication process is shown in Figure 3.5.

In the fabrication of the separation system, a 500 Å chromium (Cr) layer and a 2000 Å gold (Au) layer were sputtered on both sides of a Schott Borofloat glass substrate (SB-1, S. I. Howard Glass Co., Inc., Worcester, MA, USA) using a Unifilm direct current (DC) sputter (PVD-300, Unifilm Technology, LLC., Boulder, CO, USA). Positive photoresist was spin-coated at 5000 rpm for 30 seconds on the front-side of the glass substrate and soft baked in a vacuum oven at 120 ºC for 1 minute. The microfluidic channel was patterned through UV light exposure using the OAI Mask Aligner (Optical Associates, Inc., San Jose, CA, USA) and developed. The back side and perimeter edges of the substrate were coated with positive photoresist and hard baked in a vacuum oven at 120 ºC for 5 minutes. The exposed Cr / Au layers on the front side were subsequently etched in Cr and Au etchant, and a 100 µm

deep microchannel was realized by hydrofluoric wet etching of the glass for 70 minutes (Figure 3.5(a)). The microchannel pictures after glass wet etching process are shown in Figure 3.6.

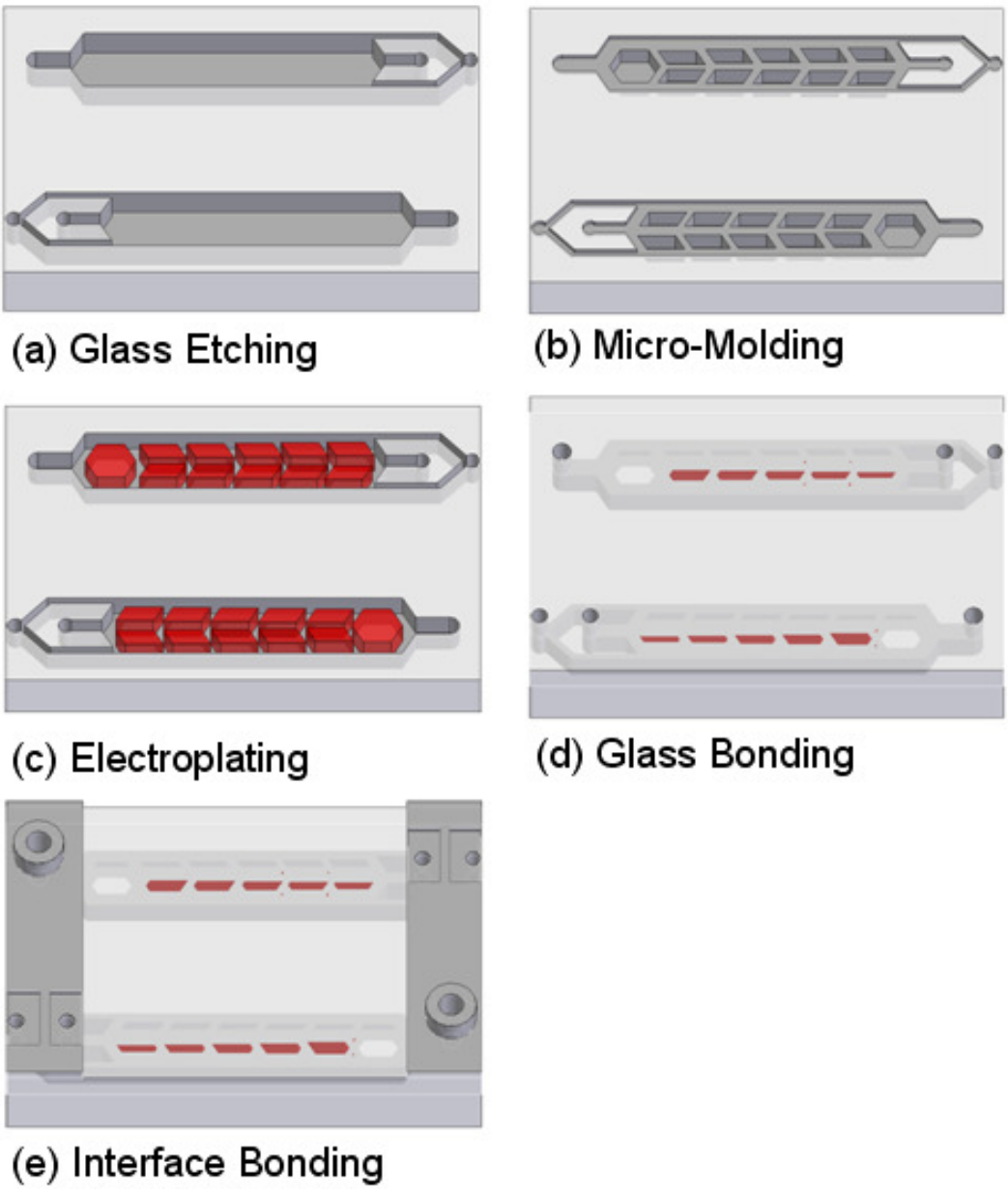

Figure 3.5. The fabrication process for the six-stage cascade PMMS system.

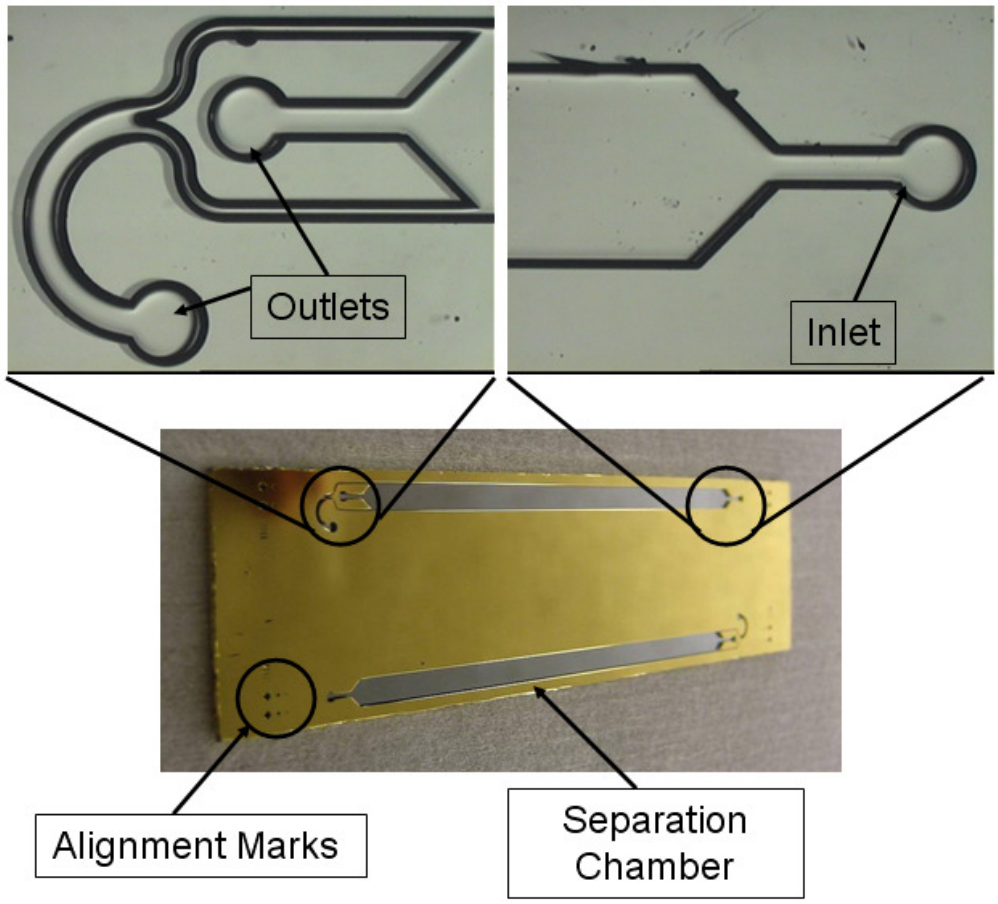

Figure 3.6. Etched microchannel in the glass substrate.

After removing the photoresist and metal masking layers, 150 Å, 1500 Å, and 1000 Å titanium / copper / chromium electroplating seed layers were sputtered over the surface of the etched glass substrate using the Unifilm DC sputter. Thick photoresist was spin coated at 300 rpm over the surface of the etched glass substrate, resulting in a measured thickness of photoresist over the 100 µm deep microchannel area of 130 µm. The substrate with uncured photoresist on the top surface was planarized by leaving it on a flat, level surface for 30 minutes before soft baking. Afterwards, the substrate was soft baked on a hot plate at 110 ºC for 20 minutes. The ferromagnetic capture structure electroplating molds were patterned by UV light

exposure using the Karl Suss MA-6 Mask Aligner (Karl Suss America, Inc., Waterbury Center, VT, USA) and development in photoresist developer (Figure 3.5 (b)). The microseparator pictures at this stage are shown in Figure 3.7.

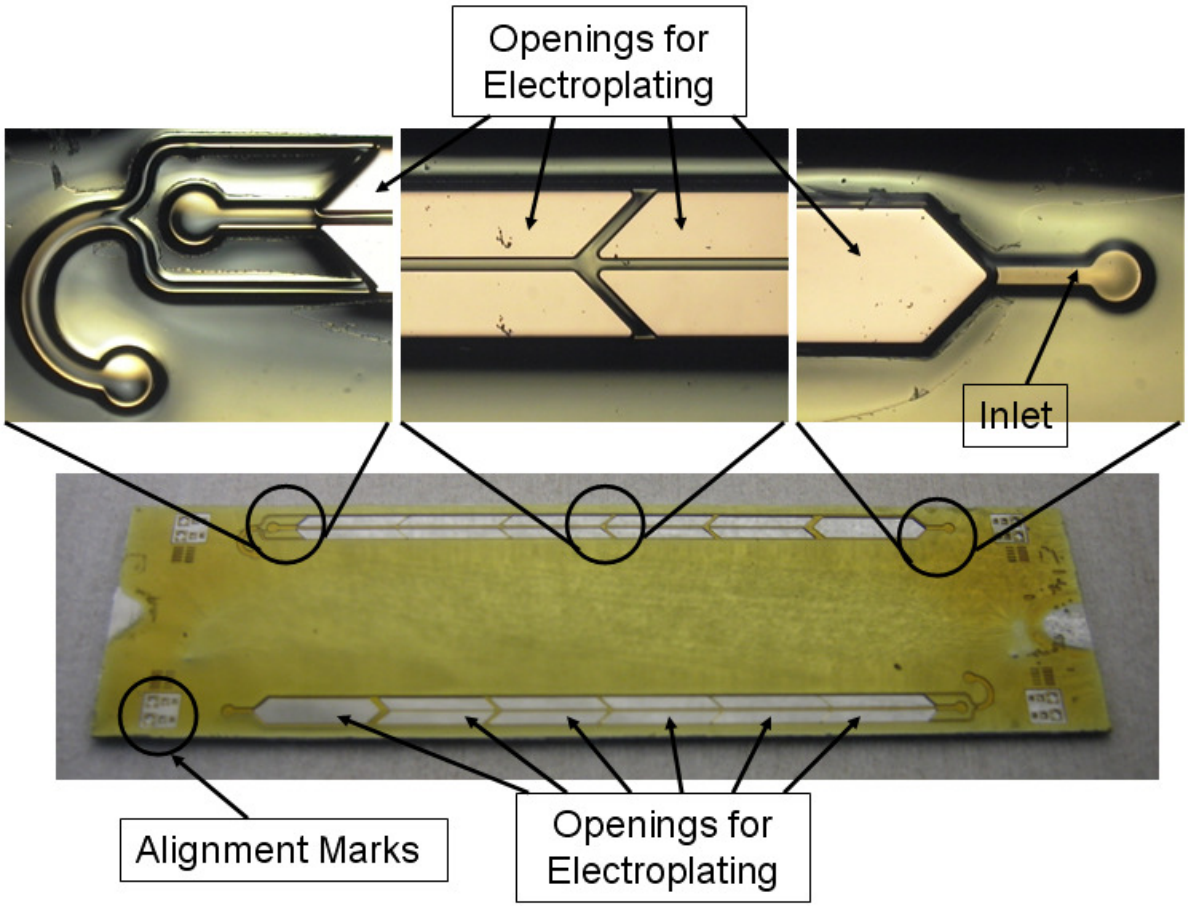

Figure 3.7. The mold for electroplating is patterned inside the microchannel.

The ferromagnetic capture structures located within the patterned flow channel, 100 µm thick, were realized by electroplating nickel iron (NiFe) permalloy using a $Ni_{81}Fe_{19}$ electroplating bath [88] on the pre-defined seed layer after removing the exposed Cr layer. The electroplating process was carried out at room temperature with a current density of 20 mA/cm^2. Following the electroplating process, the thick

photoresist molds and seed layers were removed by chemical etching, resulting in the patterned ferromagnetic structures within the microfluidic channel network (Figure 3.6 ©). The microseparator pictures at this stage are shown in Figure 3.8.

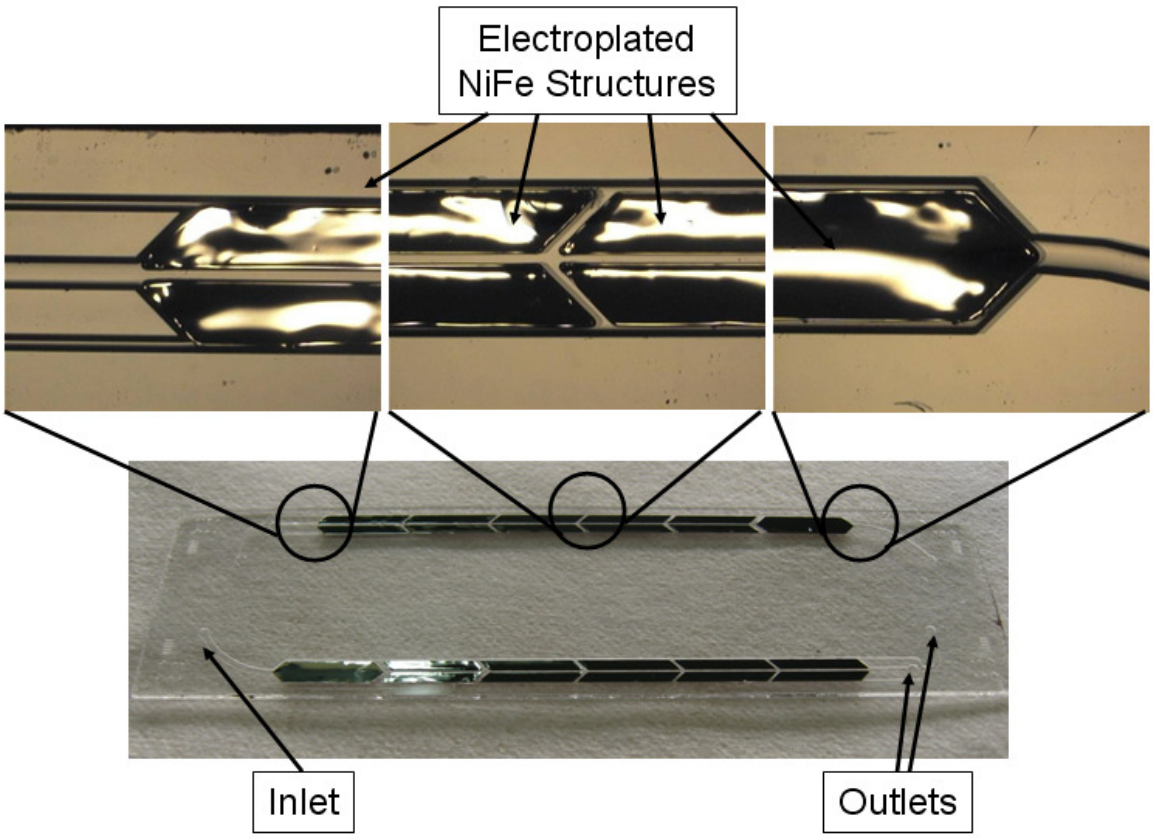

Figure 3.8. The NiFe ferromagnetic structures are electroplated inside the microchannel region.

A Viper™ SLA® stereolithography system (3D Systems, Co., Rock hill, SC, USA) was used to fabricate a drilling guide, microfluidic interfaces, and the system package. The STL format design files were edited and converted into a file format for Viper™ SLA® system by a Lightyear® program that can control the number of parts to be built and the supporting structures for each part. The converted file was loaded into the Viper™ SLA® system and a build was started using a linked computer

system in rapid prototyping manufacturing and manufacturing institute (RPMI) labs at Georgia Tech. The typical UV laser power for SLA process was 100 mW. The fabrication time were mostly determined by the height of tallest part. With a 100 mW power, a build time for the system package was around 4 hours. After the build for SLA parts was completed, they were cleaned by isopropyl alcohol in a ultrasonic bath for 15 minutes and rinsed again with flowing isopropyl alcohol. The cleaned parts were baked in UV oven for 30 minutes. The drilling guide was used to enable correct positioning of the inlet and outlet ports in the top glass substrate. The drilling guide is shown in Figure 3.9.

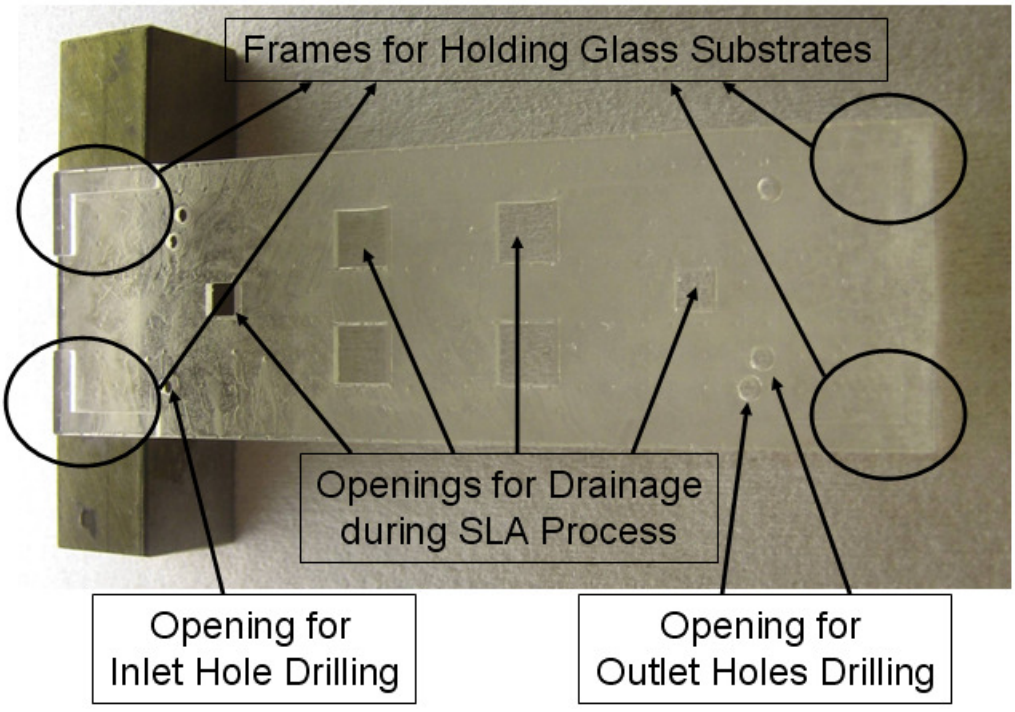

Figure 3.9. The drilling guide for the inlet and outlet holes.

The inlet and outlet holes were defined in the blank top glass using a 1.0 mm diameter diamond drill bit. The drilled top glass was aligned and thermally bonded with the patterned bottom glass in a box furnace at 685 °C for 3.5 hours in a nitrogen gas environment (Figure 3.5 (d)). Finally, the SLA-based microfluidic interface was bonded to the microseparator using a UV curable resin (Renshape® SL 5510, Vantico A&T US, Inc. Lansing, MI, USA) between the glass microfluidic system and the SLA interface. The resin was cured using UV light exposure for 30 minutes (Figure 3.5 (e)).

During the fabrication process for the PMMS system, there were several issues in the etching, electroplating and bonding processes. In our initial prototype designs, 50 µm deep microchannels were easily etched by submerging the patterned glass slide in hydrofluoric wet etching solution for 28 minutes. However, the wet etching process was slowed down and almost stopped around 88 µm deep after a 50 minute etching process. Agitating the etching solution with a stirring bar made the bottom of microchannel uneven and often tore the protective Cr / Au layers during the glass etching process. This problem was solved by taking out, washing the device carefully with DI water after submerging for 50 minutes, and continuing the etching process for additional 20 minutes.

The patterning of electroplating mold inside the 100 µm deep microfluidic channel was one of the major challenges. If the temperature and time for the soft bake cycle were not long enough, the mold structures suffered severe undercut issues and often caused problems in the subsequent electroplating process. Images of the undercut photoresist mold structures because of this issue are shown in Figure 3.10.

Initially there was post bake process at 120 °C after the second photolithography procedures. However, it turned out that this hard bake process sometimes caused deformation in the electroplating molds and subsequent changes in the final electroplated ferromagnetic structures. The post bake process was removed after several observations of deformation in the mold structures.

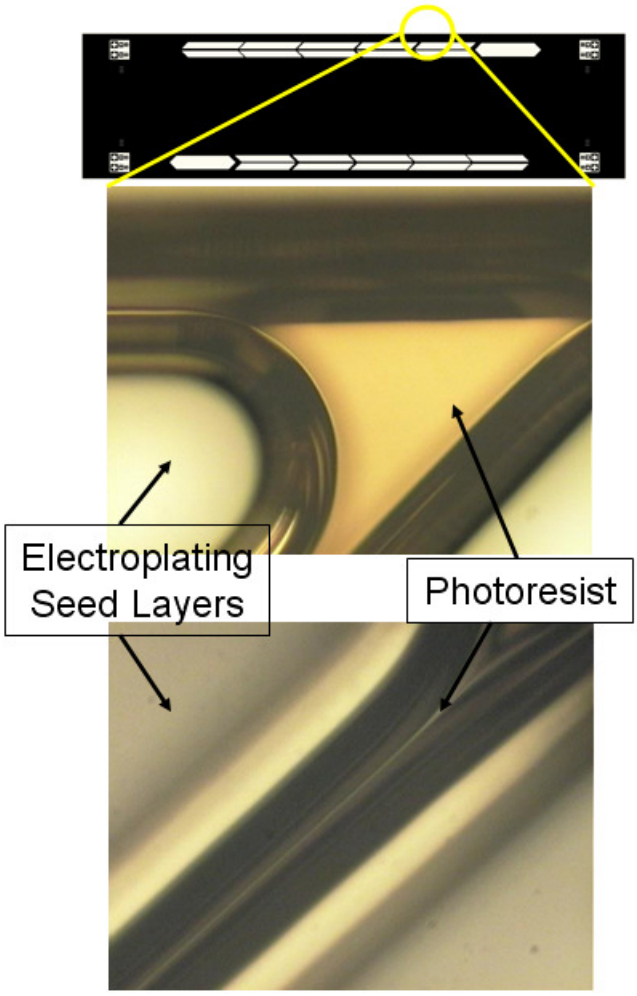

Figure 3.10. Undercut of mold structure due to soft bake issues. Micrograph focused on the photoresist surface (middle) and on the seed layers (bottom)

When the electroplating process was carried out, there was huge height difference up to 40 µm between ferromagnetic structures and even within one structure since the top surface had large curvature. Two contact points for electroplating process were made at each edge of glass slide and power supply line was connected to the one of two contact points for specified time, while the other contact point was covered and submerged in the electroplating solution. By switching the contact point, the height differences were reduced below 10 µm.

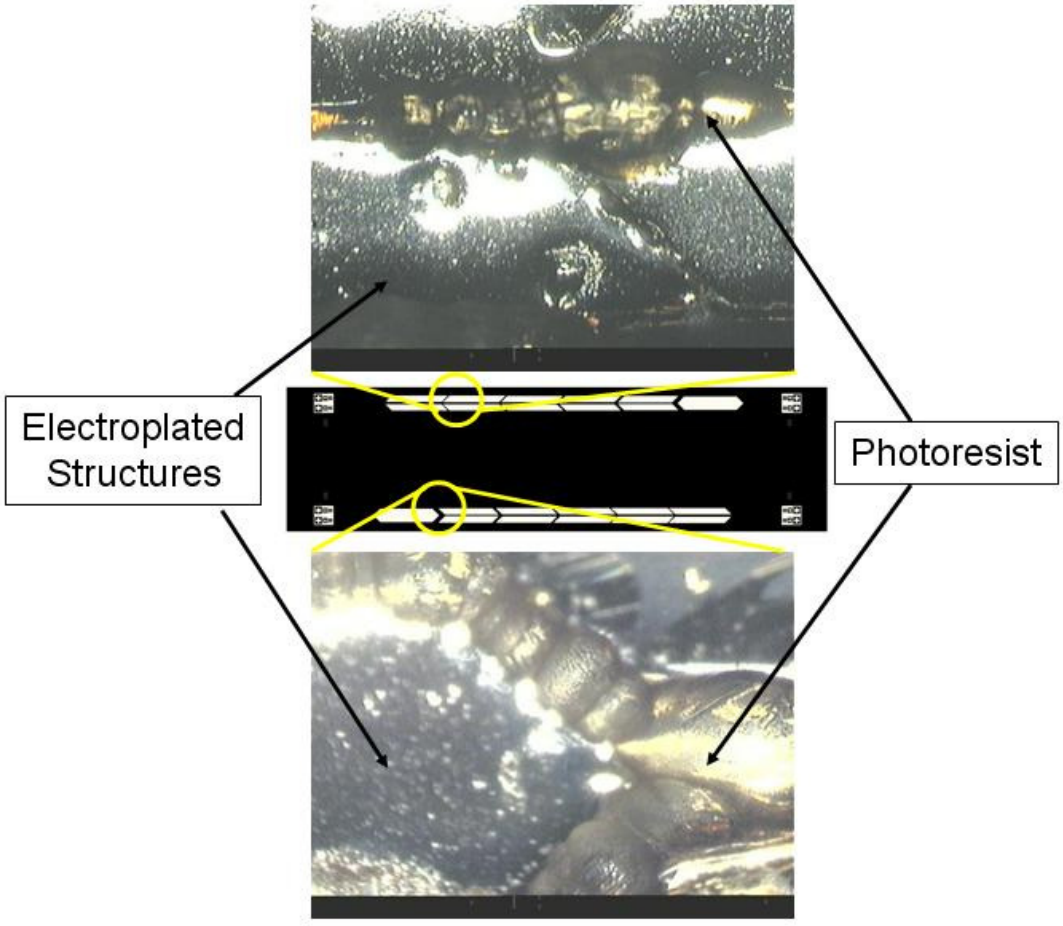

Figure 3.11. Bubbles during electroplating process.

The first method to cover non-active contact point was by painting the exposed Cu area with photoresist, but it required some dry time and it caused peeling off of electroplated layers between switching sides. Later, blue tape for vacuum seal was used for quick covering and uncovering of the contact point. Since the ferromagnetic structures required long electroplating times, it sometimes caused overheating of the photoresist, by which bubbles were made. These bubbles made the uneven surface of ferromagnetic structures worse (Figure 3.11). This issue was eased by proper soft bake and switching the contact side during electroplating.

For making inlet and outlet holes at the correct position in top glass slides, a CO_2 LASER was first used. However instead of making clean round holes, it gave a shattered edge shape or a burnt and melt-down shape. Thus, a conventional bench top drill press machine was used with an SLA-based drilling guide.

The most severe problems in the fabrication process occurred during the glass-to-glass bonding process. The technique used in the initial bonding process was glass fusion bonding, and it requires an exact match in the thermal expansion coefficients between the two glass slides. If there was a slight difference in thermal expansion coefficients between the top and bottom glass substrates, those glass substrates would be shattered into pieces after the thermal procedures. In several cases, the glass slides after thermal process came out broken because the top glass slides were ordered from the manufacturer later than the bottom glass substrates even though they were from same vendor (Figure 3.12).

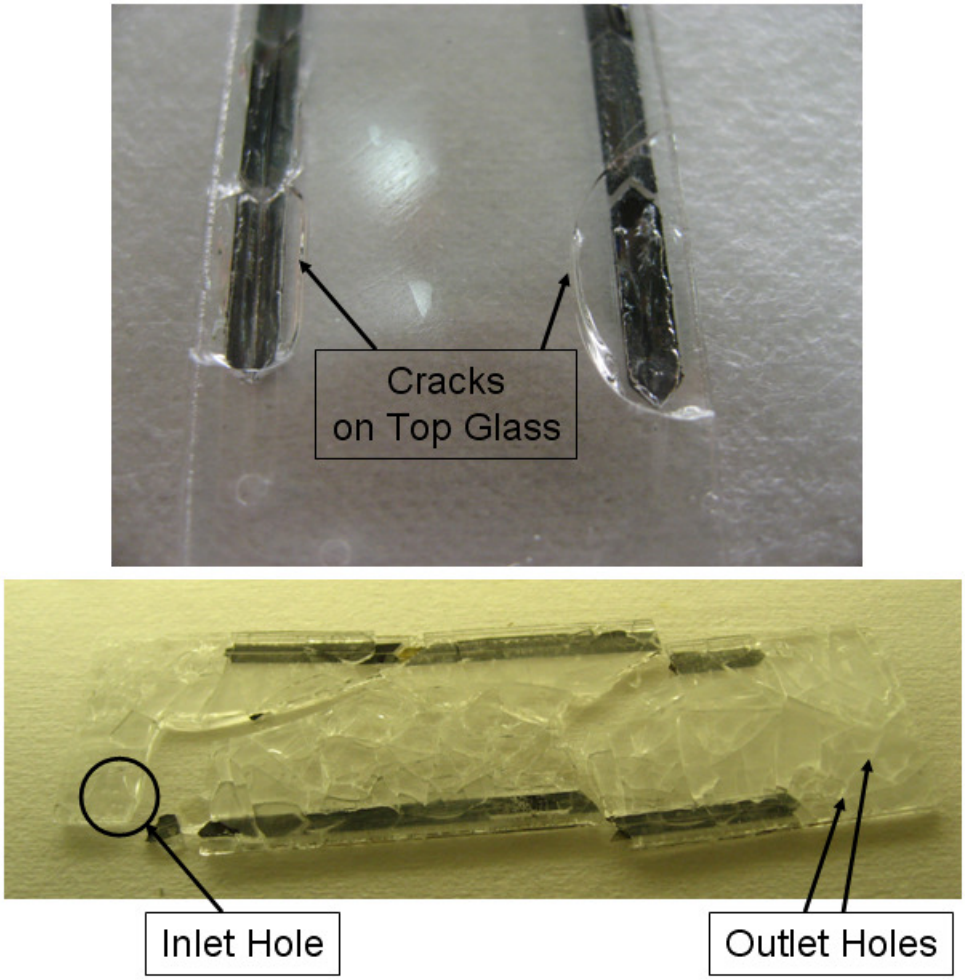

Figure 3.12. Broken devices during glass-to-glass thermal bonding process.

Unlike its predecessors, the six stage cascade system has a much bigger chamber and electroplated areas. This caused deformation in the bottom glass slides during the bonding process in many cases, and the top and bottom glass could not be completely bonded. The Curie temperature of $Ni_{81}Fe_{19}$ alloy powder is 567 °C and the thermal bonding process at 685 °C is known to decrease the permeability of $Ni_{81}Fe_{19}$ alloy [89]. As an alternative approach, the top and bottom glasses were aligned and bonded using UV curable adhesive resin (Renshape® SL 5510, Vantico A&T US, Inc. Lansing, MI, USA) applied between the two glasses by capillary force

and cured under a UV lamp for 30 minutes. UV adhesive bonding process solved most of problems associated with the thermal bonding process, but it created other problems like occlusion of the microfluidic channel by the introduced UV curable adhesive resin as well as open gaps between the top glass and the electroplated structures causing some blood cells to pass over the ferromagnetic structures during the experiments.

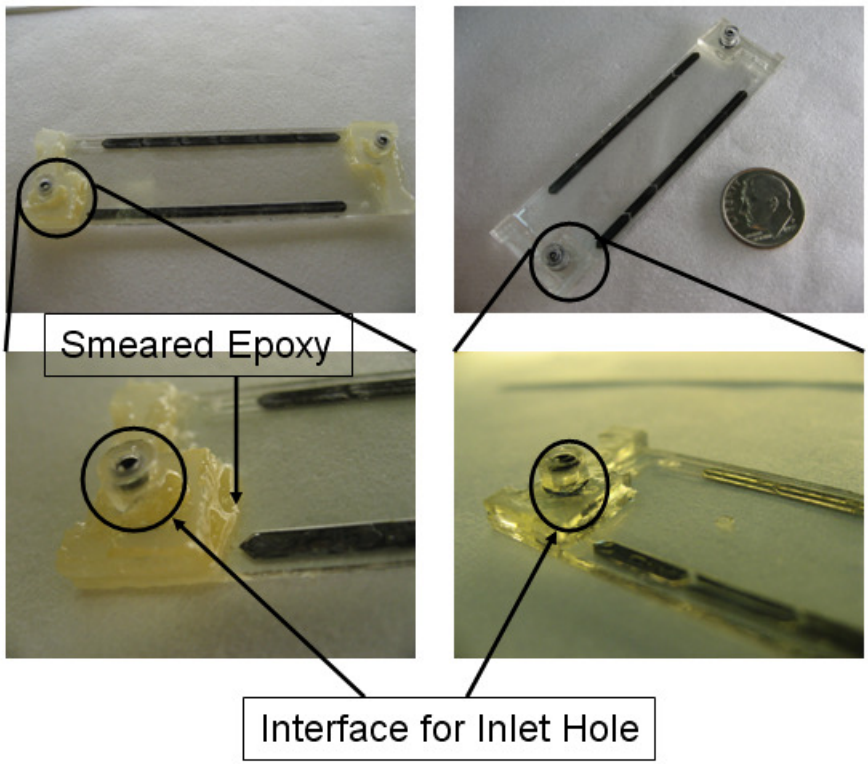

Figure 3.13. Bonding of interface by epoxy type adhesive (left) and UV curable adhesive resin (right).

The interface bonding process was carried out with epoxy type adhesive, but it required more than 2 hours for sufficient bonding and was hard to control. Later UV curable adhesive resin was used for clean and fast bonding between the interface and the glass substrates (Figure 3.13).

3.5 Experimental Methods

Human venous blood was collected at the Georgia Tech on-campus health center under an Institutional Review Board-approved protocol for blood collection for research purposes. The samples were drawn into evacuated glass tubes containing ethylenediamine tetraacetic acid (EDTA) as an anticoagulant. A 3.0 mM deoxidizing isotonic solution was prepared by dissolving sodium hydrosulfite (Sigma-Aldrich Co., St. Louis, MO, USA) in a calcium and magnesium free phosphate-buffered saline (PBS) solution (Mediatech, Inc., Herndon, VA, USA) at room temperature. The deoxidization and dilution of the blood sample were achieved by adding 500 μL of the 3 mM isotonic sodium sulfite solution to 50 μL of whole blood. SYTO® 13 fluorescent dye was used to identify the nucleated cells during experiments. The blood sample with SYTO® 13 fluorescent dye was incubated for 2 hours.

Before introducing the sample, the PMMS system was first treated with Pluronic® F108 tri-block copolymer surfactant (BASF Co., Florham Park, NJ, USA) solution to reduce the adhesion of blood cells on the channel surfaces. The surfactant solution was used to fill the microfluidic channel and left resident in the chamber for 5 hours. After treating the glass surfaces, the substrates were subsequently washed three times with PBS solution.

The fabricated device was mounted onto the center cavity inside the SLA alignment jig and permanent magnets were inserted into the side pockets to create an external magnetic flux. Compared to the plastic syringe, a glass syringe gave a more regular sample introduction rate at a low volumetric flow rate. A 500 μL gas tight glass syringe (Hamilton Co., Reno, NV, USA) was used to load the incubated blood

sample and connect it to capillary tubing through Luertight™ fittings (Upchurch Scientific, Inc., Oak Harbor, WA, USA). Tubing with a thin inner diameter was used in an effort to reduce blood sample travel time from the tip of a syringe to the inlet of microseparation system, thus minimizing the effect of sedimentation inside the tubing. The other end of tubing was connected to the device inlet port through the SLA microfluidic interface. A PHD 2000 syringe pump (Harvard Apparatus, Holliston, MA, USA) was used to provide the desired constant volumetric flow rates during the separation process.

During experiments, the initial volumetric flow rates were set at higher value and then lowered to target volumetric flow rates to avoid sedimentation of blood samples inside the connecting tubing. The assembled microsystem was placed under a fluorescent microscope and the trajectory of blood cells under a high magnetic gradient flux was monitored using the microscope camera and video capture tools (Figure 3.14). The bottom light source was used combined with a UV light source to illuminate both fluorescent and non-fluorescent cells with a green light passing filter.

A total of 2.5 μL of fluid was collected at each outlet port using adjustable pipettes (Series 2000, Eppendorf North America Inc., Westbury, NY, USA). The separation efficiency of the PMMS system was characterized by counting RBCs in the fluid collected at each outlet port using a Coulter cell counter (Multisizer II,, Beckman Coulter, Inc., Fullerton, CA, USA). For cell counting purpose, the collected fluid is mixed with 35 mL of buffer solution (ISOTON® II Diluent, Beckman Coulter, Inc., Fullerton, CA, USA) in a vial and placed in the cell counter for measurement.

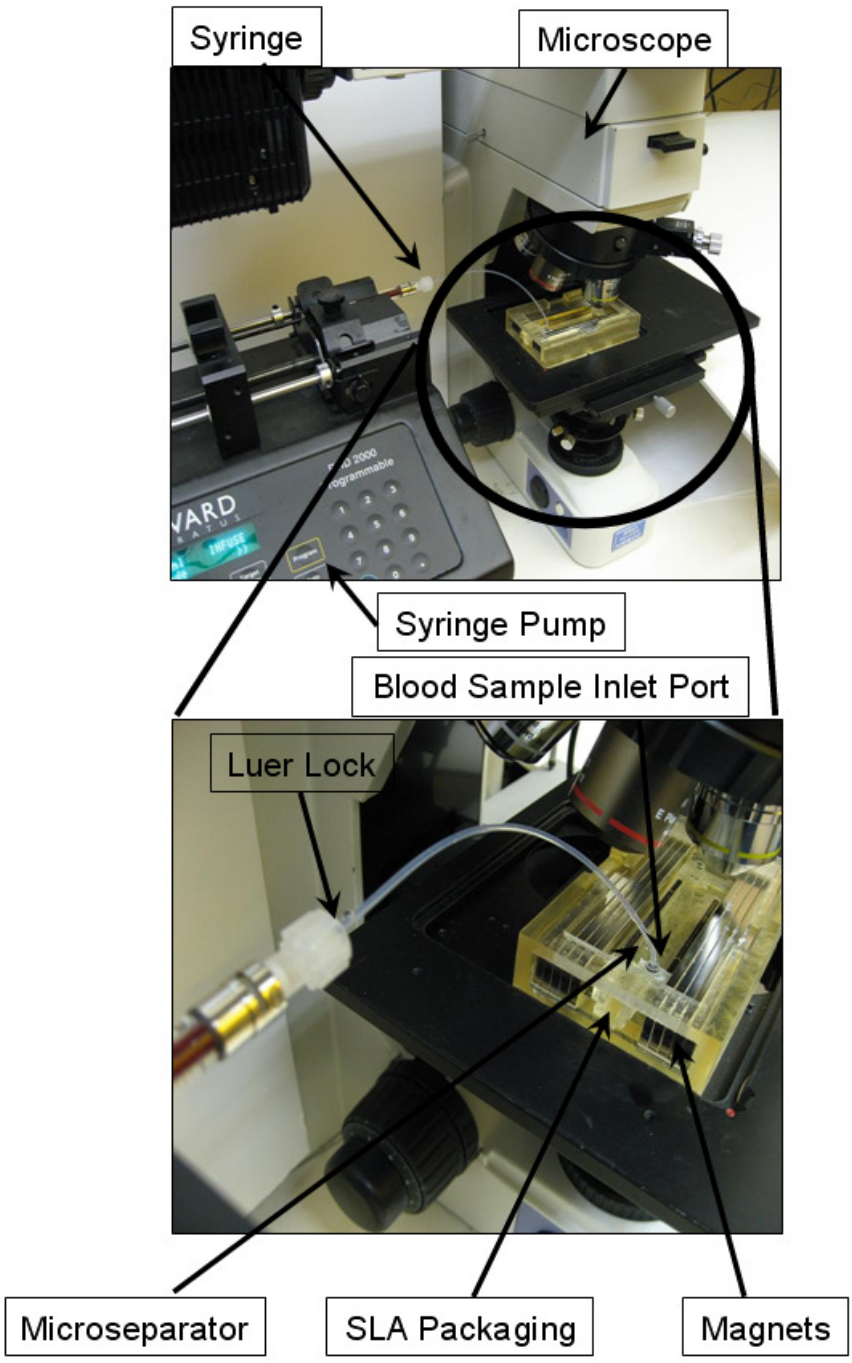

Figure 3.14. Instrument set-up for testing the PMMS system.

3.6 Results and Discussion

The original interface and package fabricated are shown in Figure 3.15. The original design for microfluidic interface does not have the "[" shaped edge for tip holder. The original package is only equipped a tip holder and several draining holes for fabrication.

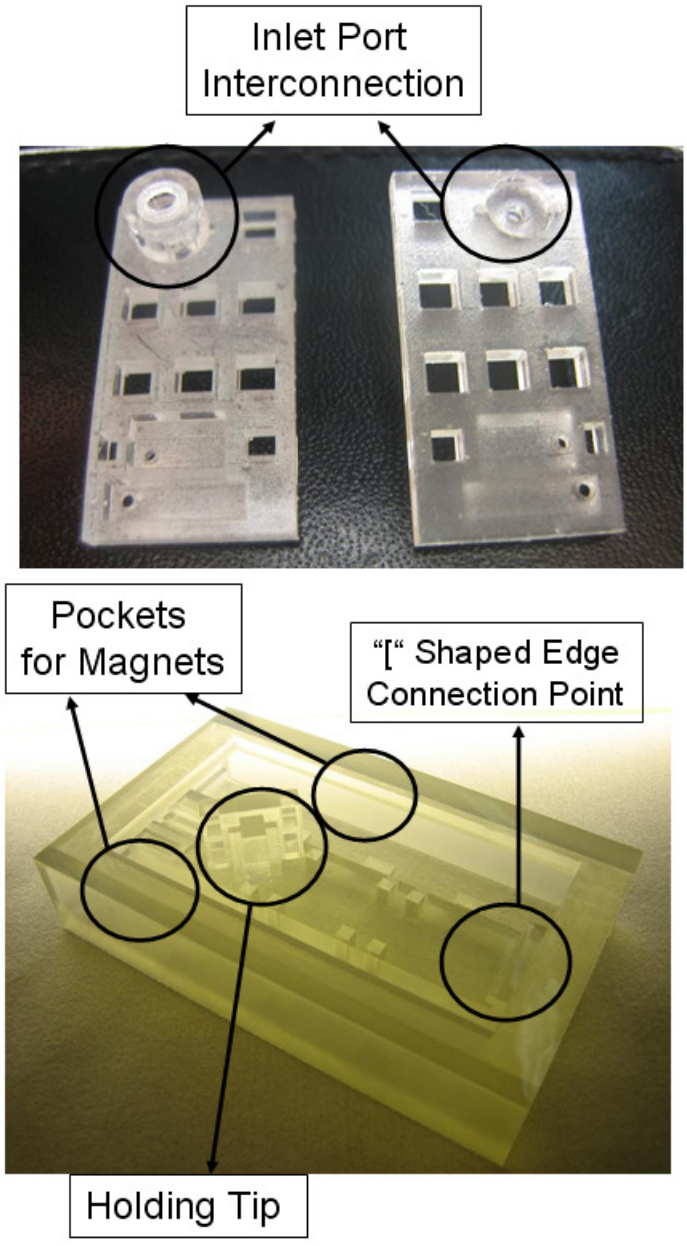

Figure 3.15. Original microfluidic interface (top) and system package (bottom).

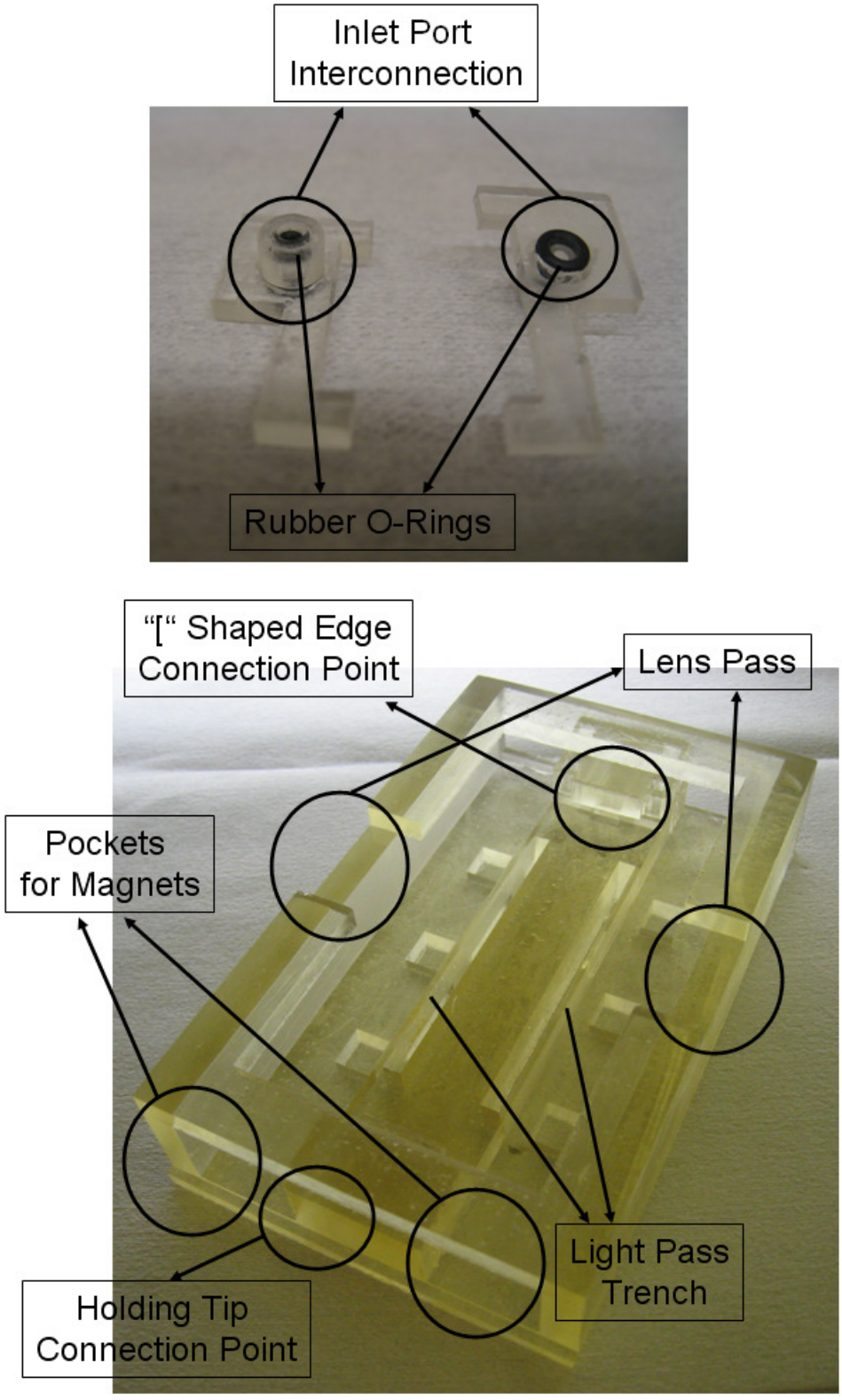

Figure 3.16. Modified microfluidic interface (top) and system package (bottom).

The modified microfluidic and system package is shown in Figure 3.16. The removable holding tip was used for easier installation and removal of the microseparator chip between experiments. The holding tip is shown connected to the system package. Two open cavities under the microchannel area were designed to provide light passage from the bottom-side microscope light source and two lens pass were made as shown in the package design.

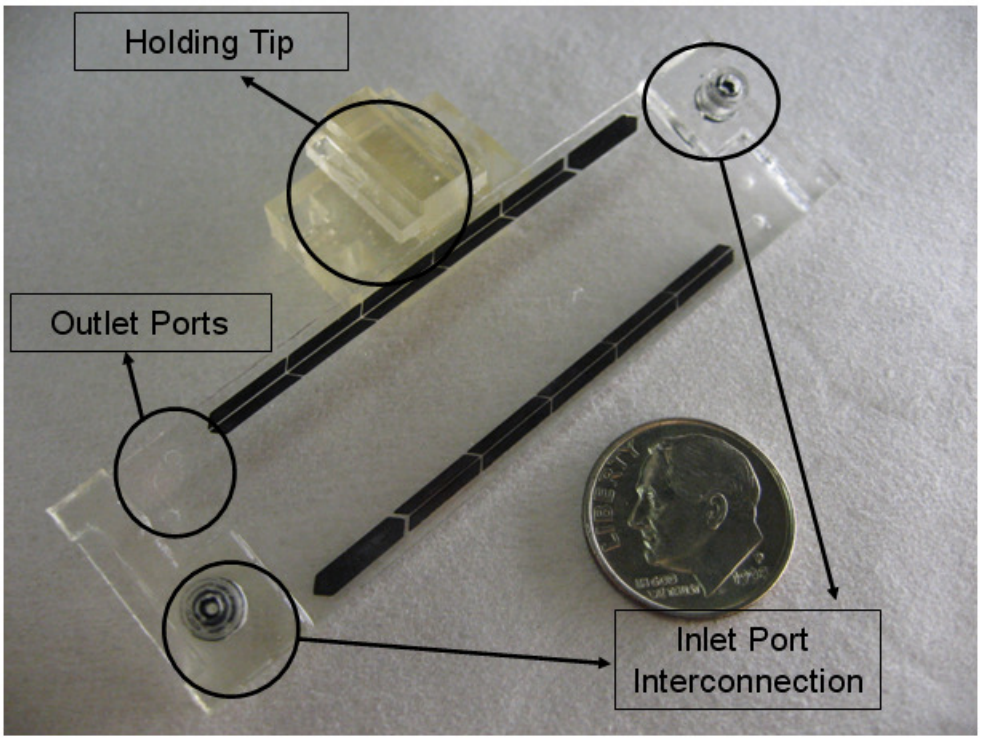

Figure 3.17. The fabricated PMMS system with holding tip.

The fabricated six-stage cascade PMMS system is shown in Figure 3.17. The 100 µm tall ferromagnetic structures inside the microchannel can be seen. The separation systems were fabricated at the perimeter of glass substrates to minimize the distance between the separation channel and the permanent magnets and thus

maximize the magnetic field gradient and magnetophoretic force on the untagged blood cells. The inlet holes were placed away from the main channel to give more room for microscope lens movement above the separation chamber during experiments. The outlet holes remained open to air to collect the separated blood samples with the adjustable pipettes. A holding tip was used in the removable part of the alignment jig to hold the microsystem during experiments.

Figure 3.18 shows the PMMS system packaged inside the alignment jig with permanent magnets in the side pockets.

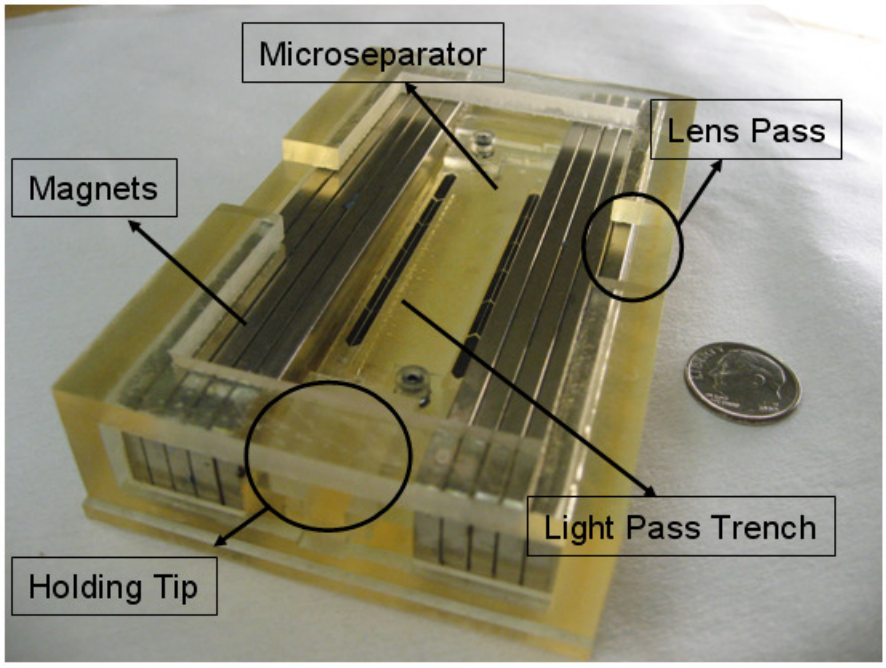

Figure 3.18. The assembled PMMS system inside package.

The PMMS system was first tested with prepared blood sample without an applied magnetophoretic force acting on blood cells by removing the permanent magnets from the package. At the flow rate of 28.8 uL/hr, 60.4 $\pm$ 5.25 % of blood

cells were collected into the center channel. The PMMS system was then tested with permanent magnets placed in the side pockets. Figure 3.19 shows images of the RBC separation inside the microchannel at an average flow rate of 28.8 µL/hr with an applied magnetophoretic force (except right top side picture). As the blood sample traveled the length of the microseparator, the RBC level in the outer channels decreased, while the number of RBCs in the center channel increased after each stage.

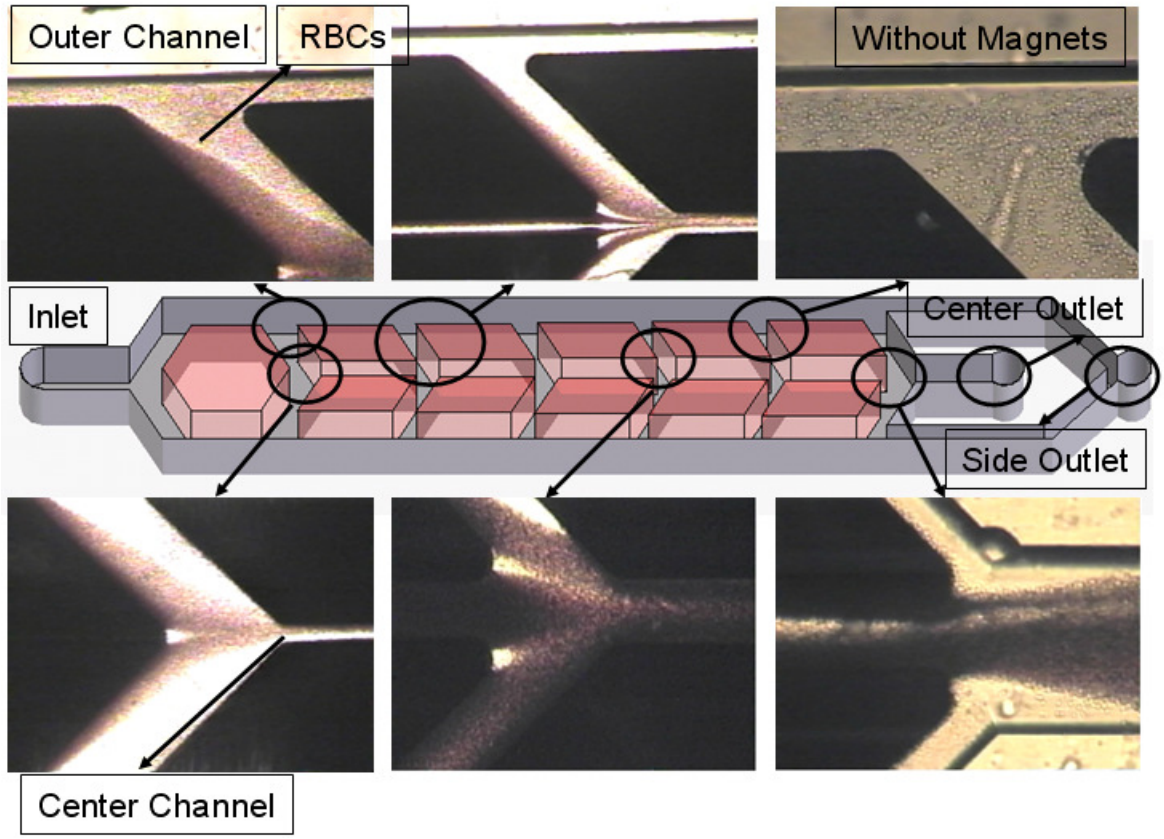

Figure 3.19. Micrographs of the blood cell separation at each stage.

At the output of the central channel in the microseparator, the separation efficiency was measured to be 89.5 $\pm$ 0.20 % for RBCs. The PMMS system was tested at higher volumetric flow rates of 50.4 µL/hr and 72.0 µL/hr. The measured

separation efficiencies were lowered to 86.2 ± 1.60 % and 59.9 ± 6.06 % respectively. As the whole blood travels at a higher flow rate, the residence time of blood cells inside the magnetic field gradient decreased, while the drag force by the flow increased. Thus, the chance for RBCs to be captured into the center channel was reduced (Figure 3.20).

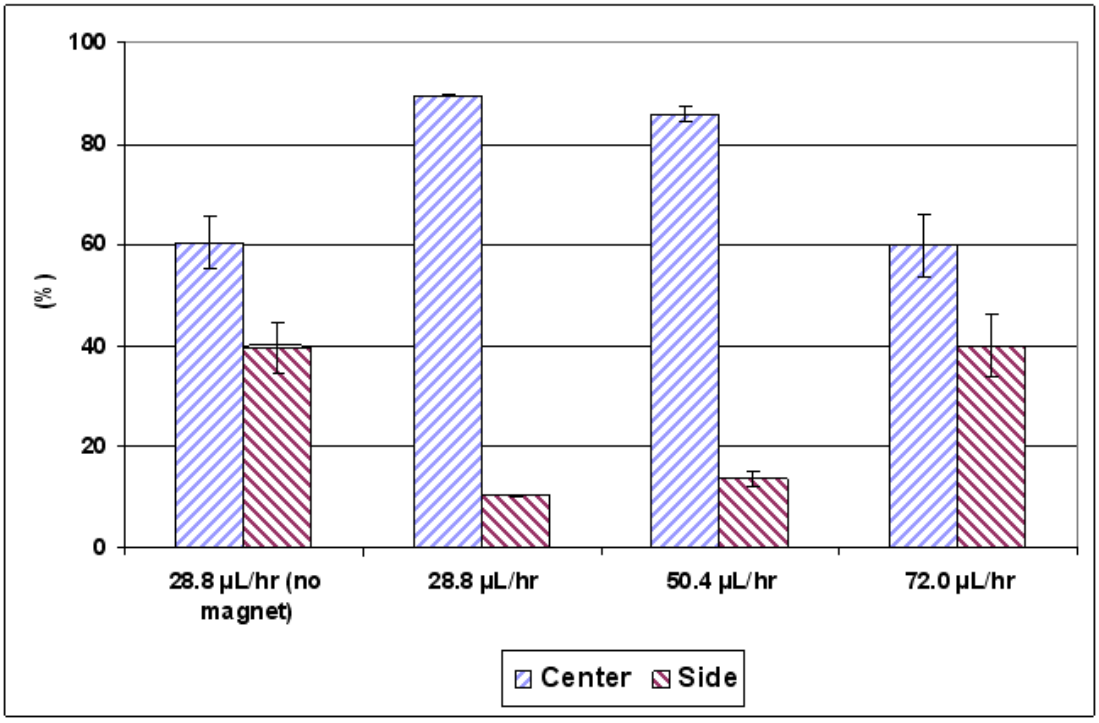

Figure 3.20. Measured separation efficiency of RBCs at each outlet for two volumetric flow rates. **Data of 50.4 uL/hr comes from UV adhesive bonded microseparator.*

No clogging from cell coagulation inside the channel was observed during the separation. However, trapped air bubbles in the channel introduced between experiments blocked the microchannel and prevented further characterization if not removed before starting the separation process.

CHAPTER 4

MAGNETOPHORESIS SYSTEM APPLICATION II

(Cancer Cell Separations)

4.1 Introduction

Cancer has been one of the largest causes of mortality in the United States with the total number of deaths related to cancer increasing annually until recently. With the technical advances in cancer early detection technologies and treatments, the overall cancer survival rate for patients has been rising. However, as a primary tumor starts to shed cancer cells into the blood stream and those circulating tumor cells cause secondary tumors to grow in various sites of cancer patients, clinicians have limited options for cancer treatment and the survival rate drops rapidly. Therefore, identifying and determining the malignancy of tumor cells in the early stages of cancer progression is very important to deter further metastasis of primary tumors and to maximize the success rate in cancer treatments. The sample size from early detected tumors is usually small and manipulating those cells has been a major challenge. The ability to perform the biological experiments efficiently with only a small volume of complex fluids makes the microfluidic system a promising candidate for point-of-care devices. Additionally, microfluidic systems offer other practical advantages including the potential for operation without the need for an expert operator and the potential to be used in resource-limited situations.

The expression level of specific membrane proteins differs for malignant tumor cells and benign tumor cells [90, 91]. For example, during complementary

experiments with head/neck cancer cells, it was found that the expression level of the protein CD29 was much higher in metastatic head / neck squamous cancer cell lines (M4e) than non-metastatic head / neck squamous cancer cell lines (212LN), therefore could potentially provide a biomarker for head and neck cancer detection [92, 93]. Depending on the expression level of CD29, the malignant tumor cells can be selectively tagged with magnetic nanoparticles by antigen-antibody reactions (Figure 4.1).

The presented continuous flow-based magnetophoresis microsystem will enable the separation and collection of a wide variety of cells in small quantity by selective molecular tagging to the cell membrane or by intercellular tagging.

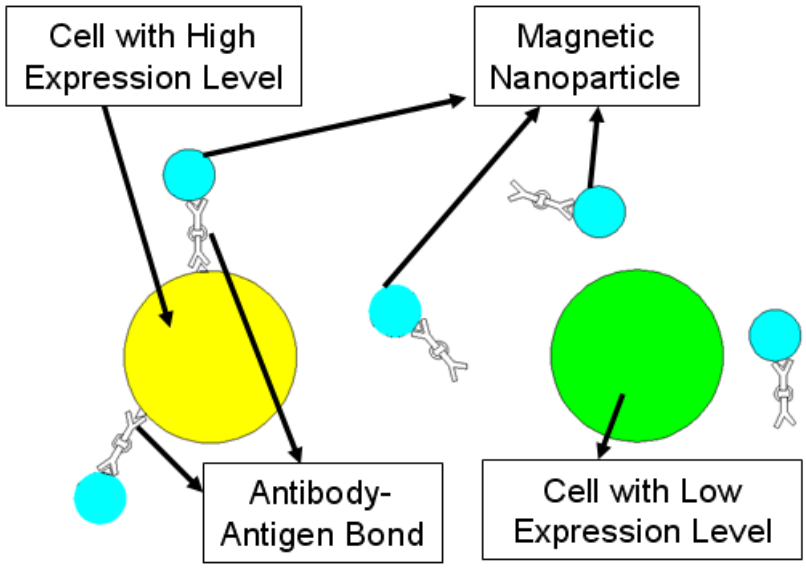

Figure 4.1. Cells with different protein expression levels (CD29) and magnetic nanoparticles.

4.2 Microsystem Design

Initially, the six-stage cascade PMMS system was used to determine the feasibility of using the magnetophoretic microfluidic separation system for the separation of tagged tumor cells from a complex sample containing a mixture of cells. During experimentation, it was confirmed that magnetophoretic microfluidic system could separate and isolate targeted magnetically tagged cells successfully. Additionally, it was found that several design and operational modifications were required due to the much higher magnetophoretic force acting on magnetically tagged cells when compared to untagged cells and due to the relatively small percentage of target cells in the sample.

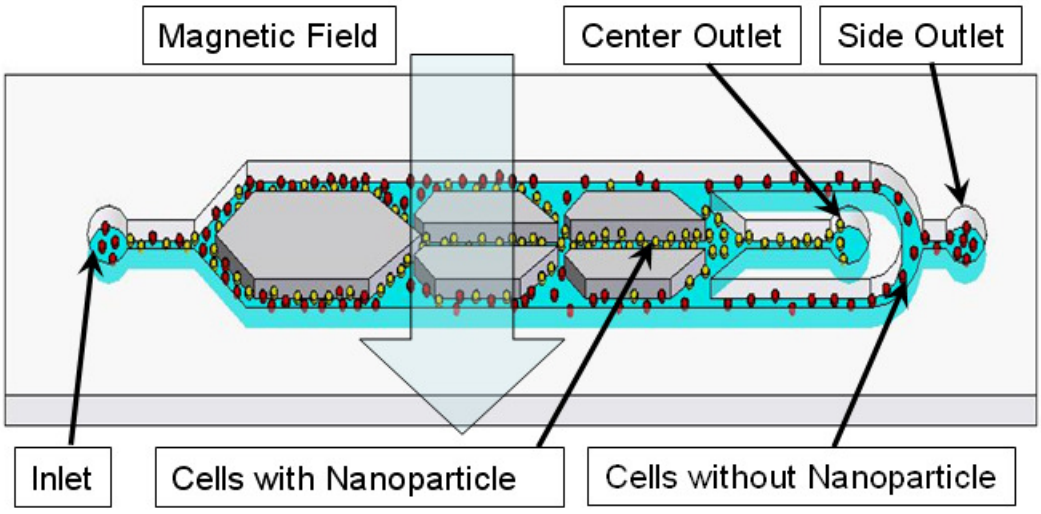

Figure 4.2. Operational principle of the multiple stage para-magnetophoresis microseparator.

Figure 4.2 illustrates the novel microsystem used to achieve continuous separation of magnetically tagged cells from untagged cells. The operational

principle of this microfluidic system is similar to that of the blood cell separator. Under a high magnetic field gradient, 'magnetic' cells in a mixed cell suspension are attracted toward the ferromagnetic capture structures and subsequently forced into the center channel while the untagged cells travel along the outer channel. The remaining tagged cells in the outer channel are attracted and separated again at the subsequent separation stages. One major change was made in the design of fluid channel network when compared to the RBC / WBC application discussed in Chapter 3. In the separation of RBCs, the cell density of the 'magnetic' cells is much higher than that of the 'non-magnetic' cells. However, in the separation of tagged tumor cells in an application such as CTCs, the cell density of the 'magnetic' cells is much lower than that of the 'non-magnetic' cells. As seen in Figure 4.2, at each separation point, there is 'V' shape area so that only 'magnetic' cells closely positioned to the edge of the ferromagnetic capture structures can be swept into the center channel, while 'non-magnetic' cells remain in the side channels.

The magnetophoresis system for malignant tumor cell separation requires two photolithography steps. The two mask designs, one for the microfluidic channel and one for the ferromagnetic structures are shown in Figure 4.3.

The design of the tagged cell separation system was similar to the design of six-stage cascade PMMS system shown in Chapter 3 for the separation of RBCs from nucleated cells. The distance between the separation chamber and the inlet hole was sufficient to provide a better image of the separation chamber area during the experiments.

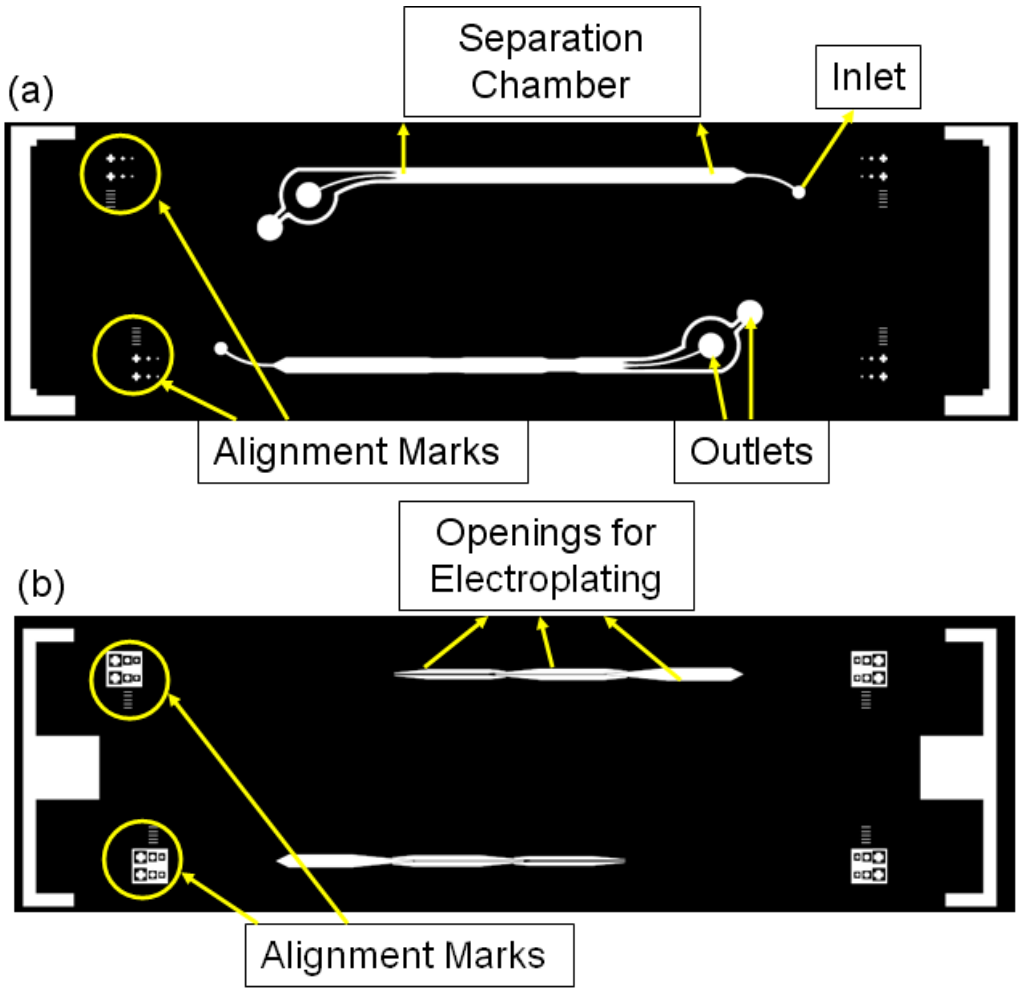

Figure 4.3. Mask designs for microfluidic channel (top) and electroplated ferromagnetic structures (bottom).

There were two major design changes from six-stage cascade PMMS system. First, the diameter of the two outlet holes was changed from 1.0 mm to 2.0 mm for easier collection of the separated cancer cells. Second, the design of the fluid transition region from the outer channels to the diagonal collection channels was modified as shown in Figure 4.4. The change in the design of the transition region was necessary because in the separation of tagged tumor cells, the cell density of the 'magnetic' cells is much lower than that of the 'non-magnetic' cells, and the magnetophoretic force on these tagged cells is much higher than that of the RBCs in a

human blood sample. By changing the design and making a 'V' shaped area at each separation stage as in Figure 4.4, only 'magnetic' cells closely positioned to the edge of the ferromagnetic capture structures can be swept into the center channel, while 'non-magnetic' cells remain in the side channels.

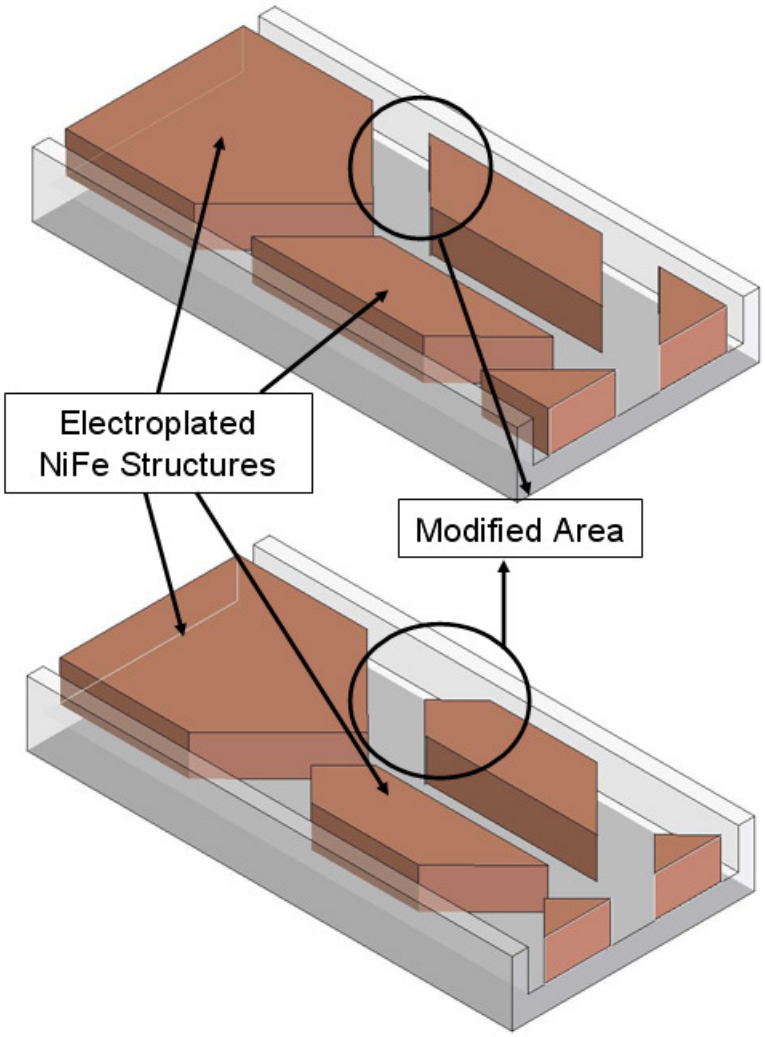

Figure 4.4. The design differences between six-stage cascade PMMS system for non-tagged RBCs (top) and the tagged cell separation system (bottom).

The mask designs were initially drawn and saved in DXF format by Autodesk® AutoCAD and sent to an outside vendor for plotting onto transparent film. Later, the patterns were transferred from the transparent film to a 4" × 4" chromium-layered glass mask using a standard photolithography process.

The microfluidic interface for the tagged cell separator was designed similarly to that of the blood cell separator shown in Chapter 3. Two O-rings were inserted to firmly hold the Teflon™ tubing and the "[" shaped space for the tip holder of the system packaging to hold the microfluidic system while conducting experiments (Figure 4.5).

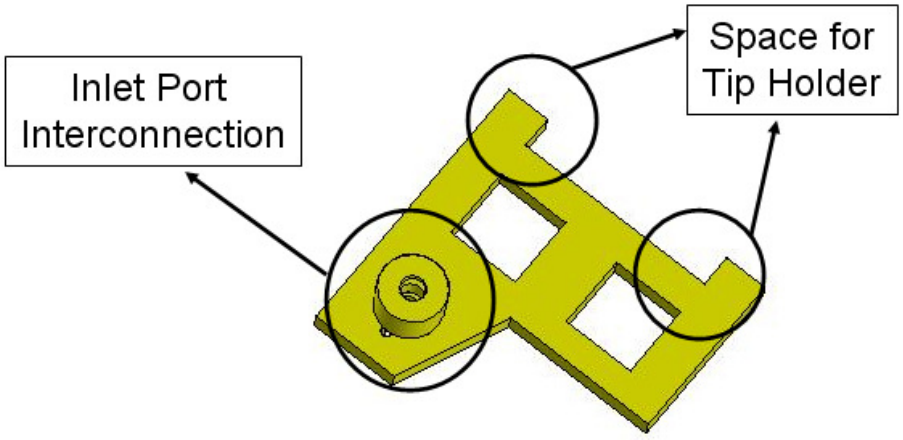

Figure 4.5. Microfluidic interface design.

The system packaging has similar features to that of the blood cell separator such as a center stage to place and hold a microfluidic separation system with a removable tip and an open cavity under the center stage for light passage. A major change made in the design of system package was the position of the adjustable side

pockets for the permanent magnets relative to the separation system. Each of the side pockets can be separated from main package and inserted into several saw-shaped locations to change the distance between the permanent magnets and the microseparator. Additional SLA-based columns, which positioned between the microseparator and the side pocket, were designed to reduce the magnetic field intensity on the microseparator (Figure 4.6).

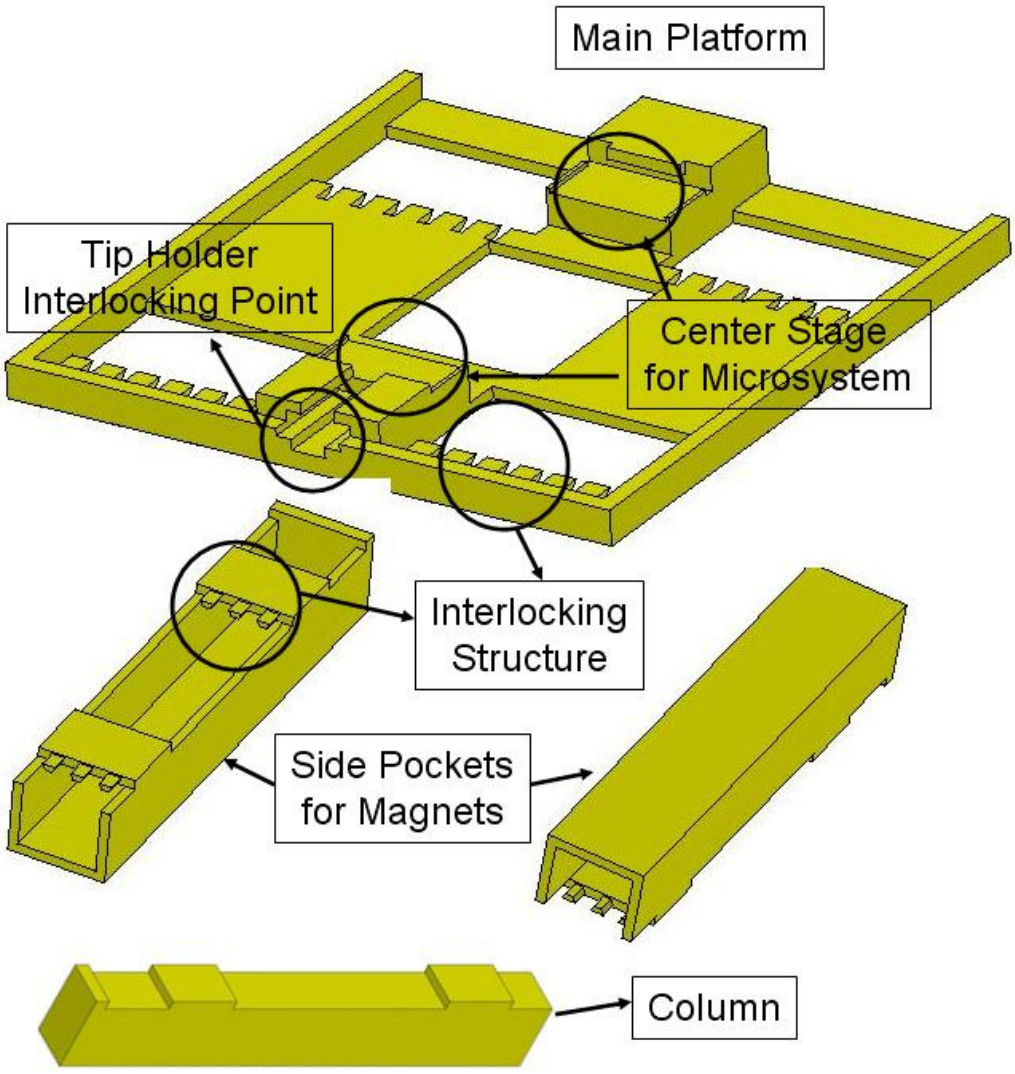

Figure 4.6. Microfluidic system packaging design.

The overall size of the system package platform is 108 mm × 108 mm × 11.5 mm (length × width × height). The width of center stage for microsystem was chosen to be 22.0 mm and the size of the movable side pocket is 108 mm × 20.5 mm × 15.5 mm (length × width × height).

The drilling guide design for correct positioning of the inlet and outlet ports in the top glass substrate is shown in Figure 4.7. For the drawing of the microfluidic interface, system packaging, and drilling guide, the Solid Edge® program was used and the design was saved as a STL file for a SLA process.

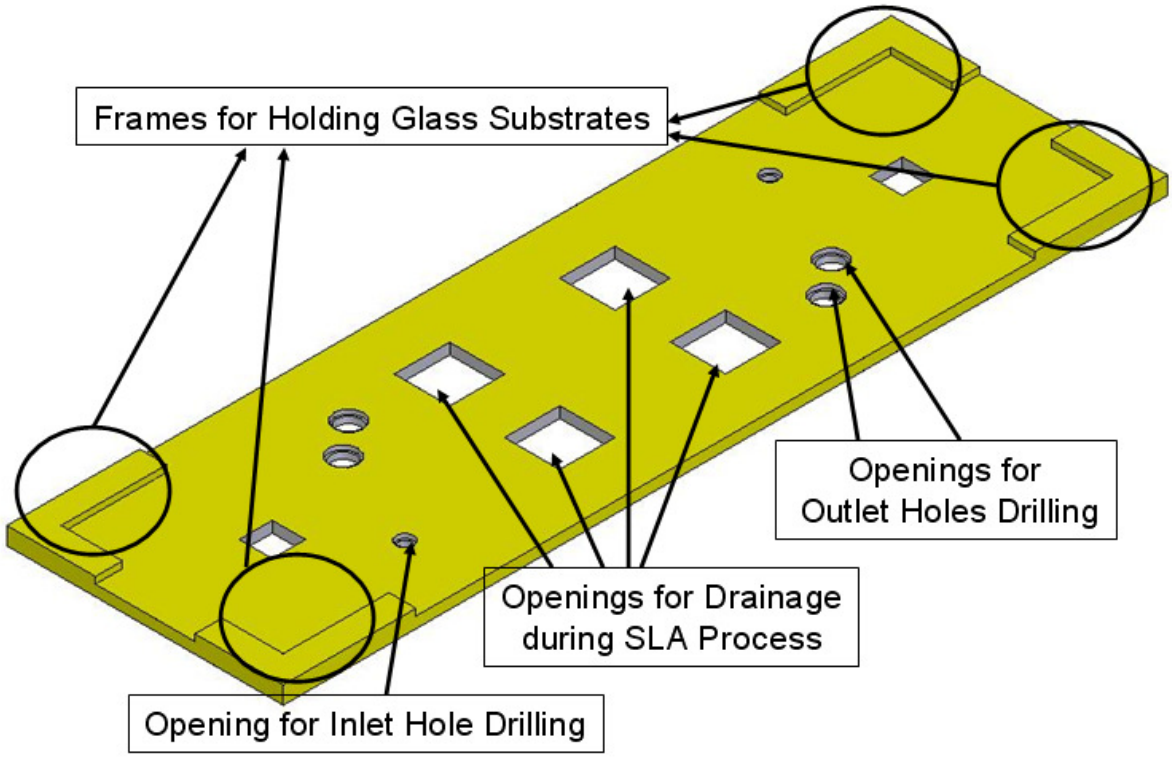

Figure 4.7. The drilling guide for the inlet and outlet holes.

4.3 Microsystem Fabrication and Packaging

The microsystem was composed of microfluidic channels, ferromagnetic separation structures, inlet/outlet holes, and microfluidic interfaces. The overall fabrication process of microseparator is similar to that of six stage cascade mode blood cell separator and consists of wet etching the glass substrate to create the microfluidic channel, electroplating of ferromagnetic separation structures, glass-to-glass bonding, and bonding of the microfluidic interfaces.

After the wet etching process, the residual photoresist and metal masking layers were removed using acetone, Cr / Au etchant, and piranha cleaning. The ferromagnetic structures were electroplated as described in Chapter 3.

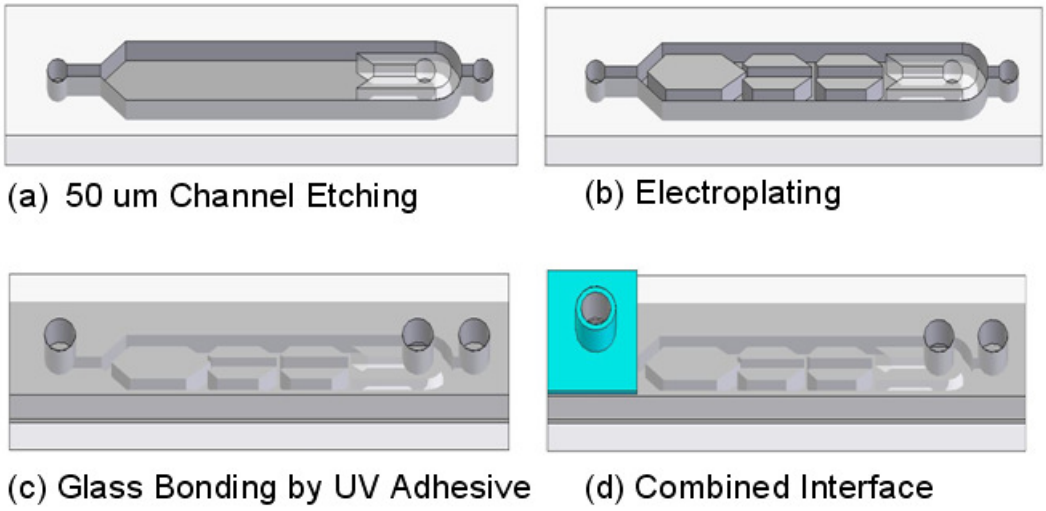

Figure 4.8. The fabrication process for the microseparator.

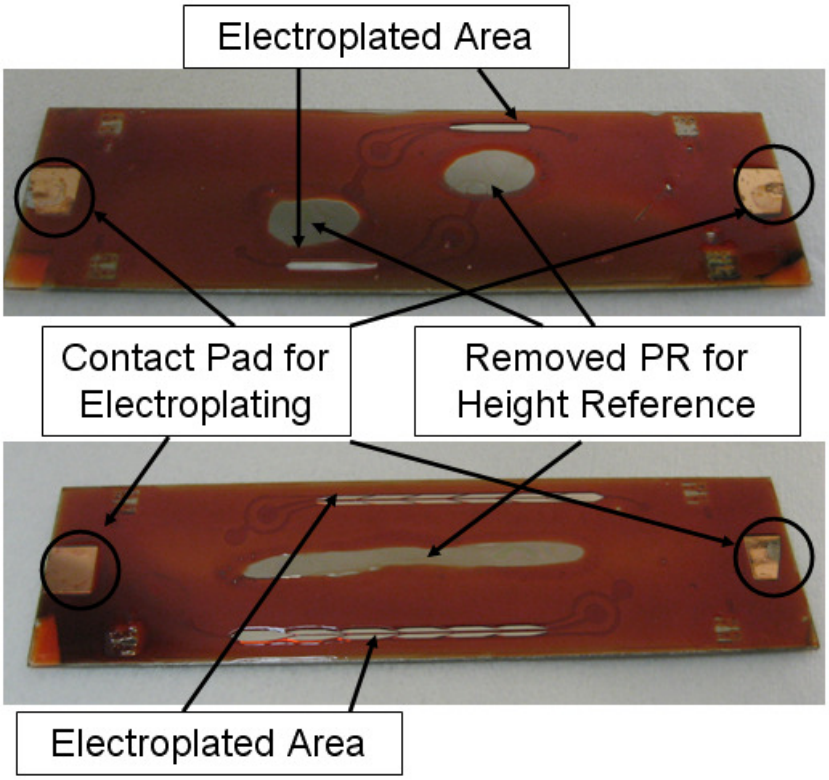

Figure 4.9. The microsystem during electroplating process.

Sputtered Ti / Cu / Cr layers were used for the electroplating seed layers and thick positive photoresist was used for the electroplating molds. The electroplating process was carried out at room temperature with a current density of 10 mA / cm^2 for 2.5 hours in the electroplating baths described in Chapter 3 (Figure 4.8 (b)). The thickness of the electroplated permalloy were measured using a P-15 Profilometer (KLA-Tencor Corp., Milpitas, CA, USA). The photoresist layer on the center part of a device was removed temporarily for a height reference (Figure 4.9). Following the electroplating process, all the thick photoresist molds and the seed metal layers were removed resulting in the 50 µm high ferromagnetic structures inside the microfluidic channels. Photomicrographs of the microseparator at this stage of the fabrication process are shown in Figure 4.10.

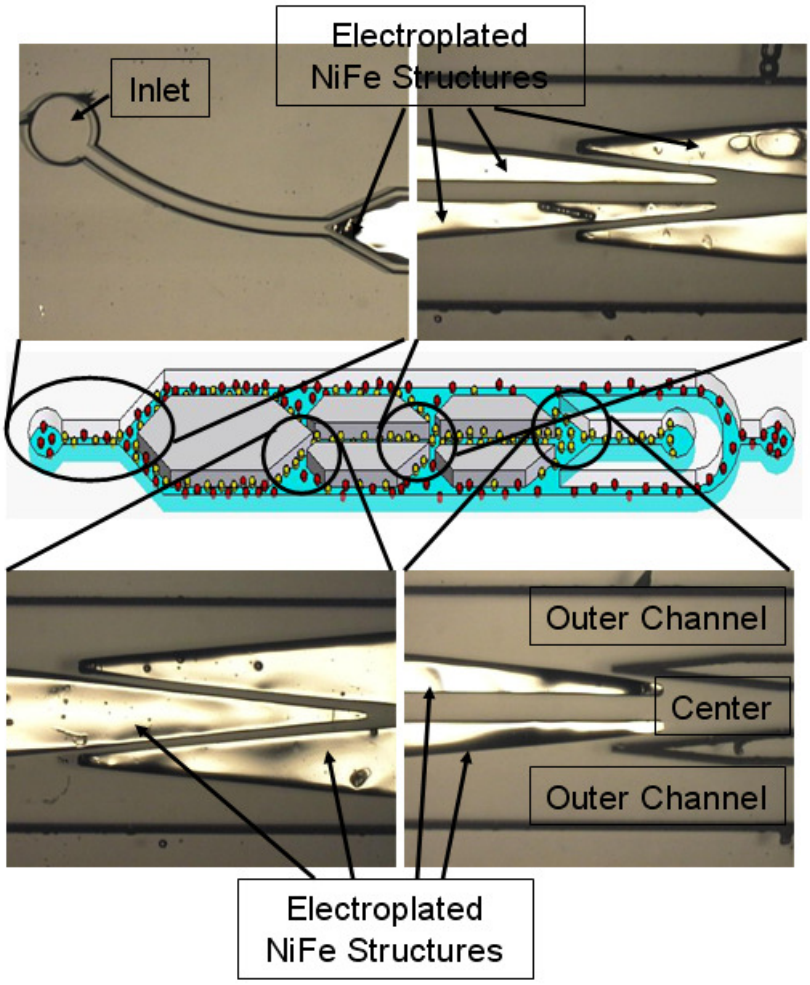

Figure 4.10. The microfluidic channel with electroplated ferromagnetic structures before bonding process.

The inlet / outlet holes were drilled by 1.0 mm / 2.0 mm diamond drill bits in the blank top glass substrate using an SLA fabricated drilling guide. The drilled top glass was aligned and bonded with the microfluidic channel defined bottom glass by introducing UV cure adhesive resin between the two glasses using capillary force and curing the adhesive under a UV lamp for 30 minutes (Figure 4.8 (c)). Finally, the microfluidic interface was bonded to the microseparator by repeating the UV adhesive bonding process (Figure 4.8 (d)).

To solve the issue of improper sealing between the top glass and the electroplated structures causing unwanted sample flow over the ferromagnetic structures during experiments, polydimethylsiloxane (PDMS) bonding was used as an alternative approach. For this bonding method, the ferromagnetic structures were over-electroplated for 3 hours to make the edge areas of ferromagnetic structures slightly protrude above the etched microfluidic channel. PDMS in the liquid stage was spin-coated on the bottom side (bonding side) of the drilled top glass at 3000 rpm for 30 seconds and pre-baked on a hot plate at 50 °C for 20 minutes. The resulting PDMS thickness was measured to be approximately 10 μm, thus adequately accommodating the height difference between the surface of the lower glass slide and the over-plated electroplated structures. The pre-baked top glass was aligned carefully with the bottom substrate and bonded on a hot plate at 50 °C for additional 2 hours. The bonding method using the PDMS layer as sealant layer alleviated the issue of sample fluid passing through the unsealed gaps between the top and the bottom substrate, but PDMS bonding process was much harder to control than the UV curable adhesive bonding process. Occlusion of the microfluidic channel while using the PDMS bonding process was a much larger problem than when using the UV curable adhesive. Figure 4.11 shows the results of the bonding process using PDMS as a bonding layer. The small bubbles on top of electroplated structures show that PDMS had successfully sealed the gap between electroplated structures and top glass slide, thus preventing fluid flow in this region. However, as shown in the pictures, often the PDMS blocked the microfluidic channels and made them useless.

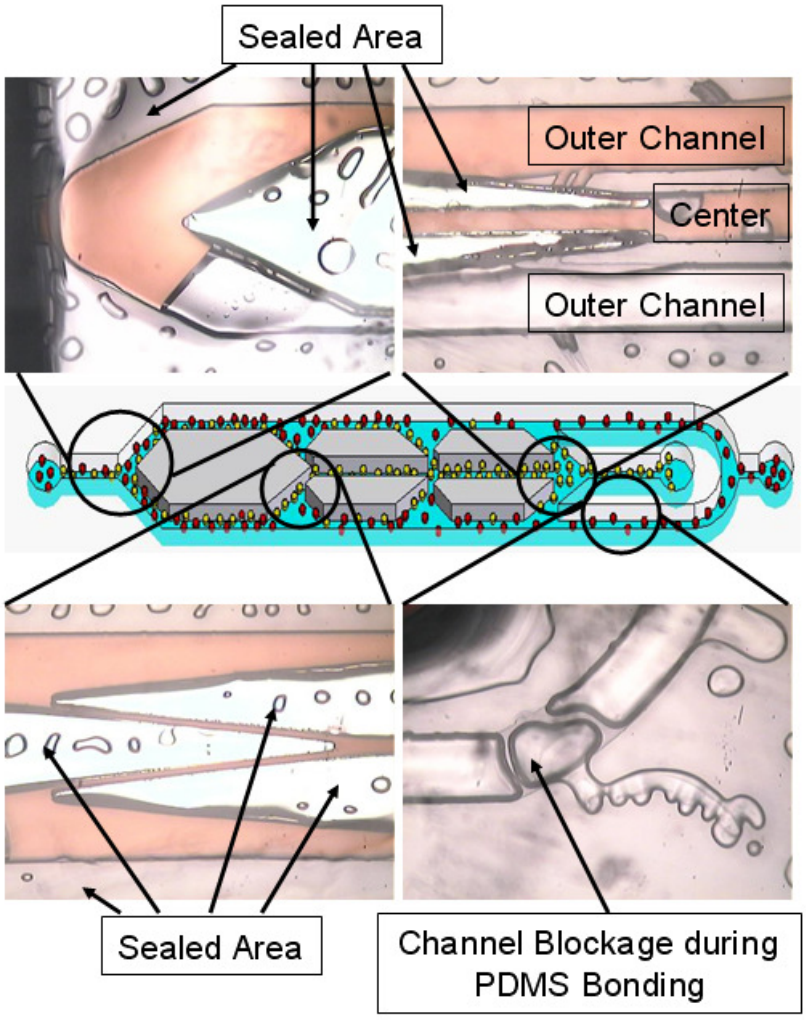

Figure 4.11. Photomicrographs of the PDMS bond between the top and bottom substrates.

Finally, a third process was developed to improve the bonding step in the fabrication process. A modified UV curable adhesive bonding process was carried out. By adding a step consisting of applying a small amount of UV curable resin on top of the electroplated structures to the previously discussed UV adhesive bonding process, the gap between the top glass substrate and the electroplated structures was eliminated.

4.4 Experimental Methods

212LN and 686LN-M4e cells were maintained in Dulbecco's modified Eagle's medium DMEM / F12 medium (1:1) supplemented with 10 % fetal bovine serum FBS at 37 °C in a humidified atmosphere with 5 % CO_2. To detach the cells from the culture container, all culture media was first aspirated. The remaining attached tumor cells were washed with PBS solution once and all PBS solution was aspirated. Cellstripper™ (Mediatech, Inc., Manassas, VA, USA) solution was added to culture container and incubated for 10 minutes in an incubator of same condition described above. After incubation, Cellstripper™ solution was removed carefully and PBS solution was added. CD29+ cells were selectively tagged using EasySep® (StemCell Technologies, Vancouver, BC, Canada) procedures. Mouse anti-CD29 IgG1 antibody (BD 555442, BD, Franklin Lakes, NJ, USA) was used to create IgG1-tetrameric-antibody complex. Cells with the CD29 surface marker were then bonded with the tetrameric-antibody complex and selectively tagged with magnetic nanoparticles. The tagged cancerous cells were prepared by flowing through the non-tagged cells in the Easy® magnet. SYTO-13 fluorescent dye was used to identify the tagged cancerous cells from other human blood cells during experiments. The tagged cancerous cell sample with SYTO-13 fluorescent dye was incubated for 2 hour before mixed with blood cells. Human venous blood was collected at the on-campus health center under an Institutional Review Board-approved protocol for blood collection for research purposes. The samples were drawn into evacuated glass tubes, containing EDTA as an anticoagulant.

The magnetophoretic microsystem was similarly treated with surfactant solution to decrease cell adhesion on the channel surfaces. After treating the glass surfaces, the substrates were subsequently washed three times with PBS solution. The setup for the experiments was similarly prepared as described in Chapter 3. The assembled microsystem and experimental setup is shown in Figure 4.12. The separation efficiency of the microseparator system was characterized by counting the tagged or non-tagged cells in each outlet with video motion capture.

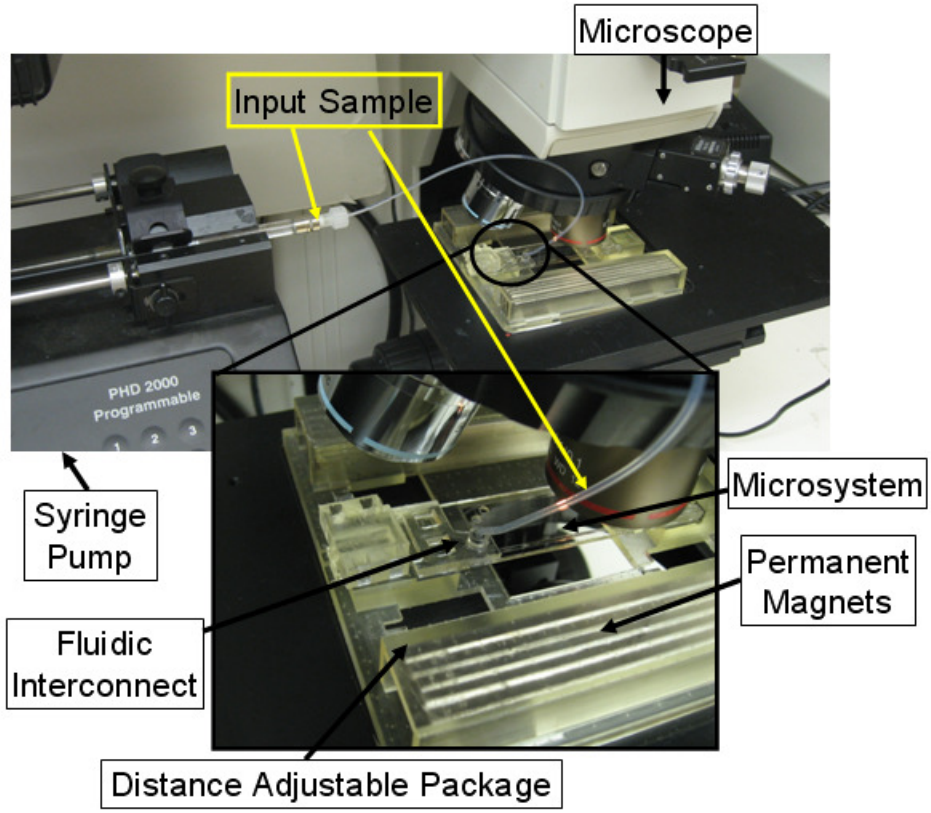

Figure 4.12. Instrument setup with microsystem in the package.

4.5 Results and Discussion

Initially three microseparators with different numbers of separation stages were fabricated. However, after simple separation experiments, a microseparator with three separation stages were chosen for further extensive experiments. Single stage and six stages design microseparator are shown in Figure 4.13.

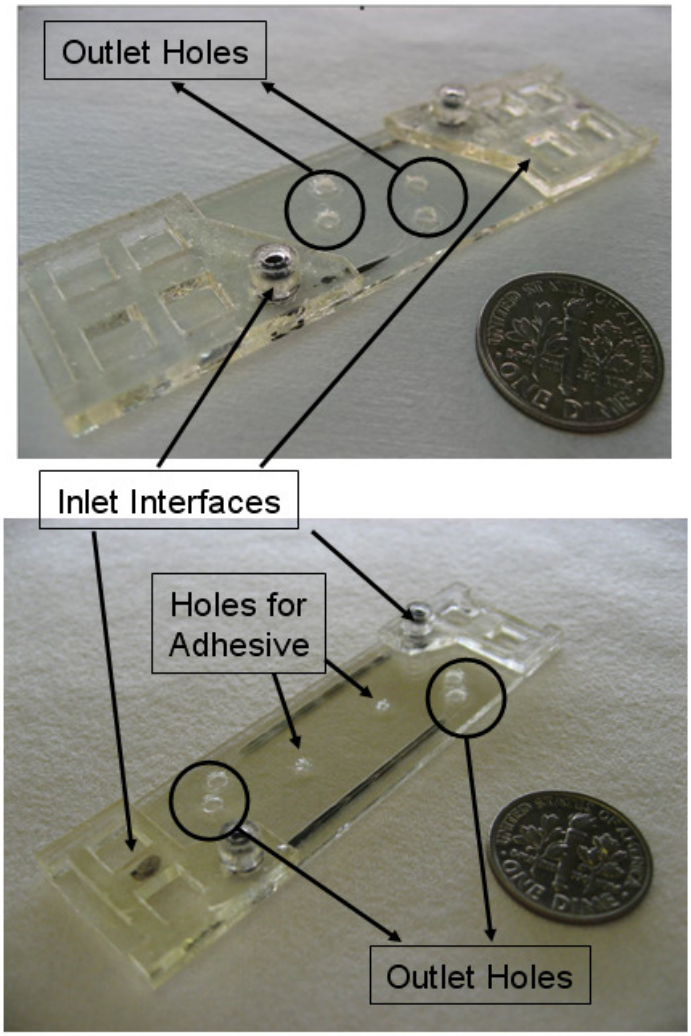

Figure 4.13. The fabricated single stage (top) and six stage (bottom) microseparator.

The fabricated three stage microseparator system is shown in Figure 4.14. The 50 µm tall ferromagnetic separation structures inside the microchannel can be seen featuring three separation stages. The UV curable resin could not be introduced successfully into the area between two microseparators using capillary force from the perimeter edges of the glass substrates. Two additional holes for UV adhesive resin introduction were drilled in top glass. Inside the microfluidic interfaces bonded to the microseparator, a rubber o-ring was inserted for more reliable interconnection. Two side channels #1 and #3 in the microchannel are merged into one side outlet and channel #2 is connected to the center outlet.

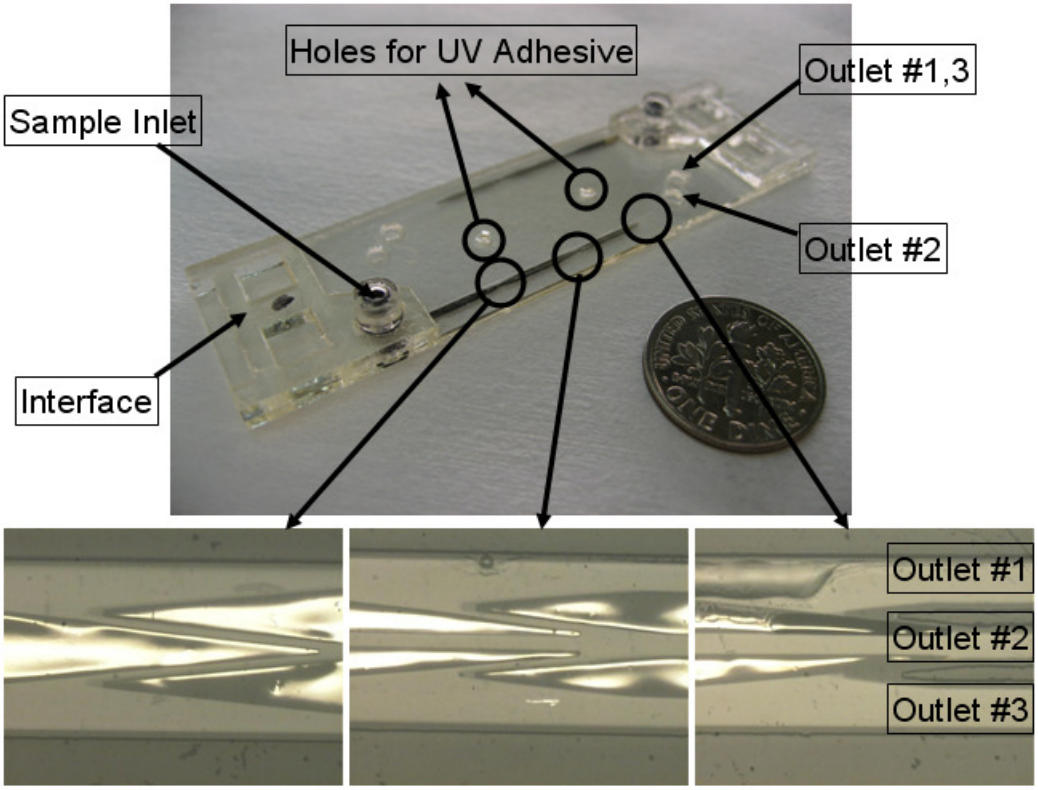

Figure 4.14. Top view of the fabricated microseparator.

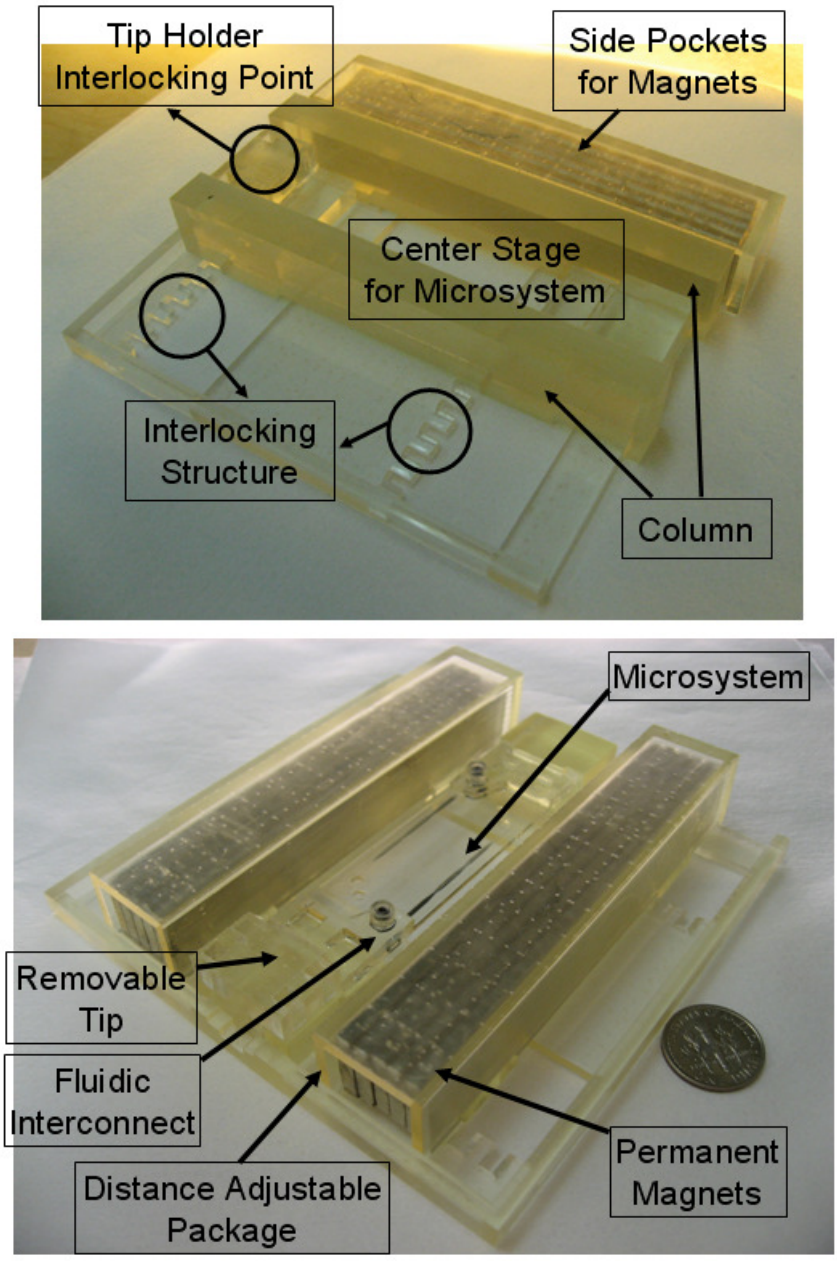

Figure 4.15. The three components of system package (top) and the assembled microseparator system (bottom).

All three components of system packaging (main platform, two side pockets for permanent magnets, and blocking column) are shown in the top figure of Figure 4.15. The bottom figure of Figure 4.16 shows the microseparator assembled onto the system packaging with permanent magnets in the distant adjustable pockets. The

removable holding tip is used for easier installation and removal of the microseparator chip between experiments. An open cavity in the system packaging under the microseparator was used to enable monitoring of the sample cells movement during separation by providing light passage from the bottom-side microscope light source. The side pockets were made to adjust the distance between the microsystem and the magnets to control the magnitude of magnetophoretic force on the tagged cells.

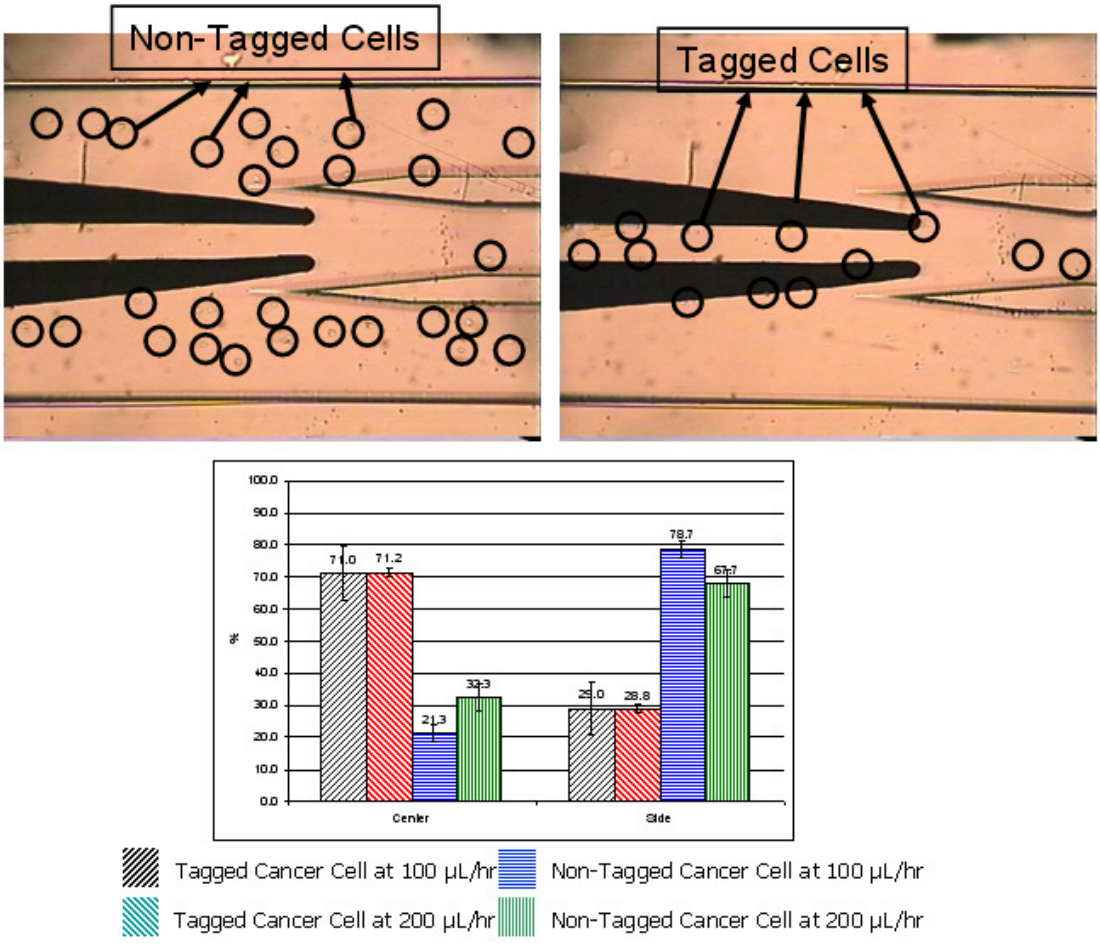

Figure 4.16. Micrograph of the microsystem with (a) non- tagged cells and (b) and tagged cells (Circled).

Figure 4.16 shows the microscope images of the tagged and non-tagged cells sample inside the microseparator under the para-magnetophoresis. As expected, the tagged cells were forced into the center channel, while non-tagged cells stayed in the side channels. At the flow rate of 100 μL/hr, 71.0 ± 8.37 % of tagged cancerous cells were attracted toward center channel, while 78.7 ± 2.53 % of non-tagged cells stayed in the side channels. When the flow rate increased to 200 μL/hr, 71.2 ± 1.38 % of tagged cells were attracted toward center channel, while 67.7 ± 4.17 % of non-tagged cells stayed in the side channels.

Separation of cancerous cells from human blood cells was carried out in the microseparator with the third stage modified as shown in Figure 4.17. The modification was made to reduce the number of non-tagged cells introduced into the center channel.

The density of blood and cancerous cells for the experiments was 2.5×10^7 cell/mL and 5×10^5 cells/mL, respectively. The cancerous cell samples were tagged with fluorescent dye to distinguish cancerous cells from the human blood cells. At the flow rate of 100 μL/hr, 20.5 ± 7.95 % of tagged cancerous cells were attracted toward center channel, while 93.7 ± 2.45 % of non-tagged cells stayed in the side channels. At 200 μL/hr, 48.9 ± 10.94 % of tagged cells were attracted toward center channel, while 97.7 ± 0.81 % of non-tagged cells stayed in the side channels. Compared to the original microfluidic channel design, a lesser number of non-tagged cells were introduced to the center channel. However the number of tagged cells captured into the center channel was also reduced.

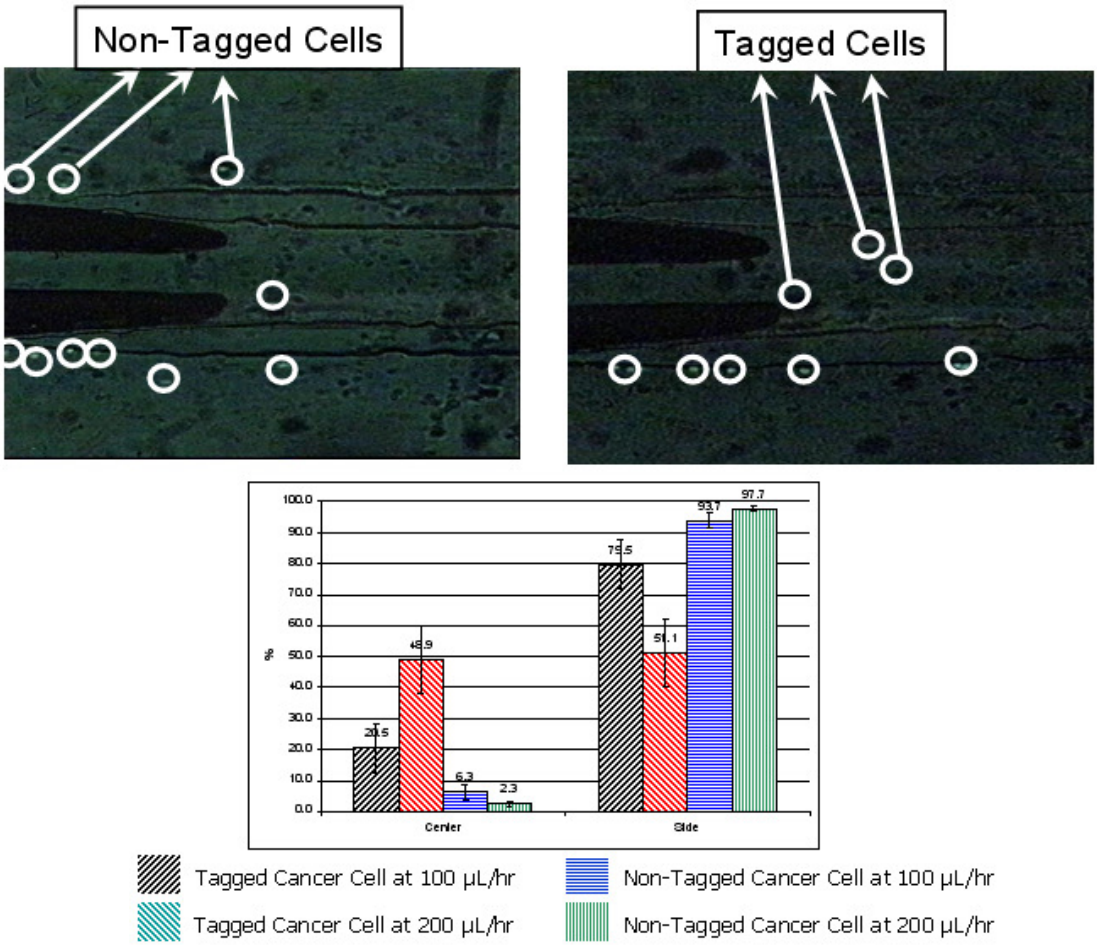

Figure 4.17. Micrograph of the microsystem with (a) non- tagged cells (Circled) and (b) and tagged cells (Circled) mixed with human blood cells.

In separating the target magnetic cells, the two major driving forces are magnetophoretic force by the external magnetic source and the drag force by the fluid flow. For the magnetophoresis microsystem to separate target particles continuously, the balance between the two forces should be considered carefully. If the magnetophoretic force becomes greater, the required capture time would be reduced, but the possibility of target particles being held inside the chamber also increases. The balance can be controlled by changing the flow rate, the distance between external magnetic source and microseparator, and the magnitude of the external

magnetic source. However, when the introducing sample consists of magnetic cells with different level of magnetic susceptibility or different number of tagged magnetic beads on the surface, the balance control for the continuous mode separation becomes extremely difficult and the separation efficiency is lowered.

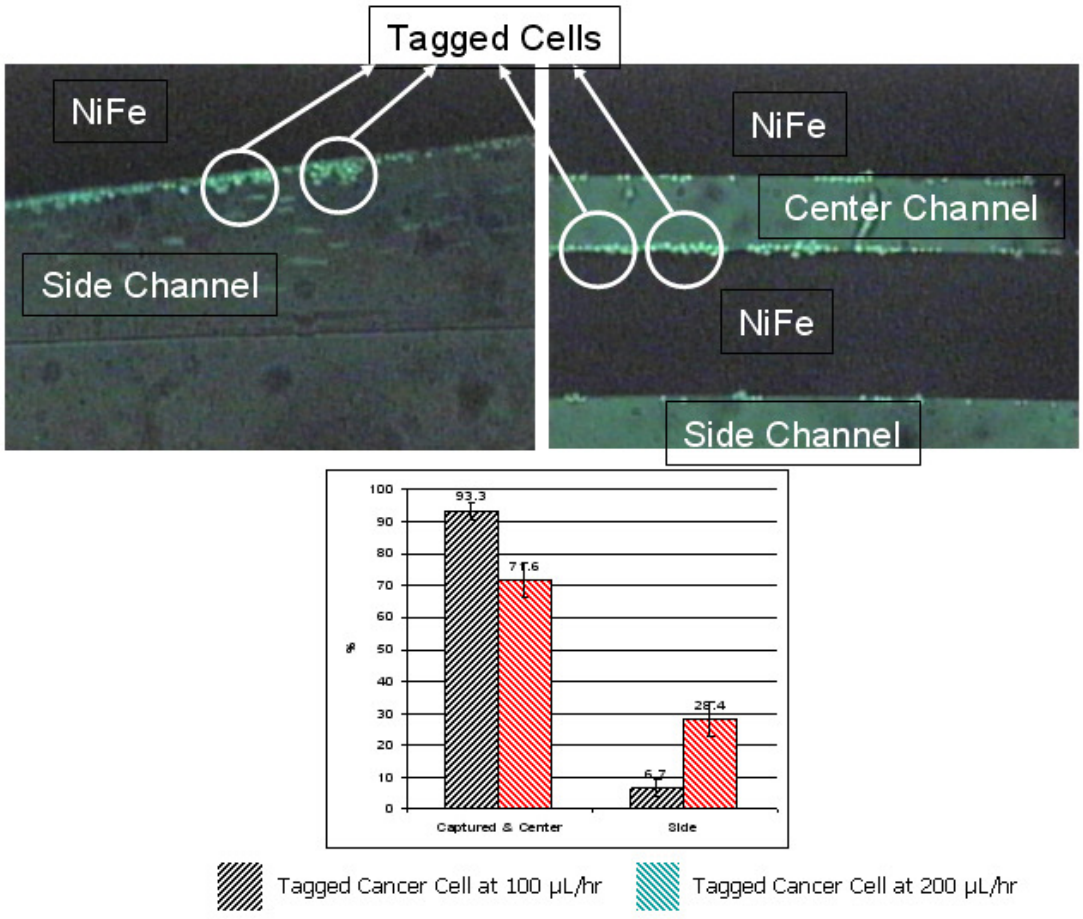

Figure 4.18. Micrograph of the microsystem with Hold-release Mode Tagged Cancer Cells separation from Human Blood Cells.

In hold and release mode operation, most of target cells with higher magnetic susceptibility are captured during the hold phase and released into capture outlet during the release phase by changing the external magnetic source, while a small

number of target cells with lower magnetic susceptibility are separated in similar fashion with continuous mode operation. For hold and release mode operation (Figure 4.18), the external magnets were positioned closest to the microseparator during the sample introduction and removed once all samples were passed through the microseparator.

The introduction of sample were conducted at the flow rate of 100 μL/hr and 200 μL/hr, 93.3 ± 2.54 % and 71.6 ± 5.27 % of tagged cancerous cells were either captured or found in the center channel, respectively.

CHAPTER 5

CONTINUOUS FLOW DIELECTROPHORESIS MICROSEPARATION SYSTEM

5.1 Introduction

The phenomenon of translational motion of a neutral body under a non-uniform field was described as early as 600 B.C. by Thales of Miletus in Turkey who observed that when amber was rubbed, it attracted small particles. Dielectrophoresis (DEP) is the translational motion of a neutral matter caused by polarization effects in a non-uniform electric field [94]. A charged body moves along the field lines in both uniform and non-uniform electric fields, but a neutral body experiences a net force only in a non-uniform electric field. A neutral body stays neutral in an electric field, but in a non-uniform electric field the forces on each polarized region are unequal, which gives rise to a net force on the neutral particle (Figure 5.1). By using dielectrophoresis, one can remove small particles from suspending media; in particular the application of dielectrophoresis for cell manipulation has attracted enormous interest from both scientists and engineers.

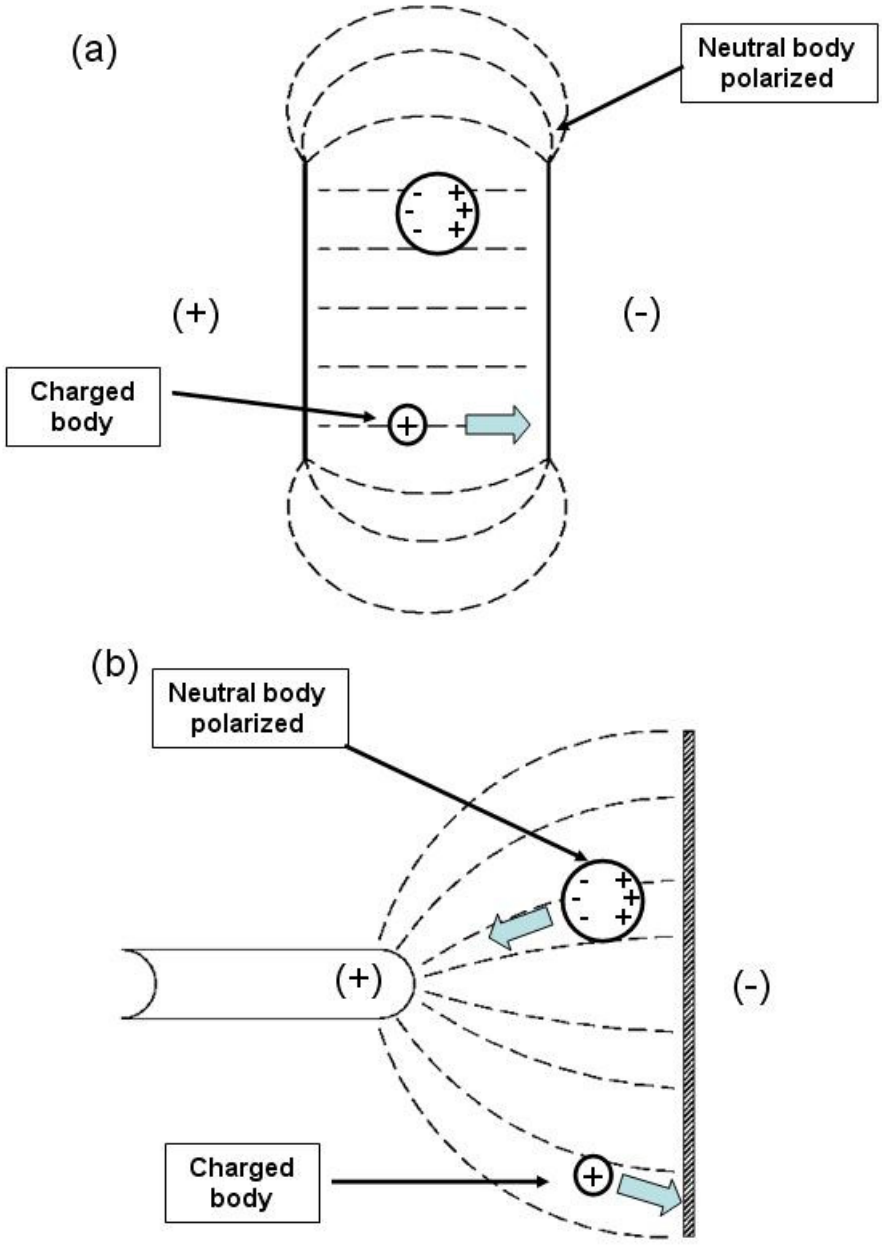

Figure 5.1. Movement of neutral and charged bodies in a uniform electric field (a) and a non-uniform electric field (b).

5.2 Theory

A neutral particle suspended in a fluid experiencing a dielectrophoretic force can be described as a small dipole under non-uniform electric field. When a small neutral particle with volume v is placed in a static external electric field $\vec{E}_e$ at equilibrium, the net force $\vec{F}$ due to an applied field is given by:

$$\vec{F} = (\vec{\mu} \bullet \nabla)\vec{E}_e \qquad (5.1)$$

where $\vec{\mu}$ is the dipole moment vector of the particle.

When a particle is isotropically, linearly, and homogeneously polarizable, the dipole moment $\vec{\mu}$ can be expressed as $\vec{\mu} = \alpha v\vec{E}_e$, where α is the tensor polarizability or dipole moment per unit volume in unit field, then Equation 5.1 becomes

$$\vec{F} = \alpha v(\vec{E}_e \bullet \nabla)\vec{E}_e \qquad (5.2)$$

Since the electric field is an non-rotational or a conservative field, by using the vector transformation $(\vec{A} \bullet \nabla)\vec{B} = \nabla(\vec{A} \bullet \vec{B}) - (\vec{B} \bullet \nabla)\vec{A} - \vec{A} \times (\nabla \times \vec{B}) - \vec{B} \times (\nabla \times \vec{A})$, Equation 5.2 can be expressed more simply as

$$\vec{F} = \alpha v(\vec{E}_e \bullet \nabla)\vec{E}_e = (\alpha \nabla \left|\vec{E}_e\right|^2 - \alpha(\vec{E}_e \bullet \nabla)\vec{E}_e)v = \frac{1}{2}\alpha v \nabla \left|\vec{E}_e\right|^2 \quad (5.3)$$

for $(\vec{E}_e \bullet \nabla)\vec{E}_e = \nabla \left|\vec{E}_e\right|^2 - (\vec{E}_e \bullet \nabla)\vec{E}_e$ from the vector transformation [94].

The effective dipole moment $\vec{\mu}_e$ of a spherical particle embedded in a dielectric medium is $\vec{\mu}_e = v\vec{P}_e = \left(\frac{4}{3}\right)\pi a^3 \vec{P}_e$, where a is radius of particle and the excess polarization $\vec{P}_e$ can be expressed as $\vec{P}_e = (K_2 - K_1)\varepsilon_O \vec{E}_i$, where ε_O is permittivity of free space, $\vec{E}_i$ is internal electric field in the sphere in the direction of the external

field, and K_1, K_2 are the relative dielectric constant of the medium and particle, respectively.

If the dielectric sphere is placed at the origin and subjected to a uniform z-directed electric field of magnitude E_O, the potential satisfies Laplace's equation and takes the form as $\Phi_1(r,\theta) = -E_O r\cos\theta + \frac{A\cos\theta}{r^2}$, where $r > a$ and $\Phi_2(r,\theta) = -Br\cos\theta$, where $r < a$.

The boundary conditions at $r = a$ are $\Phi_1(r=a,\theta) = \Phi_2(r=a,\theta)$ and $K_1\varepsilon_O E_{r1}(r=a,\theta) = K_2\varepsilon_O E_{r2}(r=a,\theta)$, where $E_{r1} = -\frac{\partial\Phi_1}{\partial r}$ and $E_{r2} = -\frac{\partial\Phi_2}{\partial r}$.

With the given boundary conditions, $\vec{E}_i$ can be solved for and is given as: $\vec{E}_i = \frac{3K_1}{K_2 + 2K_1}\vec{E}_e$.

Accordingly, the effective dipole moment $\vec{\mu}_e$ is

$$\vec{\mu}_e = v\vec{P}_e = \left(\frac{4}{3}\right)\pi a^3\vec{P}_e = 4\pi a^3\left(\frac{K_2 - K_1}{K_2 + 2K_1}\right)K_1\varepsilon_O\vec{E}_e \text{ (5.4 [95])}$$

and combining Equation 5.2, 5,3 and 5.4 gives the effective translational force $\vec{F}_e$ as

$$\vec{F}_e = 2\pi a^3\left(\frac{\varepsilon_2 - \varepsilon_1}{\varepsilon_2 + 2\varepsilon_1}\right)\varepsilon_1\nabla\left|\vec{E}_e\right|^2, \text{ where } \varepsilon_1 = K_1\varepsilon_O, \varepsilon_2 = K_2\varepsilon_O \text{ (5.5)}$$

Equation 5.5 is based on the assumption of ideal or perfect dielectrics having zero conductivity. However, in the case of real dielectrophoresis, especially for cell manipulation, both the medium and the neutral particle are conductive and polarizable. Thus, the simple permittivity ε is replaced by the complex

permittivity $\varepsilon^*(\omega) = \varepsilon - j\frac{\sigma}{\omega}$, where σ is electrical conductivity and ω is the angular frequency of the external field. Under a time dependent external electric field, the time-averaged dielectrophoretic force is:

$$< \vec{F} >_e = 2\pi a^3 \varepsilon_1 \,\mathrm{Re}\{f_{CM}(\omega)\} \nabla E_{rms}^2, \; f_{CM}(\omega) = \frac{\varepsilon_2^*(\omega) - \varepsilon_1^*(\omega)}{\varepsilon_2^*(\omega) + 2\varepsilon_1^*(\omega)} \quad (5.6)$$

f_{CM} is the Clausius-Mossotti factor and E_{rms} is the root mean square value of the external electric field [96].

From Equation 5.6, the response of cells or particles suspended in a liquid medium in a non-uniform electric field because of an the applied AC source is strongly dependent on the frequency of the applied field and the conductivity of the fluid medium. Depending on their complex dielectric constant, some cells experience attractive forces in the electric field gradient and others experience repulsive forces (under the same frequency of the applied field and the conductivity of suspending medium condition). Most cells experience a positive DEP force in the high frequency range and a negative DEP force in the low frequency region. At the crossover frequency, or transition frequency, no DEP forces are exercised on the cells. The frequency response of each type of cell is dependent on various cell characteristics, such as the membrane characteristic, the internal structure, and the cell size variation.

The major advantage of DEP compared to other separation schemes is that the variability in the frequency response of cells is selective enough for DEP microsystems to differentiate between similar cell types. Also, DEP is more advantageous in that it does not require any labeling of cells. Microfluidic systems using DEP have been shown to manipulate biological cells successfully using

intrinsic dielectric affinity differentiation and have demonstrated highly selective isolation of target rare cells from the mixture of various blood cells without any tagging.

5.3 Capture and Release Mode DEP Microsystem for Cell Separation

In early microfluidic separation systems using dielectrophoresis, separation of cells was carried out in discontinuous mode, or capture and release mode [96~99].

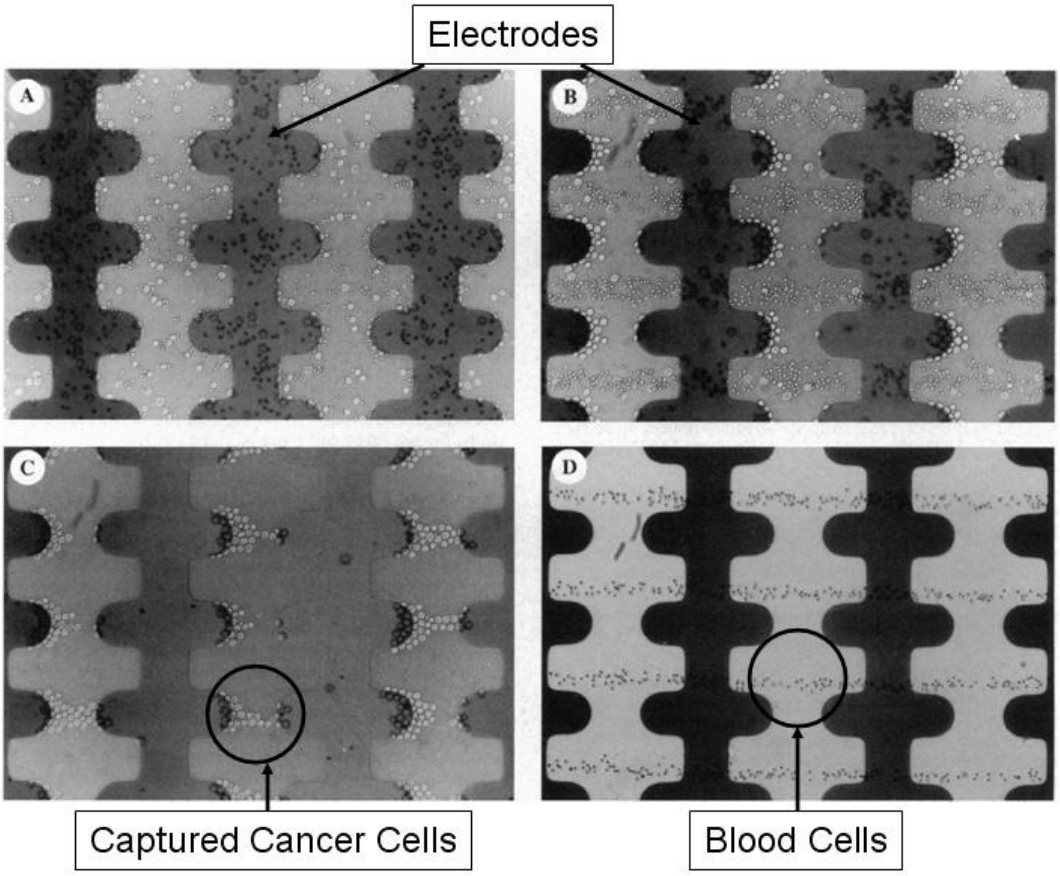

Figure 5.2. Separation of MDA231 human metastatic breast cancer cells (larger cells) from dilute peripheral blood. (A) During initial sample introduction (B) During blood cell release (C) Cancer cells captured on the electrode tips while blood cells had been swept downstream. (D) electrode close to outlet where only blood cells flowing through. ***(Images from [98]).***

First cell mixtures with different dielectric properties are introduced into a chamber with closely positioned but separated electrodes. An AC electrical signal creating non-uniform electric field between electrodes is applied at a frequency at which only target cells experience strong attractive DEP force so that non target cells are swept downstream with elute flow while target cells are captured at the tip of the electrodes. Once non target cells are swept into the outlets, the target cells are released with the elute flow by turning off the electrical field.

Becker et al successfully separated MDA231 breast cancer cells from T lymphocytes and erythrocytes in an isotonic solution consisting of 8.5 % sucrose plus 0.3 % dextrose buffer, with a DEP microfluidic system (Figure 5.2).

In the late 1960s, J. S. Crane and H. A. Pohl showed that live and dead yeast cells show different dielectrophoretic reactions [99] and Markx et al have demonstrated separation of viable and non-viable yeast cells successfully with a microfluidic system [100]. Tai et al presented an automatic DEP separation systems consisting of several microfluidic valves and pumps (Figure 5.3)

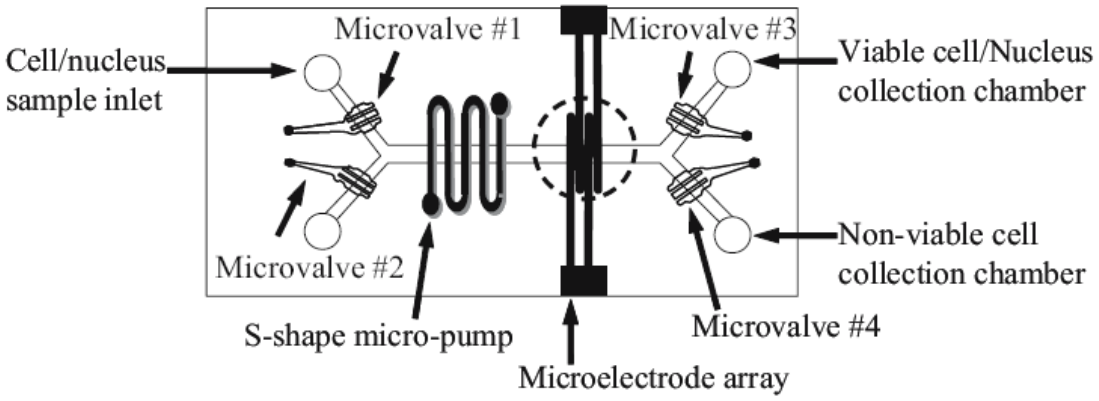

Figure 5.3. Schematic illustration of an automatic cell/nucleus separation and collection chip with a microchannel, an S-shape micropump, four microvalves and a DEP microelectrode array. ***(Image from [101]).***

5.4 Continuous Mode DEP Microsystem for Cell Separation

Early DEP microsystems required several discontinuous steps of retaining, washing and, then releasing particles of interest. Unfortunately, the automation of these steps complicated the overall microfluidic system design. Also, the use of discontinuous separation systems is limited in high throughput applications because of their discontinuous nature. Continuous mode DEP separation can increase the throughput. Continuous mode DEP systems should have several outlets and the electrodes are positioned to guide different types of cells into different outlets.

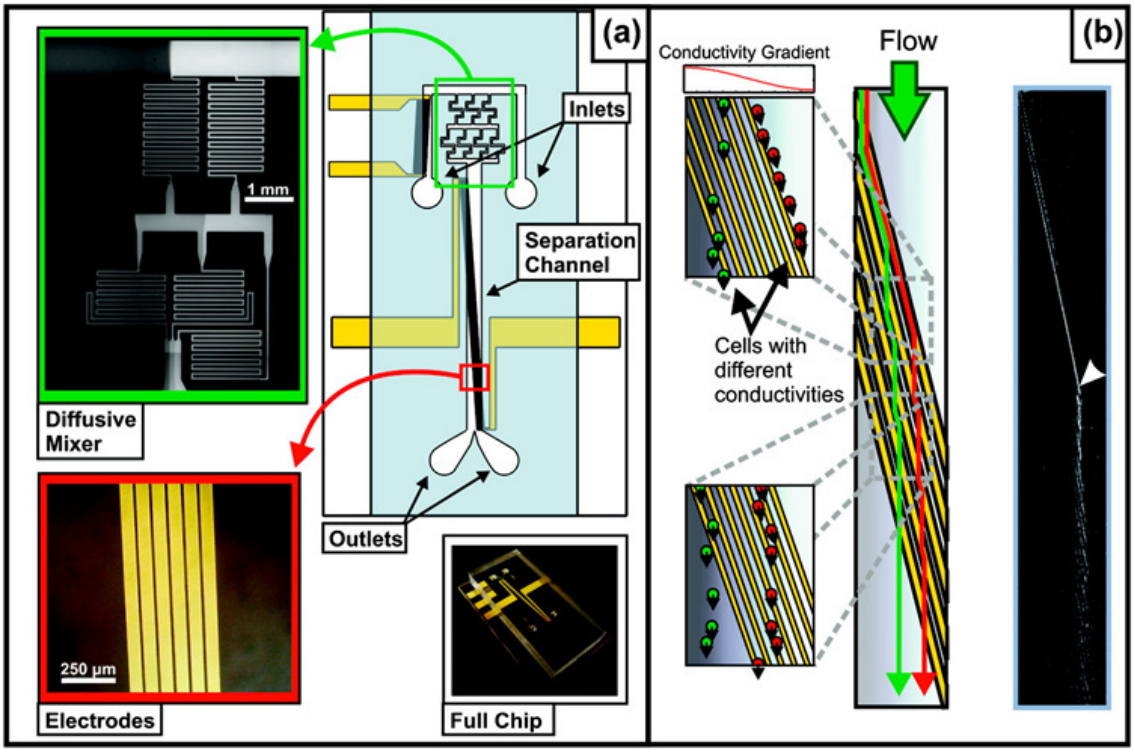

Figure 5.4. Device concept and architecture of continuous separation system using isodielectric methods. ***(Image from [102]).***

Recently, several continuous mode DEP microseparators were developed. M. D. Vahey and J. Voldman have demonstrated continuous separation of nonviable yeast cells from viable ones based on equilibrium methods [102]. The method used

in their device was isodielectric separation which is analogous to isoelectric focusing. Isoelectric focusing is a method in separating particles based on their electric charge differences. For example, a protein placed in a medium where the pH of its surrounding is below its isoelectric point will be positively charged and move toward the cathode. If there is a pH gradient in the medium, the protein will pass through a gradient of increasing pH and stop at the position where its isoelectric point matches the pH of its surrounding. Instead of using a pH gradient with electrophoresis, they separated cells in an electrical conductivity gradient using dielectrophoresis.

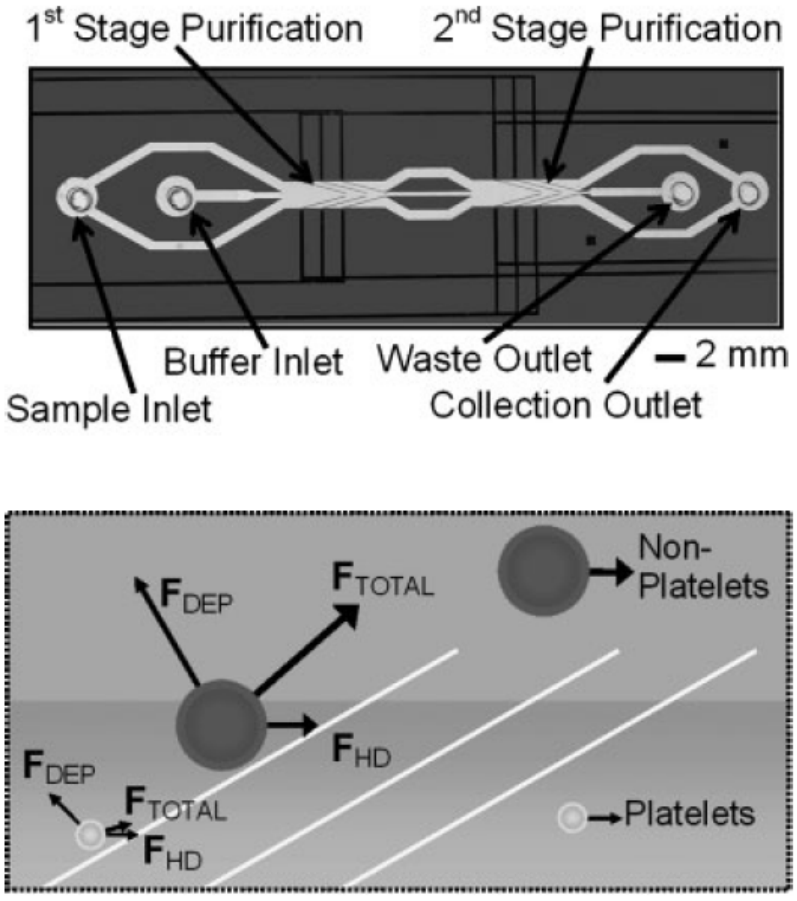

Figure 5.5. Device architecture of two stage DEP cell sorter using the difference in the magnitude of negative DEP forces. ***(Image from [103]).***

Pommer et al reported separation of platelets from diluted whole blood [103]. Unlike other DEP separation system using positive DEP force as the guiding force, they utilized the differences in the magnitude of negative DEP forces.

Li et al employed electrode array structures biased by an on-chip resistive ladder network to control individual electrode voltages in creating non-uniform 'isomotive' fields. By using non-uniform isomotive DEP fields, positive and negative DEP particles were pushed into different region and separated [104].

However, the capability of continuous separation in most of microsystems has only been demonstrated for samples that are much less dense than human whole blood.

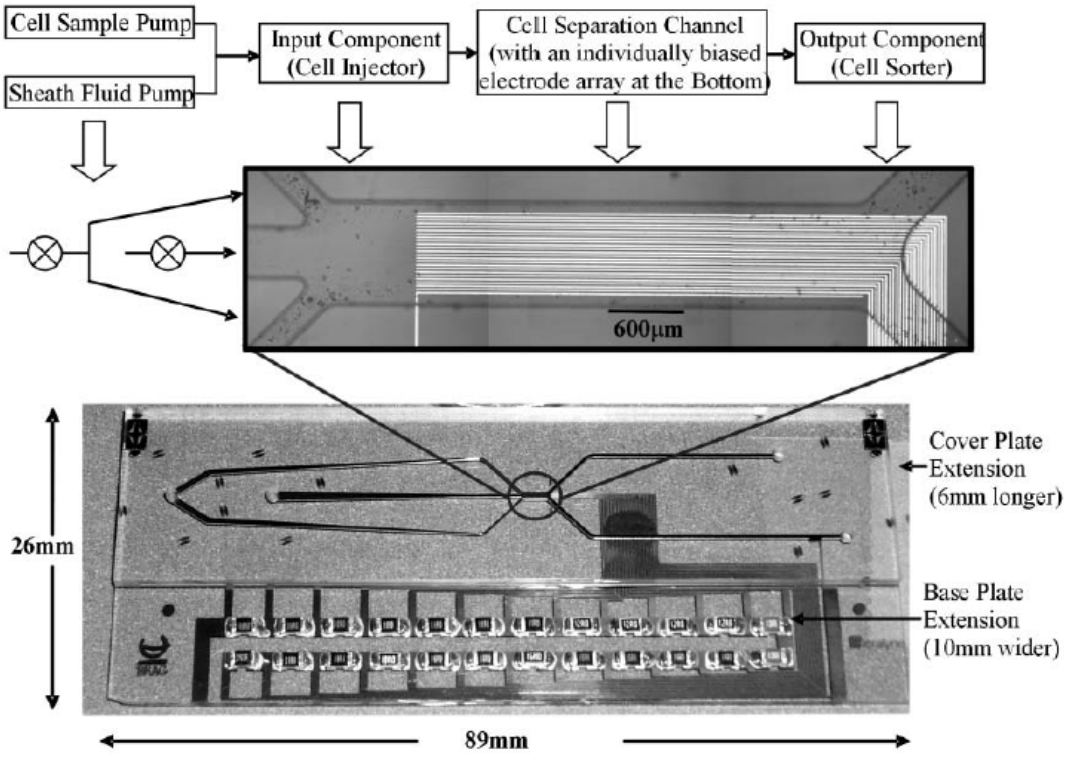

Figure 5.6. DEP microfluidic separator using non-uniform 'isomotive' forces created by electrode array structures biased by an on-chip resistive ladder network. ***(Image from [104]).***

5.5 Applications of Microscale Dielectrophoresis System

Two dielectrophoretic microsystems were developed and characterized in this work. The first dielectrophoretic microsystem was developed to determine the crossover frequency of different cell types. The second dielectrophoretic microseparator with two inlets for sample stream and sheath flow and two outlets for target cells and non-target cells was developed for high throughput continuous blood cell manipulation. The development and characterization of both dielectrophoretic microsystems is presented in detail in Chapter 6 and 7.

CHAPTER 6

DIELECTROPHORESIS SYSTEM APPLICATION I

(Blood Cell Separation)

6.1 Introduction

The response of biological cells or particles suspended in liquid media exposed to a non-uniform electric field is strongly dependent on the frequency of the applied field and the conductivity of the fluid medium. Also, the frequency response of each type of cell is dependent on various cell characteristics, such as the membrane characteristic, internal structure, and cell size variation. The resulting variability in the frequency response of different cells is selective enough for DEP microsystems to differentiate between similar cell types. Becker et al [98] have shown that in the isotonic solution of 8.5 % sucrose plus 0.3 % dextrose buffer, the crossover frequencies for MDA231 breast cancer cells, T lymphocytes, and erythrocytes are 15, 58, and 95 kHz, respectively. I. Doh and Y. H. Cho have shown the different DEP response of viable and non-viable yeast cells in terms of the medium conductivity and applied electric field frequency [105]. Also, DEP is more advantageous in that it does not require any labeling of cells in separating different type of cells.

In Chapter 3 and Chapter 4, blood and cancer cell separators using magnetophoresis were presented. Even though the presented magnetophoretic separation systems have shown high separation efficiency with considerably high volumetric flow rate for RBCs, separation of cancerous tumor cells from non-magnetic cells in human blood requires additional downstream separation apparatus.

With its highly selective and non-invasive nature, a DEP system was chosen as the downstream separation system for further sub-classification of different cell types.

In the following sections, the design and fabrication of a continuous flow dielectrophoretic microsystem capable of switching the input cell stream and separation of different cell types in a suspending medium are presented. With the switching capability, the microsystem can be used to extract cell free media from whole blood samples. Quantitative measurements of switching efficiencies of blood cells using a continuous flow DEP system are reported. Experimental results of DEP switching using human whole blood are discussed along with the separation of different cell types in human whole blood.

The significance of this research is the development of a microsystem for high-throughput continuous separation/manipulation of blood cells achieved with comb-type electrodes angled away from the laminar flow direction. In order to manipulate biological cells more efficiently, the DEP system utilizes induced hopping movement of blood cells between neighboring electrodes depending on their dielectric properties.

6.2 Microsystem Design

A conceptual view of the implemented continuous flow dielectrophoretic microsystem is shown in Figure 6.1 (a). Overall, the microsystem consists of two inlets, two outlets, and one separation chamber having comb-shaped electrodes. The sample is introduced into the device through the center inlet. The fluid is focused by two sided sheath flow (buffer #1, #2) and travels in a laminar flow. The DEP forces

are created by the downstream comb-type angled electrodes and the various types of cells in the fluid will move differently according to their native dielectrophoretic characteristics. The electrodes are centered on the input sample channel and the outlet #1 channel with decreasing comb tooth length from the input to the output of the microseparator along the length of the DEP chamber. This guides the target cells into the desired outlet.

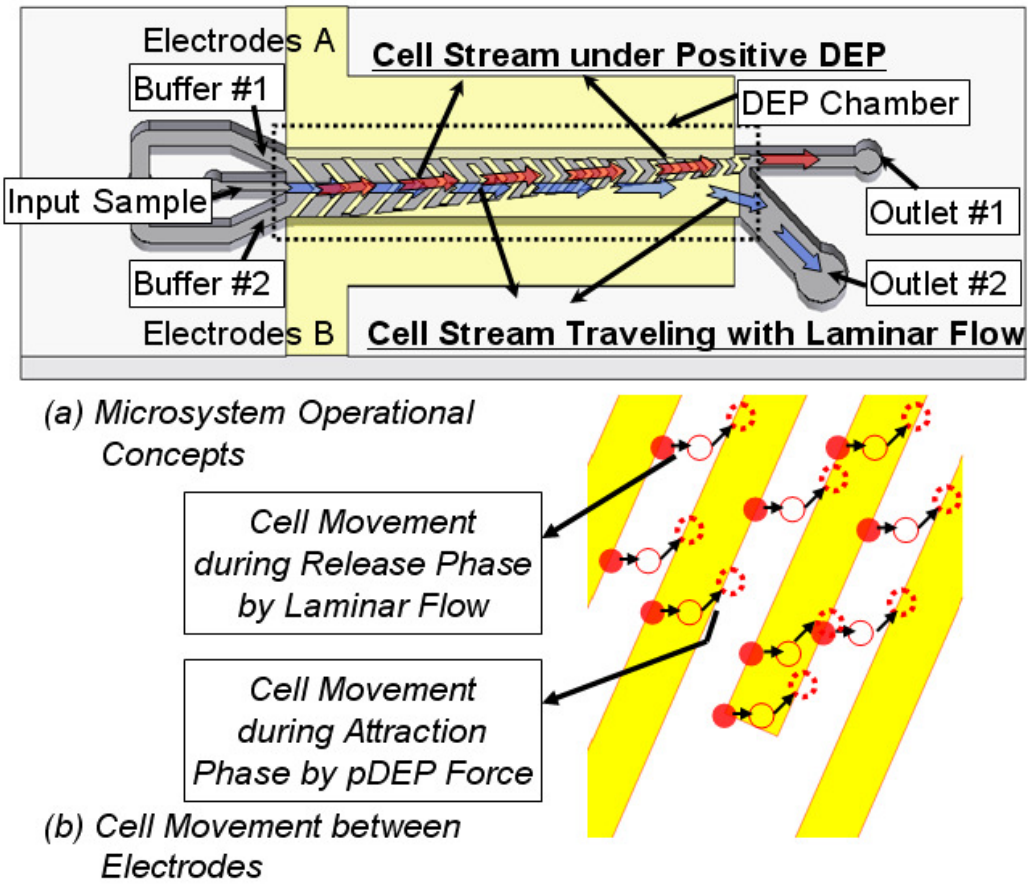

Figure 6.1. The operation principle of the hopping mode continuous DEP microsystem.

The cell streams during continuous flow operation of the dielectrophoretic microsystem are depicted with the red and blue arrows in Figure 6.1 (a). Without any

force acting on the cells, all cells in the microfluidic channel introduced through the sample inlet, travel with laminar flow and are collected into outlet #2 (blue-line). Under a high gradient electric field created by the alternating electrodes, the cells that experience positive DEP force are attracted toward the electrode edges; thus the cell stream is deflected toward outlet #1 (red-line), while the cells experiencing negative DEP force are levitated above the surface and swept with laminar flow to outlet #2 (blue-line).

To separate out the cells more efficiently using positive DEP force, the DEP system utilizes the induced hopping movement of the blood cells between neighboring electrodes by adjusting the release phase and attraction phase properly. Individual cell movement during one hopping period is described in Figure 6.1 (b).

The DEP microsystem for blood cell separation requires two photolithography steps. Two mask designs for the microfluidic channels and comb-shaped electrodes are shown in Figure 6.2. In the design of the microfluidic channel, there were additional ditches surrounding the inlet and the outlet microfluidic channel and separation chamber to protect them during the bonding process. The mask designs were initially drawn and saved in DXF format by Autodesk® AutoCAD and sent to an outside vendor for plotting services on transparent film. Later, mask patterns were transferred from the transparent film to a 4" × 4" chromium-layered glass mask using a photolithography process.

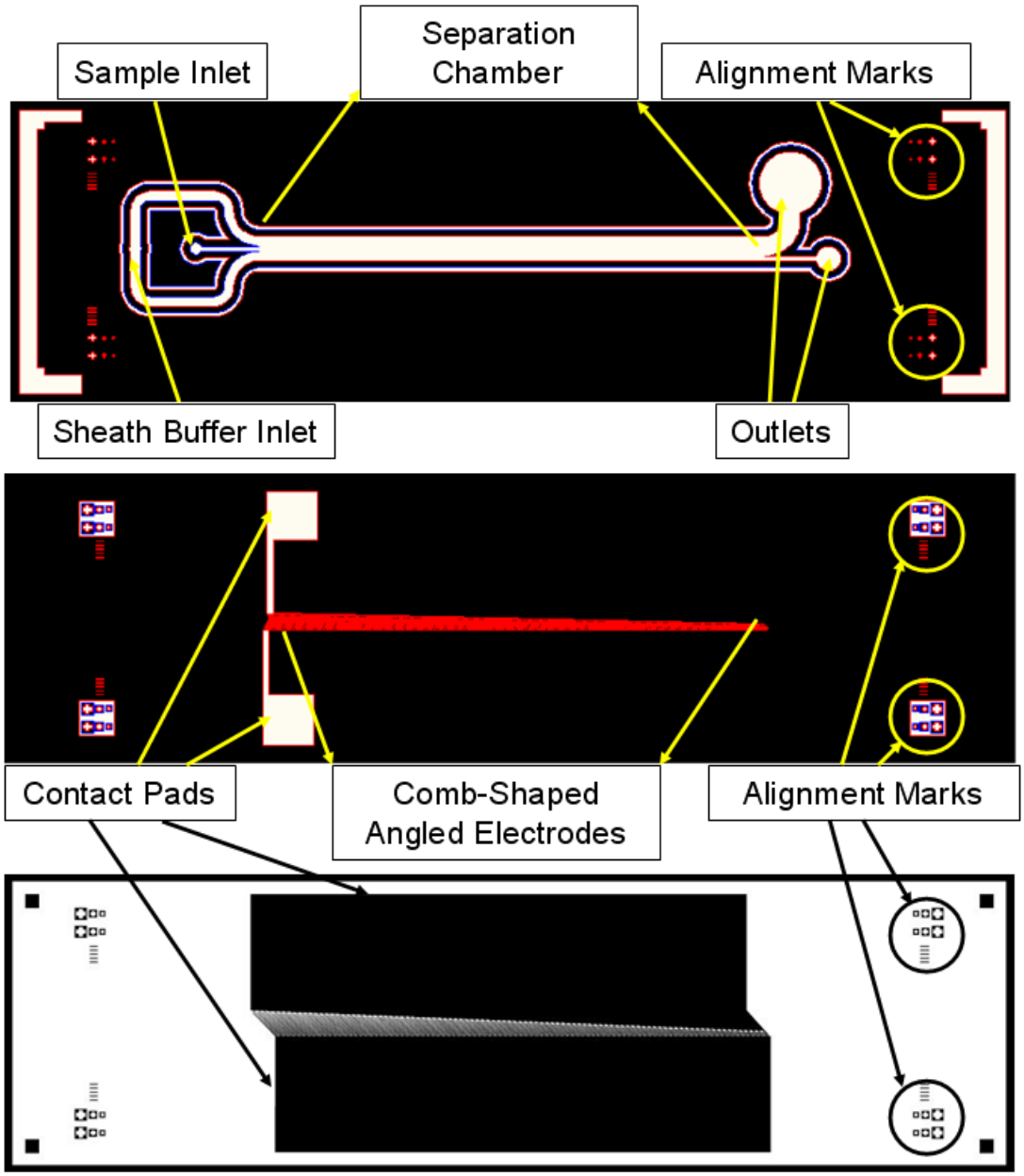

Figure 6.2. Mask design for microfluidic channels (top), original comb-shaped electrodes (center), and modified comb-shaped electrodes (bottom).

The microfluidic interface for the DEP microsystem was designed similarly to those of the magnetophoretic cell separators. The major difference is that it has two inlet ports for sheath buffer flow and sample input. Each port has two O-rings inserted to firmly hold a tubing and a "[" shaped edge to give spaces for the system package tip holder that holds the microfluidic system while conducting experiments. Since the overall size of the interface is larger than previously developed interfaces, there are two additional deep "[" shaped edge for the introduction of UV curable adhesive (Figure 6.3).

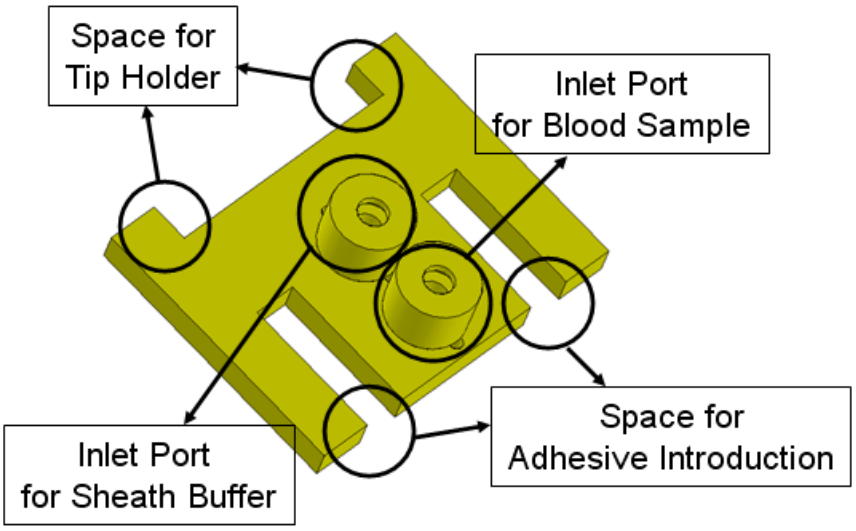

Figure 6.3. Microfluidic interface design.

The dielectrophoresis system packaging is composed of one center stage to place and hold the assembled microsystem and ten accessing holes for electrical wire. The system packaging design is shown in Figure 6.4.

Similar to the other system packages described in Chapter 4 and Chapter 5, it has open cavities under the microchannel to enable monitoring of the blood cell

movement during experiments by providing light passage from the bottom-side microscope light source. The overall size of the system packaging is 103 mm × 35.0 mm × 9.5 mm (length × width × height). The width of center stage for microsystem was chosen to be 21.0 mm.

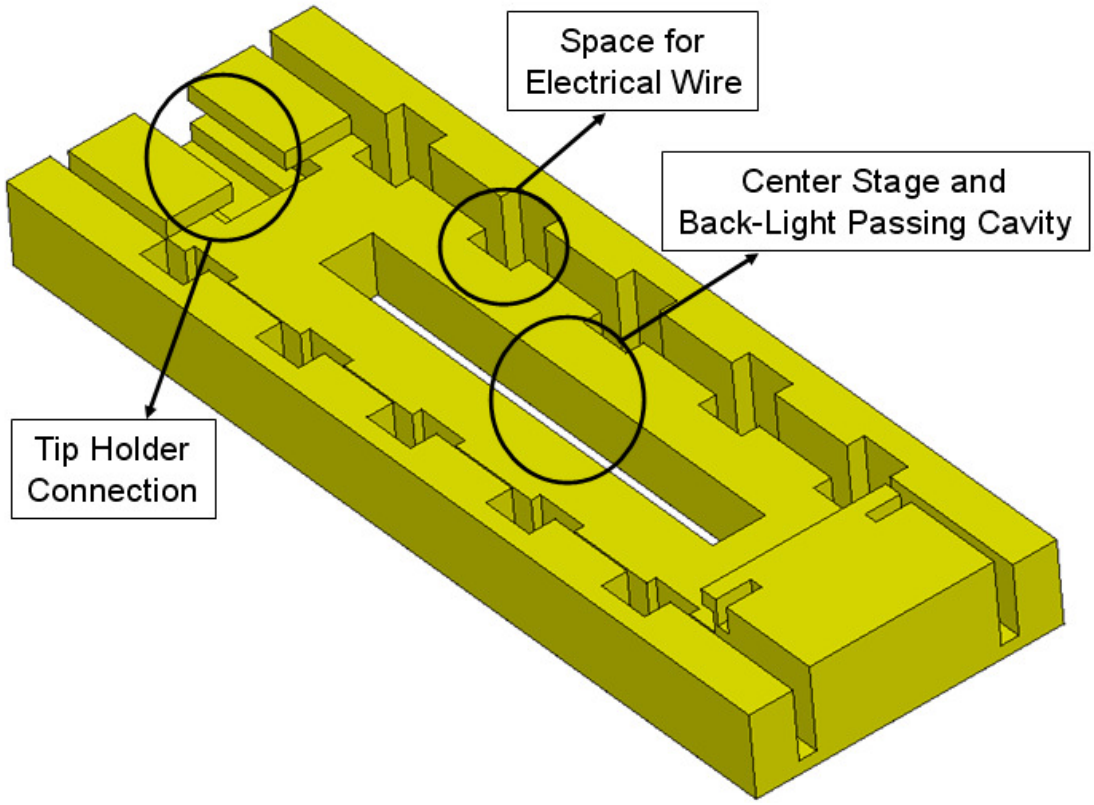

Figure 6.4. Microfluidic interface and system packaging design.

The drilling guide design for correct positioning of the inlet and outlet ports in the top glass substrate is shown in Figure 6.5. For the drawing of the microfluidic interface and system packaging, Solid Edge® program was used and the design was saved as a STL file.

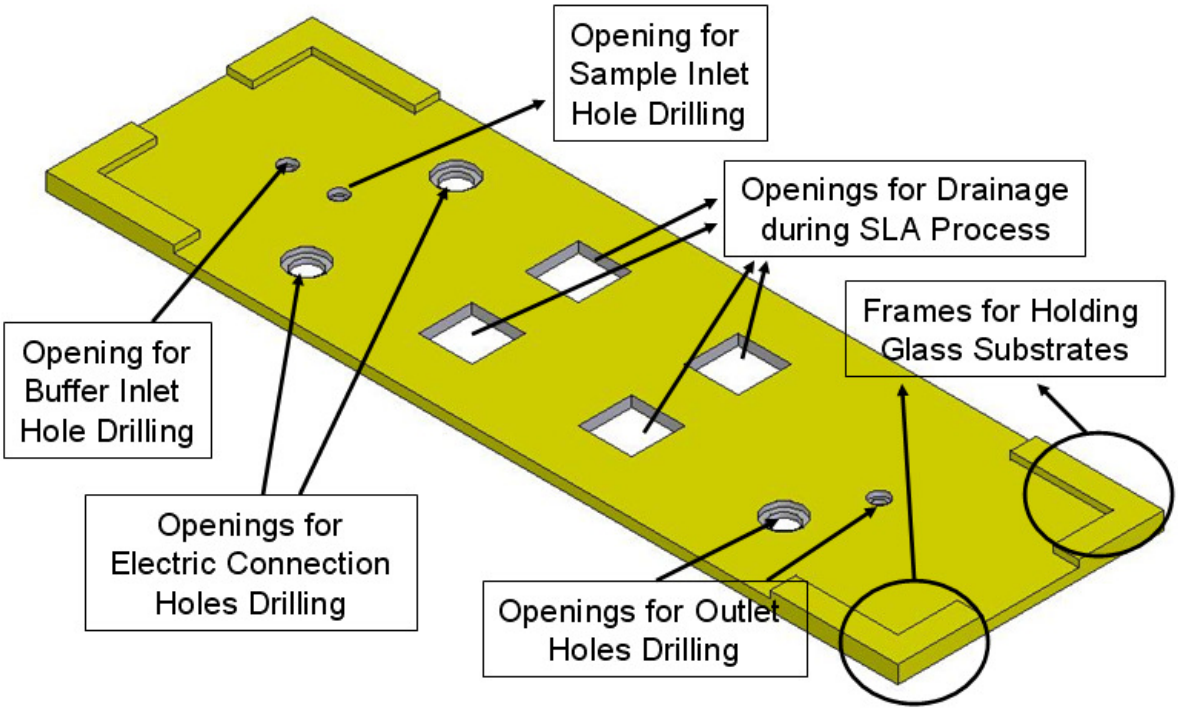

Figure 6.5. The drilling guide for the inlet and outlet holes.

6.3 Microsystem Fabrication and Packaging

The continuous flow DEP microsystem consists of a glass microchannel, angled comb-shape planar electrodes, microfluidic interface, and system packaging. The overall fabrication process for the microchannel is similar to those of magnetophoretic microsystems.

Cr / Au layers were used as protective coatings during the hydrofluoric acid wet etching process as previously described in Chapter 3. The 50 μm deep microfluidic channels were realized by hydrofluoric wet etching of glass for 30 minutes (Figure 6.6 (a)). After wet etching, the residual photoresist and metal masking layers were removed using acetone, Cr / Au etchant, and piranha cleaning. The 500 Å / 2500 Å thick Cr / Au layers for electrodes were sputtered with the DC sputterer on the front-

side surface of the etched glass substrate. Thick negative photoresist was spin-coated on the etched side of the glass substrate and soft baked in a vacuum oven at 120 ºC for 30 minutes. The downstream comb-type angled electrodes were defined through UV light exposure using the Karl Suss MA-6 Mask Aligner, and the photoresist was developed in photoresist developer. Exposed Cr / Au layers were etched away and then the photoresist on the surface of microseparator was stripped (Figure 6.6 (b)).

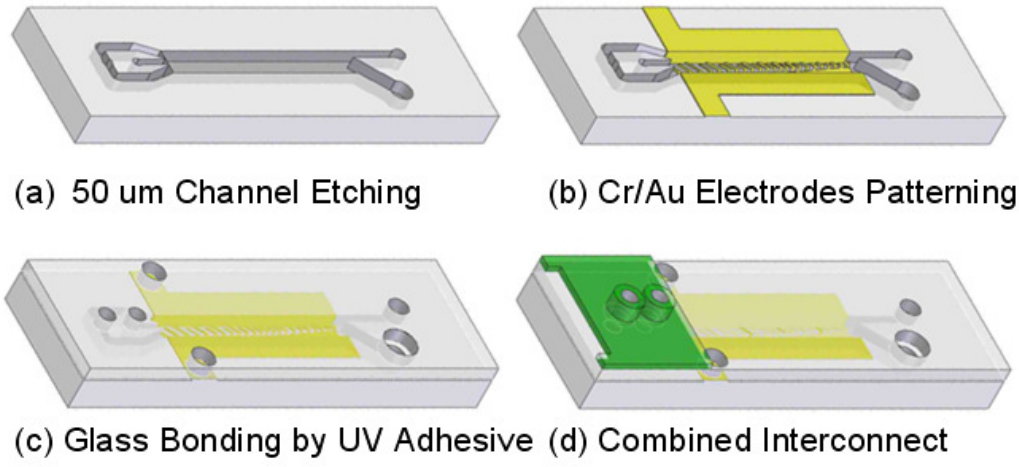

Figure 6.6. The fabrication process of the DEP microseparator.

The inlet holes were drilled by a 1.0 mm diameter diamond drill bit and the outlet holes along with the electrode connections / test holes were drilled by a 2.0 mm diameter diamond drill bit. A fixture fabricated using SLA was used for drill bit positioning. The drilled top glass was aligned and bonded with the microfluidic-channel-defined bottom glass by using UV curable adhesive resin. Capillary force was used to draw the resin between the two glass slides, and they were then cured under a UV lamp for 30 minutes (Figure 6.6 ©). The SLA-based microfluidic interface was bonded to the microseparator by repeating the UV adhesive bonding

process (Figure 6.6 (d)). Finally, two electric wires were connected to each electrode pad through the electrode connection holes using conductive silver paste.

There were two major issues in the fabrication process of the DEP microsystem; disconnected electrodes and trouble with bonding between the two glass slides. In the original electrodes layout shown in Figure 6.2, all comb-shape electrodes were connected to each contact pad through a narrow line. Since those electrodes were sputtered on the etched bottom glass, electrical disconnection often happened on the narrow line at the edge of microfluidic channel.

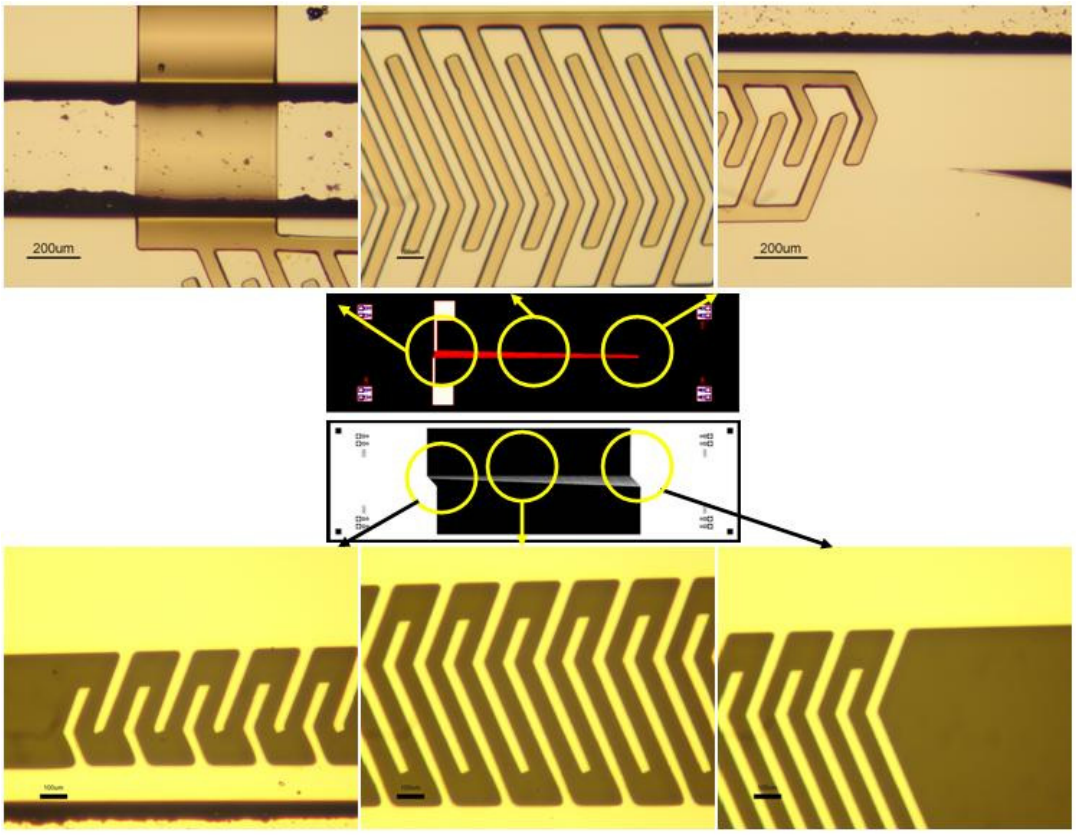

Figure 6.7. Original electrode layout (top) and modified electrode layout (bottom).

Moreover, as shown in the top figure of Figure 6.7, the width of the connecting wire between each comb-shape electrode was similar to that of each electrode and this increased the resistance between the contact pad and the electrode, especially for those positioned far away from the contact pad. Therefore the DEP force created by the electrodes far away from the contact pad became negligible.

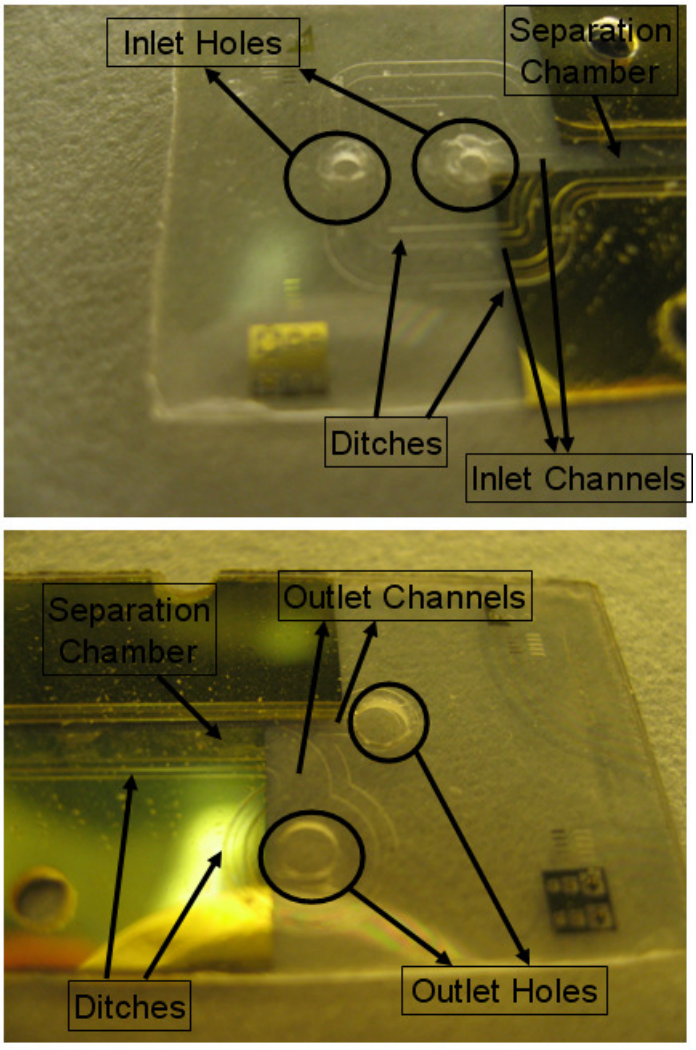

Figure 6.8. Ditches for UV adhesive bonding process.

To fix the above-mentioned problems, the electrode layout was modified such that all comb-shape electrodes were connected to the contact pad through a large area wire as shown in the bottom figure of Figure 6.7. The UV adhesive bonding process provided clean and firm bonding between the two glass slides, but as mentioned in Chapter 3, the microfluidic channel was often blocked and the shape of the separation chamber was distorted by the UV curable adhesive. To address this issue, additional ditches were etched surrounding the inlet and the outlet microfluidic channel and separation chamber as shown in Figure 6.8.

6.4 Experimental Methods

Human venous blood was collected into evacuated glass tubes, containing EDTA as an anticoagulant. A solution of 8.5 % (w/v) sucrose plus 0.3 % (w/v) dextrose buffer was used to dilute the human whole blood sample to a ratio of 10:1, thus lowering the suspending media conductivity. SYTO-13 fluorescent dye was used to identify the nucleated cells during the experiments. The diluted blood sample with SYTO-13 fluorescent dye was incubated at 37 °C for 2 hours.

Before introducing the sample, the microseparator was treated similarly with Pluronic® F108 tri-block copolymer surfactant solution to reduce the adhesion of blood cells on the channel surface during the experiments. The microsystem was assembled into the SLA system packaging and the attached electric wires were connected to the output of a 33250A Function / Arbitrary Waveform Generator (Agilent Technologies, Inc., Santa Clara, CA, USA). A function generator capable of providing burst mode AC signal can create the periodic dielectrophoretic force in the

DEP microsystem that enables the cells experiencing the positive DEP force to hop between adjacent electrodes. A 500 µL gas tight glass syringe (Hamilton Co., Reno, NV, USA) and a 3 mL luer lock syringe were used to load the incubated blood sample and the buffer solution. The syringes were connected to capillary tubing through a Luertight™ Fitting (Upchurch Scientific, Inc., Oak Harbor, WA, USA). The opposite ends of the capillary tubing were connected to the two inlet ports on the DEP microseparator through the SLA fabricated microfluidic interconnects. A PHD 2000 syringe pump (Harvard Apparatus, Holliston, MA, USA) was used to provide the desired constant volumetric flow rates during the experiments.

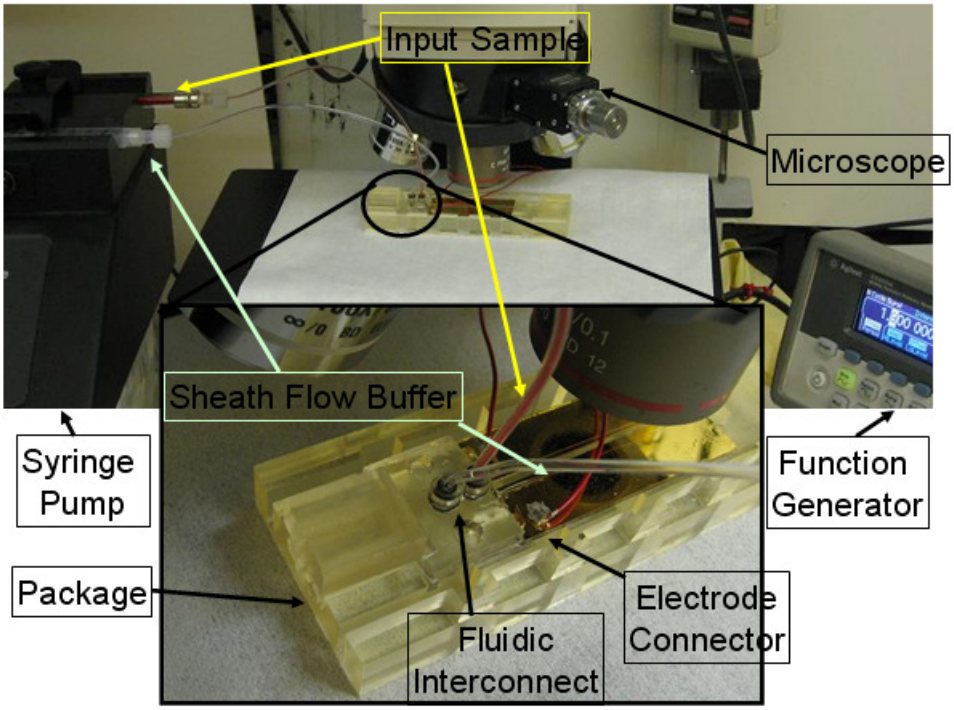

Figure 6.9. The instrument setup for blood cell separation in the DEP microseparator.

The assembled microseparator was placed under a fluorescent microscope and the trajectory of blood cells was monitored and recorded using the microscope camera and video capture tools (Figure 6.9). The switching efficiency of the dielectrophoretic separation system was characterized by counting the number of the RBCs from each outlet port using a Coulter Cell Counter (Multisizer II, Beckman Coulter, Inc., Fullerton, CA). The separation efficiency was measured by counting the number of the WBCs from each outlet port using video imaging capture tools.

6.5 Results and Discussion

Initially various DEP microsystem designs were proposed and fabricated including 3D electrode design as shown in the top figure of Figure 6.10. However, because of several fabrication constraints, this 3D electrodes design was discarded and the microseparator with two inlets and two outlets was chosen for further experiments. The initial electrode layout is shown in the bottom figure of Figure 6.10.

The fabricated microsystem is shown in Figure 6.11. Three input channels and comb-type angled electrodes which are centered on the input sample channel and the outlet #1 channel are shown. An additional narrow microchannel was etched around the main separation channel to prevent UV adhesive resin from flooding into the main channel during the UV bonding process.

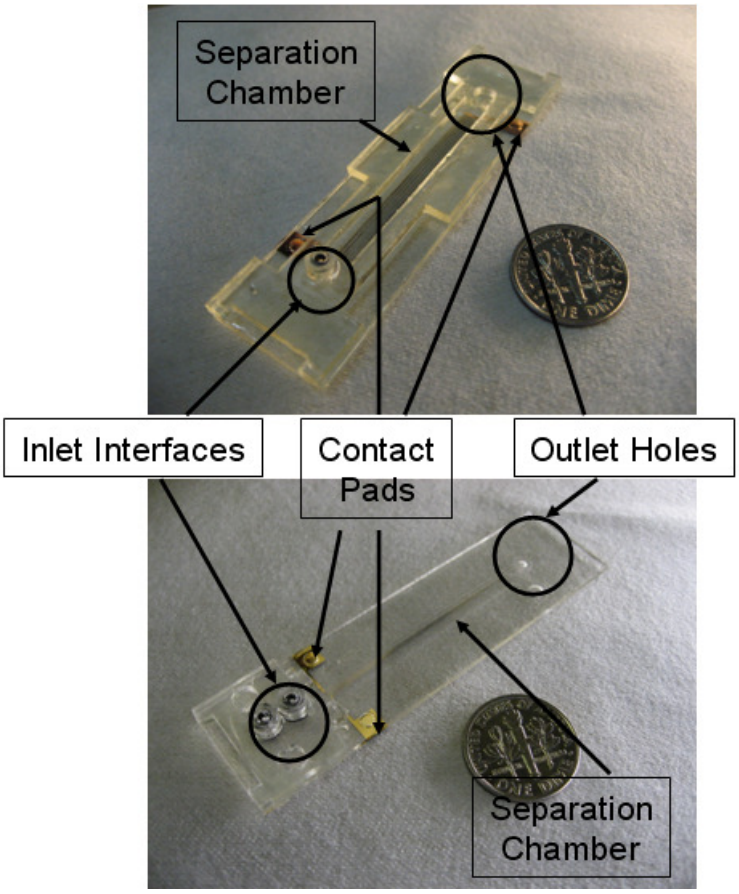

Figure 6.10. 3D electrode design (top) and DEP microseparator with original electrode layout (bottom).

The microfluidic interface with two interconnection ports is shown bonded to the microseparator in the bottom figure of Figure 6.11. Two electrode connections / test holes on each electrode were drilled to test the electrical connections after the conductive wires were bonded using silver paste. Successful electrical connection was verified by measuring the resistance between one of the conductive wire ends bonded to the connection hole and the exposed Cr / Au layers in the electrode test hole. The typical resistance was measured to be around 0.7 ohm.

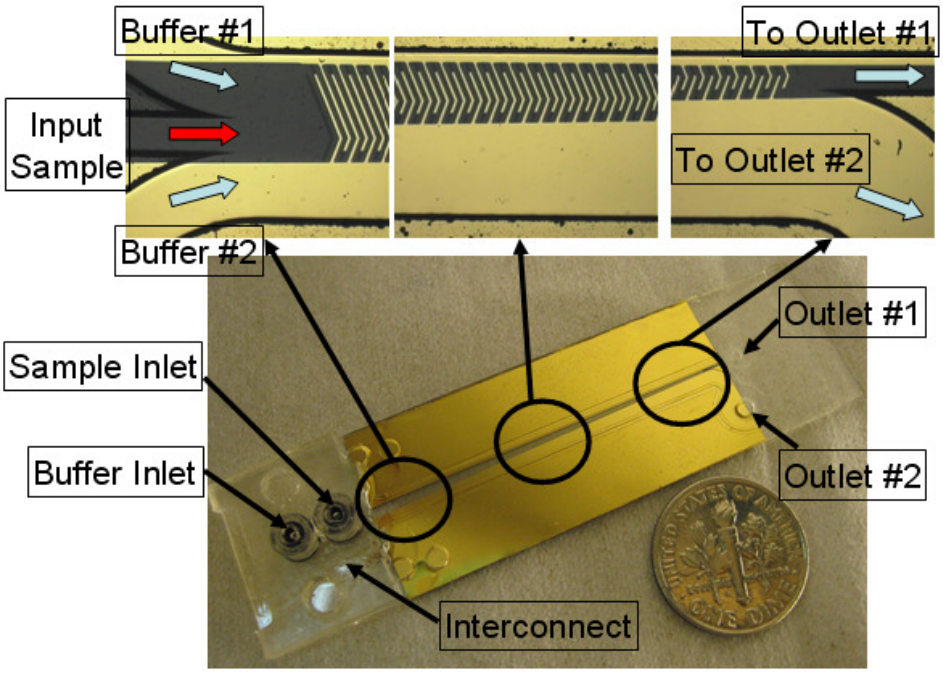

Figure 6.11. The fabricated DEP microsystem.

The microsystem was tested for the response of different blood cell types to the DEP force. Based on the results of the different blood cell responses, the experiments to switch the blood cell stream and separate different blood cell types were carried out.

Figure 6.12 shows the continuous flow dielectrophoretic separation system packaged inside the system packaging with electrical connections attached to the electrode pads. The system packaging for dielectrophoresis is composed of one center stage to hold the dielectrophoretic separation system, several small square holes for electrical wire connections, and one long rectangular cavity under the microchannel area to enable monitoring of blood cell movement during the experiments by providing light from the bottom-side microscope light source. The removable holding tip was used for easier installation and removal of the microseparator between experiments.

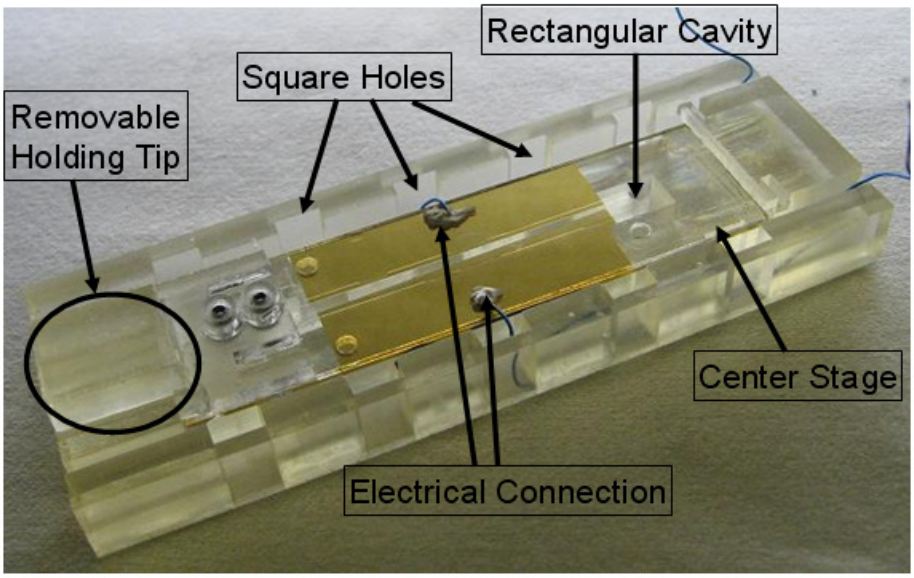

Figure 6.12. The Assembled DEP microsystem.

The DEP response of each blood cell type was monitored to find the transition frequencies while letting the blood sample flow at 5.0 μL/hr to reduce the sedimentation without the sheath flow. The transition frequency for WBCs was found to be around 500 kHz. The crossover frequency for RBCs was hard to determine because of the proximity between each cell. The density of RBCs was 5.0 × 10^8 cells/mL and when RBCs experienced positive DEP forces, they tended to make a chain, which demonstrated a much lower transition frequency than single RBC. Some RBCs start to show a positive DEP reaction as low as 260 kHz, while most RBCs showed a positive DEP response above 600 kHz. The transition frequencies of both blood cell types showed dependency on the conductivity of the buffer used for focusing sheath flow. When the original buffer solution was used as sheath flow buffer, the overall transition frequency was lowered to 150 kHz. The blood sample flow from the inlet port became focused into one stream by the side

sheath flow and stayed focused throughout the length of the separation channel. Images of the blood cell stream with no applied electric field are shown in Figure 6.13 (a).

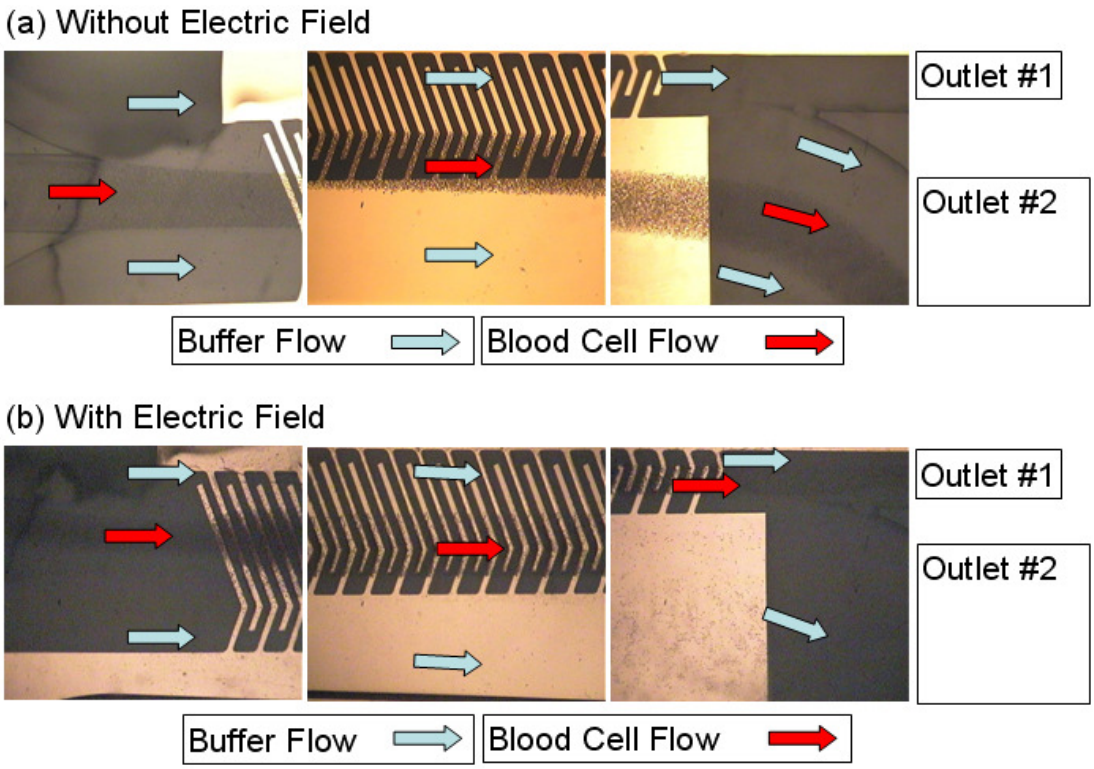

Figure 6.13. The micrographs of blood cells at the entrance, middle and exit of the channel during switching mode operation.

Without an applied DEP separation force, 99.21 ± 0.08 % of the cells from the input sample traveled in the laminar flow direction and were collected into outlet #2. A 2.0 MHz, 8 Vp-p AC signal was supplied in burst mode (0.2 second ON and 1.3 second OFF) to create the hopping movement of the blood cells between adjacent electrodes. Figure 6.13 (b) shows switching of the input blood cell stream from outlet #2 to outlet #1 under positive DEP force. For the switching operation, 96.16 ± 2.48 % of the cells were deflected from the original flow direction and collected into

outlet #1. The volumetric flow rate for this experiment was 20.0 μL/hr (3.0×10^3 cells/sec). The periodicity of the burst mode (periods for release and attraction phase) used for the switching operation was chosen based on the time for the cells to cross one or two electrodes during one period. The switching efficiency of the dielectrophoretic microseparator was characterized by counting the number of cells in 2.5 μL of the fluid collected at each outlet port using a Coulter Cell Counter (Multisizer II, Beckman Coulter, Inc., Fullerton, CA).

The WBCs separation from RBCs experiments were conducted using modified sheath flow buffer. The modified buffer solution consisted of 10 parts of original buffer solution and 1 part of a calcium and magnesium free PBS solution (Mediatech, Inc., Manassas, VA, USA). A 3 MHz, 8 Vp-p AC signal was supplied in burst mode (0.33 second ON and 1.17 second OFF) to perform the separation of WBCs from the whole blood sample. The volumetric flow rate of the blood sample was 10.0 μL/hr (1.5×10^3 cells/sec). Using the stated experimental condition, the RBCs did not experience a positive DEP force and traveled in the laminar flow direction and were collected into outlet #2. The WBCs demonstrated positive DEP attraction to the electrode edges and moved toward outlet #1. Figure 6.14 shows images of the cell separation in the microsystem. The separation efficiency was measured by counting the fluorescent WBCs passing through each outlet. 59.39 ± 4.24 % of the WBCs were deflected from the original flow direction and collected into outlet #1, while all RBCs traveled in the laminar flow direction and were collected into outlet #2.

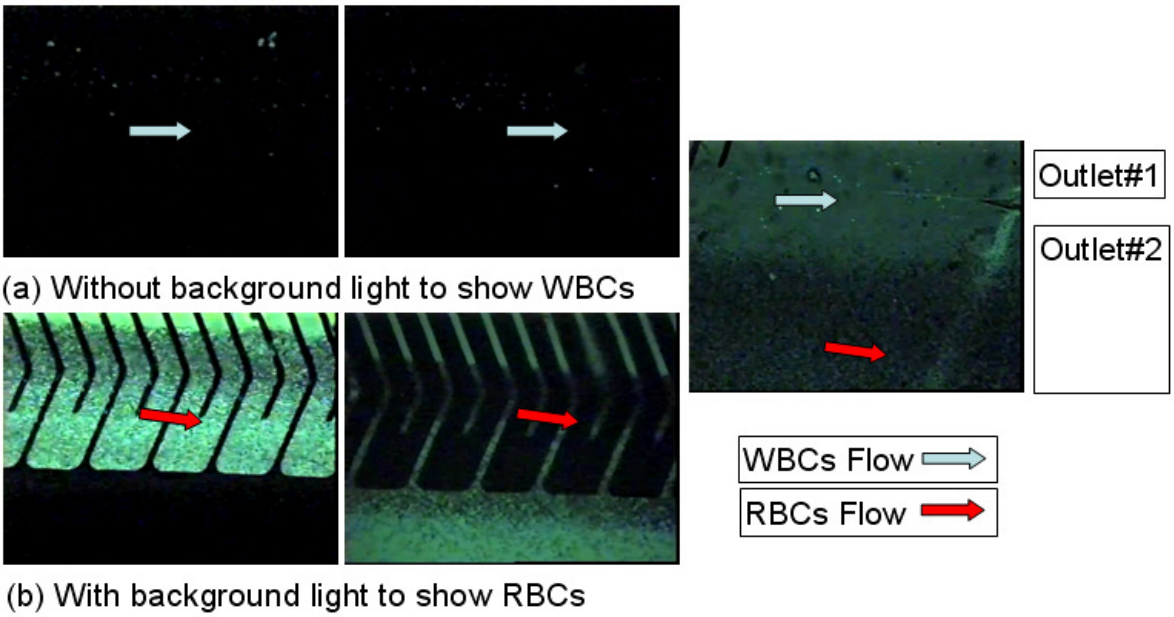

Figure 6.14. WBCs separation from the whole blood sample in the DEP microseparator.

The microsystem has successfully demonstrated the ability to switch the whole blood stream with high efficiency by using focusing sheath flow and positive DEP force. The separation of WBCs from RBCs was also demonstrated. The separation was not as efficient as in switching operation, but all RBCs were collected in outlet #2, thus outlet #1 only contained WBCs. If all the WBCs deflected from main sample stream were considered as separated WBCs, the efficiency is 74.79 ± 4.21 %.

During the experiments with the DEP microseparation system, it was observed that some WBCs adhered to the sputtered gold electrodes until they experienced a strong negative DEP force. Gold is generally known as a bio-compatible material, but when the WBCs encounter the small step in electrodes edges, it may trigger adhesion of WBCs to the surface of the electrode edge. No clogging from cell coagulation inside the channel was observed during the separation.

However, trapped air bubbles in the channel that were introduced between experiments blocked the microchannel and distorted the cell stream flow if not removed before the switching or separation process.

The continuous flow dielectrophoretic microseparation system has successfully demonstrated the ability to switch blood cell streams in laminar flow, based on the native dielectrophoretic properties of the cells without the need for tagging or chemical modification of the blood sample. With the high efficiency switching capability, the microsystem can be used to extract cell free media from whole blood samples. The separation capability of the presented microsystem was not as high as the switching capability, but the unique design and operation principle of microsystem enabled the collection of pure target cells in the collection outlet in continuous fashion, and there are many applications that could benefit from such a separation such as the removal of pure cancerous cells from normal blood cells.

CHAPTER 7

DIELECTROPHORESIS SYSTEM APPLICATION II

(Cancer Cell Separation and Characterization)

7.1 Introduction

In Chapter 3, the removal of RBCs from a human whole blood sample using magnetophoresis was presented. While the presented magnetophoretic separation system has successfully separated RBCs in a blood sample with high separation efficiency at considerable volumetric flow rates, to further sub-categorize different cell types, additional downstream separation system is required. The frequency response of each type of biological cell under dielectrophoresis is dependent on various cell characteristics. This variable frequency response enables a DEP microsystem to differentiate successfully between similar cell types. Also, a DEP separation system is advantageous in that it does not require any labeling of cells in order to separate different cell types. Therefore, dielectrophoresis was chosen as a downstream separation scheme for cancer cell separation. In Chapter 6, the development of a continuous flow dielectrophoretic system for blood cells was presented. The dielectrophoretic microsystem has successfully switched blood cell streams between two outlets and separated WBCs from other blood cell types. During the separation of WBCs, it was found that even though the crossover frequencies of RBCs and WBCs were quite close. Manipulating the conductivity of the solution of the sheath flow buffer, changes the conductivity of the sample solution, allowing successful separation.

In the following sections, qualitative measurement of crossover frequencies for different cell types suspended in various buffer solutions will be presented with brief description of the design and fabrication of a dielectrophoretic microsystem capable of measuring the crossover frequencies of different cell types. Also, quantitative measurements of separation efficiencies of head / neck cancer cells from blood cells are reported using the previously developed DEP microsystem.

7.2 Microsystem Design

The overall design of the dielectrophoretic microsystem used to measure the crossover frequencies of various cell types suspended in buffer solutions with different conductivities is similar to that of the previously described DEP microsystem in Chapter 6. The difference from the previously described DEP microsystem is that the microsystem does not have a sheath flow inlet for focusing the sample cell stream because it does not need the high-throughput separation capability in continuous mode operation. The microsystem consists of a single inlet, three outlets, and one measurement chamber with comb-shaped electrodes. The DEP forces are created between the comb-shaped electrodes and the cells in the sample are exposed to the DEP force while flowing at the specified flow rate. By monitoring the motion of the cells under the DEP force in different suspending buffer solutions, the crossover frequencies of different cell types were measured.

For fabrication, the DEP microsystem requires two photolithography steps. The mask layouts for the microfluidic channel and comb-shaped electrodes are shown in Figure 7.1.

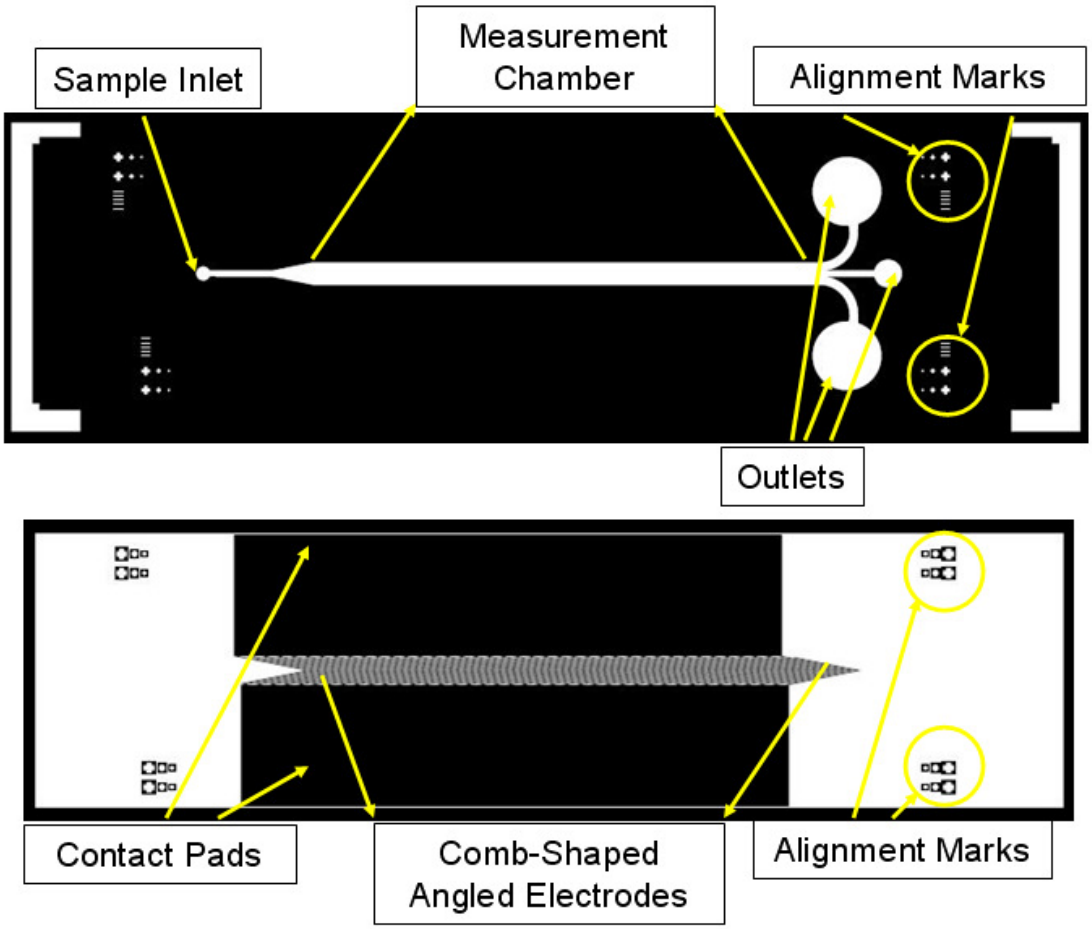

Figure 7.1. Mask design for microfluidic channel (top) and comb-shaped electrodes (bottom).

For the previously described DEP microseparator to separate different cell types continuously, the fluid in the DEP chamber should move in a laminar flow. When there was an undesired bump on the wall of a separation chamber or an air-bubble in a microchannel, the shape of the fluid flow became distorted and the DEP microsystem could not separate cells effectively. Additional ditches were placed surrounding the microfluidic structures to protect them from distortion in shape resulting from infiltrated UV curable adhesive during the bonding process. Since the

new DEP microsystem does not need to perform a continuous flow separation, the additional ditches surrounding the inlet / outlet microfluidic channels and the separation chamber were removed from the design.

The mask designs were drawn with Autodesk® AutoCAD and saved in DXF format. The file was sent to an outside vendor for plotting on a transparent film. Later, mask patterns were transferred from the transparent film to a 4" × 4" chromium-layered glass mask using a photolithography process.

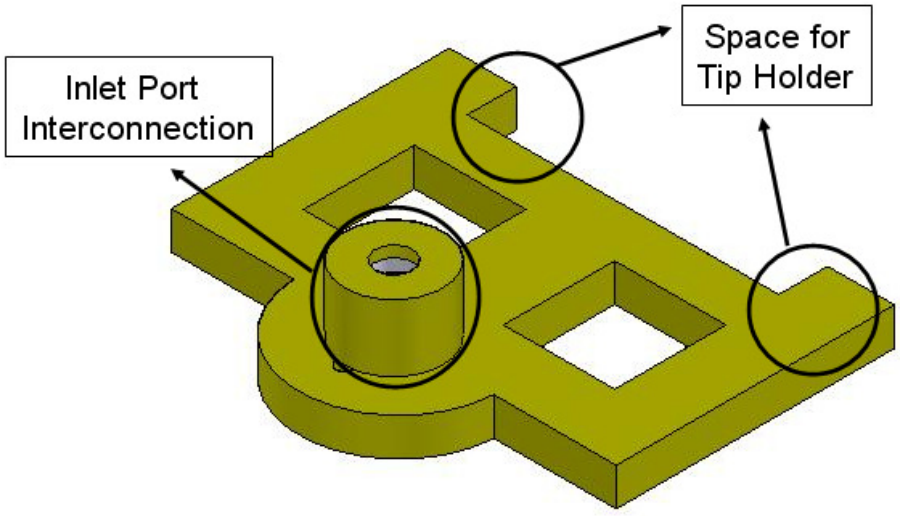

Figure 7.2. Microfluidic interface design.

The microfluidic interface of this DEP system was designed similarly to that of previously presented ones. It has two O-rings inserted to hold a tubing firmly and "[" shaped edge to allow space for the system packaging tip holder to secure the microfluidic system while conducting experiments (Figure 7.2). The system packaging design was unchanged from that of DEP blood cell separator presented in Chapter 6.

The drilling guide design for correct positioning of the inlet / outlet ports and electric connection / test holes in the top glass substrate is shown in Figure 7.3. The design of the microfluidic interface and drilling guide were drawn using Solid Edge®.

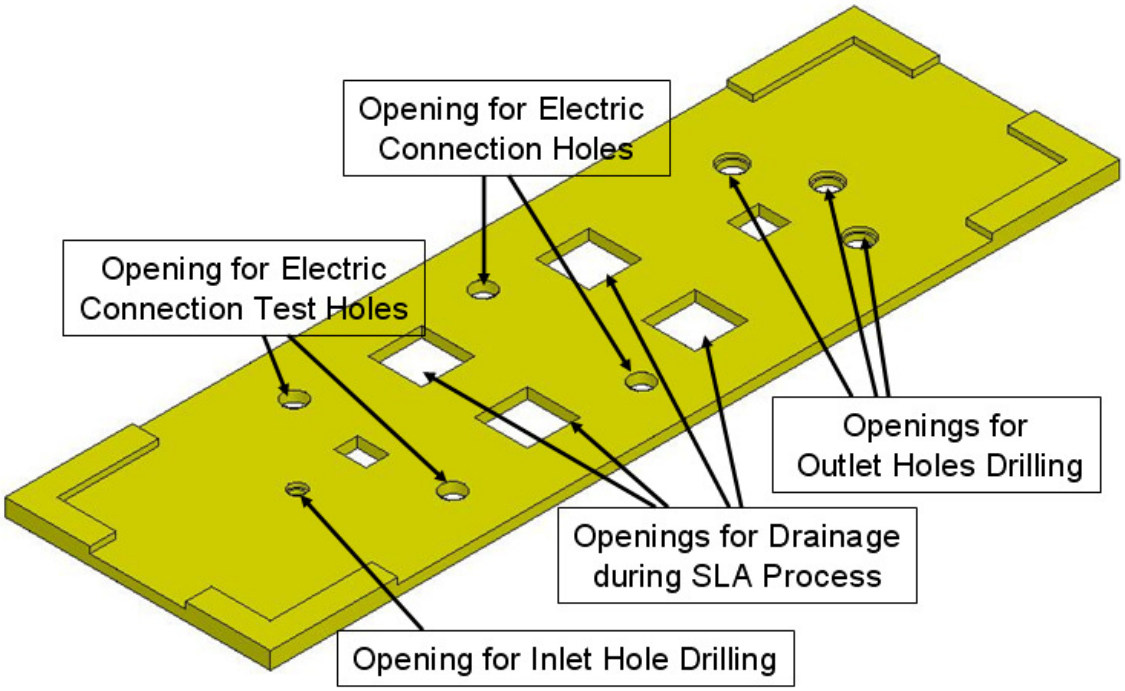

Figure 7.3. The drilling guide for the inlet / outlet and electrical connection holes.

7.3 Microsystem Fabrication and Packaging

The DEP microsystem consisted of a glass microchannel, comb-shape planar electrodes, microfluidic interfaces and system packaging. The overall fabrication processes for the microchannels are almost identical to those of the dielectrophoretic microsystem described in Chapter 6 and shown in Figure 7.4.

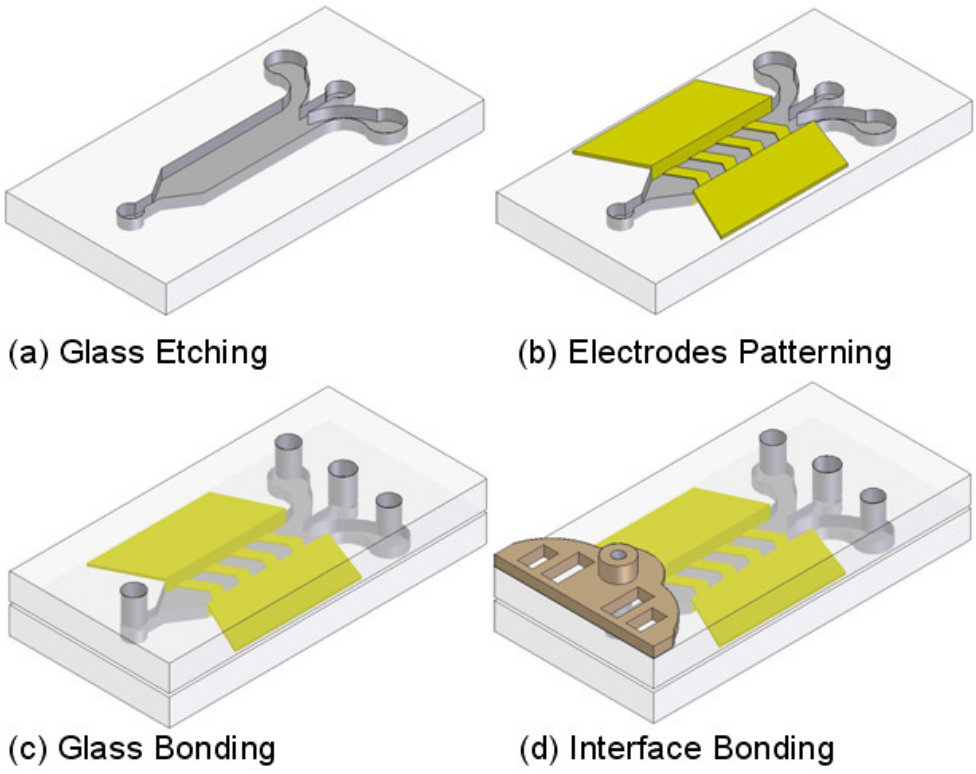

Figure 7.4. The fabrication process of the DEP microsystem for measuring the crossover frequency.

The 50 μm deep microfluidic channels were patterned and etched into a glass slide by hydrofluoric acid wet etching with photoresist and Cr / Au protective layers. Pictures of the microchannel after etching are shown in Figure 7.5.

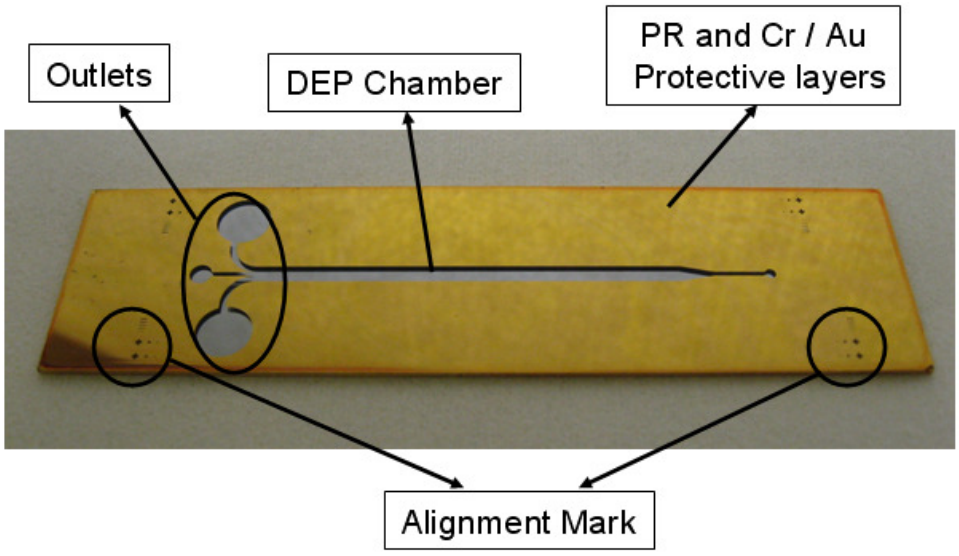

Figure 7.5. The channel etched device.

Once the glass etching process was completed, the residual photoresist and Cr / Au layers were removed (Figure 7.4(a)). New Cr / Au electrodes layers were sputtered using a DC sputterer and patterned with another photolithography step (Figure 7.4(b)). The inlet / outlet and electrical connection holes were drilled by using an SLA-based drilling guide on a new glass slide and glass-to-glass bonding between two glass slides was performed to enclose the microfluidic channel area using UV curable resin (Figure 7.4(c)). The microfluidic interface was fabricated by an SLA process. In the previous DEP microsystem described in Chapter 6, the sheath flow introduction channels encircled the sample inlet. This made a bonding process more difficult since UV curable adhesive should be introduced separately and carefully in the encircled area. Even with the additional ditch structures protecting the microchannels, the encircled area was so tiny in size that the separate introduction of UV curable adhesive often led to bonding failures. By removing the sheath flow introduction channels, which encircle the sample inlet, the bonding process using UV

curable adhesive resin became much simpler and the additional narrow ditch around the main separation channel was not needed for successful bonding. A glass-to-plastic bonding process was carried out in a similar fashion to that of glass-to-glass bonding (Figure 7.4(d)).

Finally, wires were connected to the contact pads on the glass chip through the electric connection holes with silver paste (CW2200 MTP CircuitWorks® Conductive Pen, ITW Chemtronics®, Kennesaw, GA, USA). The electrical resistance between the wire end and an electric connection test hole was measured to ensure a good connection. The wire bonding process is shown in Figure 7.6.

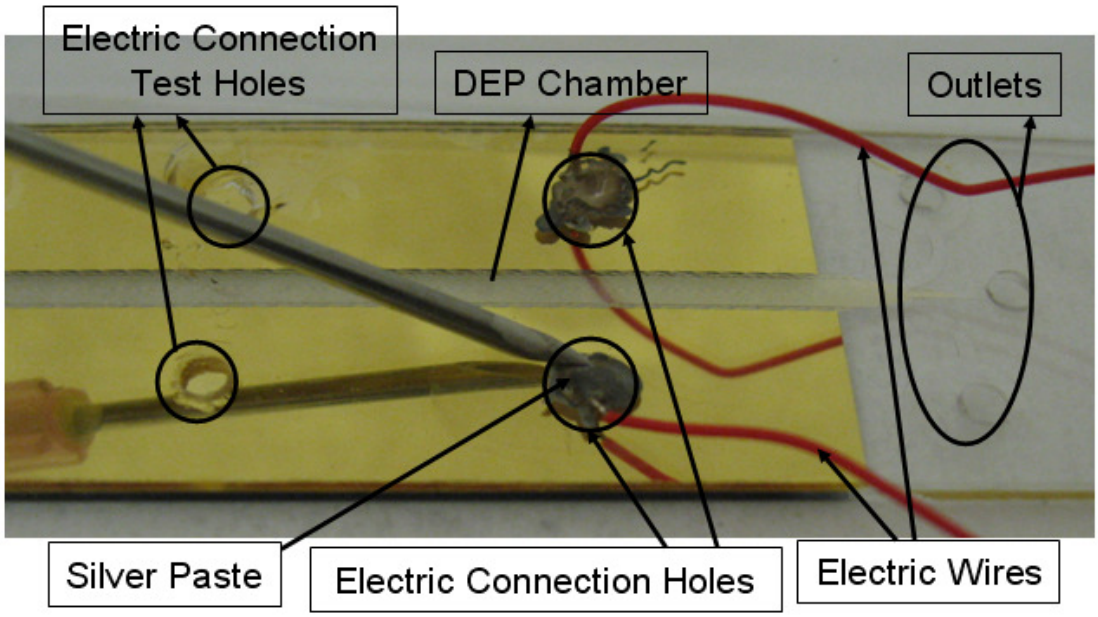

Figure 7.6. The electric wire bonding process.

7.4 Experimental Methods

A solution of 8.5 % (w/v) sucrose plus 0.3 % (w/v) dextrose buffer and a calcium and magnesium free PBS solution were used to create four suspension media (Buffer #1 ~ #4) with different conductivities. Buffer #1 consisted of a solution of 8.5 % (w/v) sucrose plus 0.3 % (w/v) dextrose buffer. Buffer #2 consisted of 97.5 parts buffer #1 and 2.5 parts PBS solution. Buffer #3 was made from 5 % by volume PBS mixed with buffer #1 with PBS solution contributing 5 % of Buffer #3. Buffer #4 was mixed using 92.5 % by volume buffer #1 plus 7.5 % by volume PBS. Human venous blood was collected into evacuated glass tubes, containing ethylenediamine tetraacetic acid as an anticoagulant and re-suspended into the prepared buffer solutions.

The procedures for the head / neck cancer cell culture and preparation are similar to those described in Chapter 4. In this case, only 212LN cancer cells were used as a cancer cell sample. The cancer cells were cultured in DMEM / F12 medium (1:1) supplemented with 10 % FBS at 37 °C in a humidified atmosphere with 5 % CO_2. The cells were detached from culture container with Cellstripper^{TM} solution following wash / aspiration / incubation procedures. The cancer cells were collected by centrifugation and re-suspended in the four different buffer solutions. Later, the detached cancer cells were filtered through a cell strainer with a 20 μm mesh size to ensure that only isolated cancer cells were present in the sample fluid.

Before introducing a sample, the DEP microsystem was treated with surfactant solution to decrease cell adhesion on the microchannel surfaces. The microsystem was subsequently washed three times with PBS in a similar fashion as

previous experiments. The overall setup for the experiments was identical to that in Chapter 6. The microsystem was assembled with the system packaging, and the electric wires were connected to the output of a function generator. A 500 uL gas tight glass syringe was used to load the prepared cell sample and connect it to capillary tubing through a Luertight™ Fitting while the opposite end of the capillary tubing was connected to the inlet port on the DEP microseparator through the SLA fabricated microfluidic interface. A syringe pump was used to provide a constant volumetric flow at low flow rates.

7.5 Results and Discussion

The fabricated microsystem has one inlet, three outlets, and one measurement chamber with comb-shaped electrodes. Two electric connection wire and two electric connection test holes are also shown in Figure 7.7. The fabricated microsystem is shown in Figure 7.7.

The DEP response of RBCs and cancer cells in different suspending solution were monitored to find the transition frequencies under the microscope. In buffer #1, cancer cells started to show positive DEP reaction at frequencies as low as 50 kHz and most cells were strongly attracted toward the positive DEP region above 150 kHz, while the positive reaction of RBCs started around 150 kHz and became obvious above 250 kHz. With buffer #2, positive DEP reaction of cancer cells initiated around 120 kHz and most cells clearly showed positive reaction above 250 kHz, while the RBCs' DEP reaction started around 250 kHz and became clear above 350 kHz.

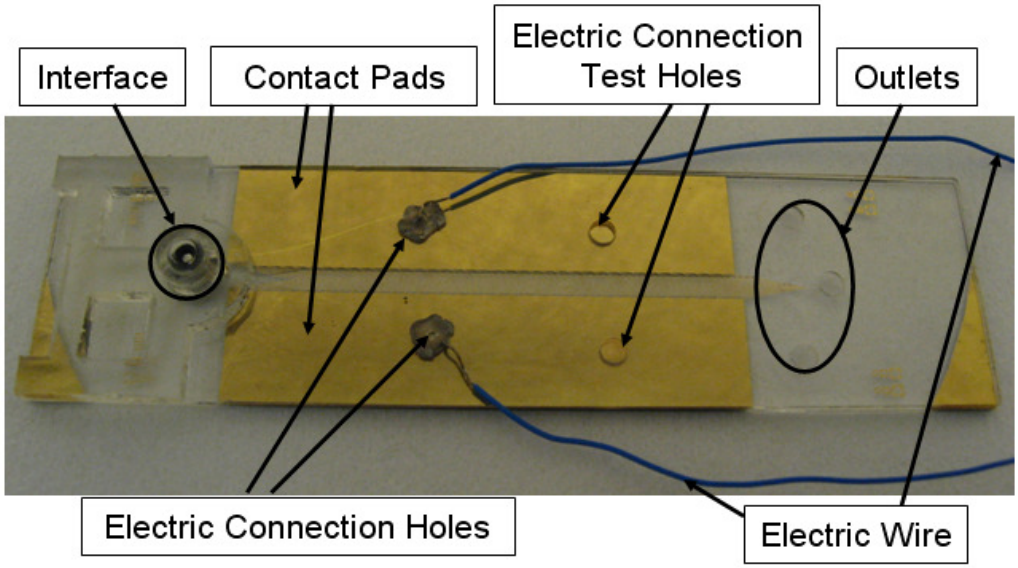

Figure 7.7. The fabricated DEP microsystem.

In buffer #3, cancer cells showed positive DEP reactions beginning around 140 kHz, but most cells were attracted around the dense electrical field area only above 600 kHz. The positive reaction of RBCs in buffer #3 began around 400 kHz and became obvious above 500 kHz. With buffer #4, positive reaction of cancer cells began around 210 kHz, but the reaction was weaker compared to those in different buffers at even higher frequencies. The RBCs in buffer #4 started to show weak positive DEP reactions above 500 kHz range, but it was hard to find the frequency where all the RBCs displayed obvious positive DEP reactions. The results are summarized in Table 7.1.

Overall, as sample cells were suspended in the buffer containing more PBS solution, the transition frequency increased and the magnitude of positive DEP force on the cells decreased. Moreover, the rate in the change of transition frequencies of RBCs between different suspension buffers was different from that of cancer cells,

which led to the transition region overlapping in the buffers containing more PBS solution.

Table 7.1. The DEP response of head / neck cancer cell line (212LN) and RBCs in different buffer solutions (F_I corresponds to the frequency where first positive DEP reaction was observed. F_M corresponds to the frequency where most cells showed positive DEP reaction.)

212LN Cells	Buffer #1	Buffer #2	Buffer #3	Buffer #4
F_I	50 kHz	120 kHz	140 kHz	210 kHz
F_M	150 kHz	250 kHz	600 kHz	Not observable

RBCs	Buffer #1	Buffer #2	Buffer #3	Buffer #4
F_I	150 kHz	250 kHz	400 kHz	500 kHz
F_M	250 kHz	350 kHz	500 kHz	Not observable

Head / neck cancer cells separation from human blood cells were conducted using the DEP microsystem described in Chapter 6. Buffer #1 was used as both sheath flow buffer and cell-suspending media. Two different sets of experiments using different frequencies and burst conditions were performed to separate the cancer cells from the cancer-spiked whole blood sample. First set of experiments used a 300 KHz, 8 Vp-p AC signal supplied in burst mode (0.217 second ON and 1.033 second OFF). Second set of experiments used a 400 KHz, 8 Vp-p AC signal supplied in burst mode (0.225 second ON and 0.975 second OFF). The volumetric flow rate of the sample was 20.0 μL/hr and the densities of the cancer cells and blood cells were 2.0×10^3 cells/μL and 2.5×10^4 cells/μL, respectively.

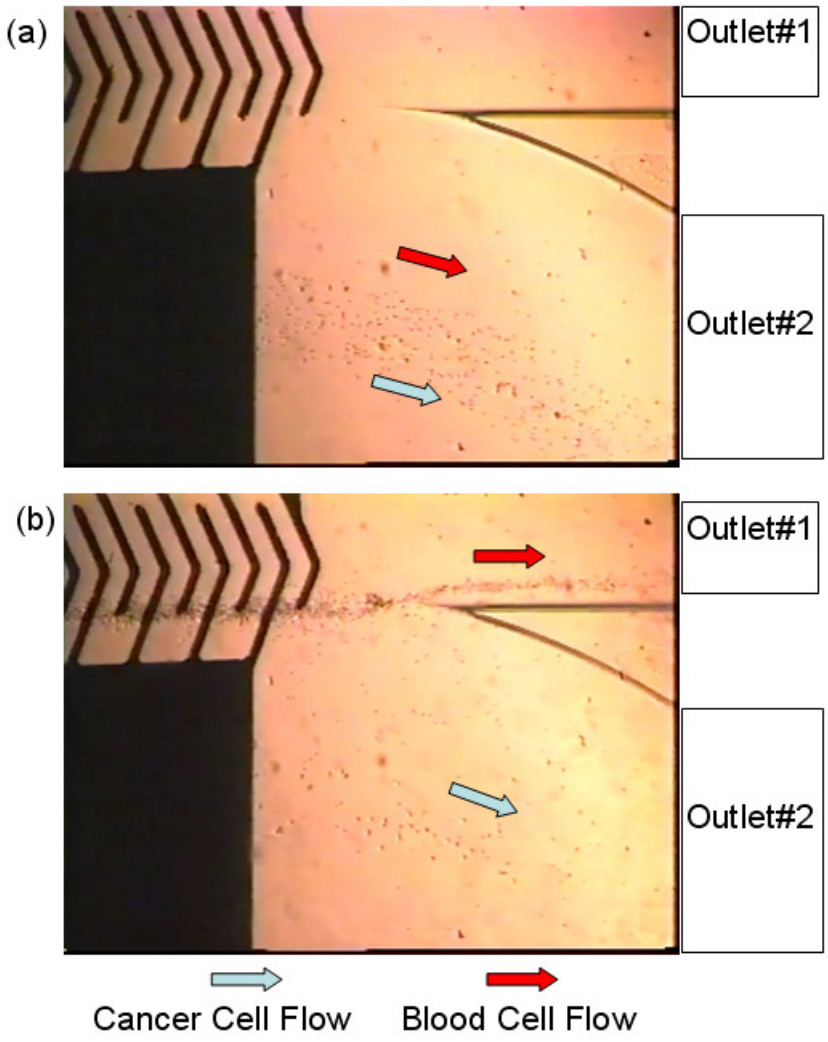

Figure 7.8. Mixed cells flow in the laminar flow without external electric signal (a) and head / neck cancer cells separation from human whole blood with external electric field.

Using the stated experimental condition, the cancer cells experienced small amount of positive DEP forces and traveled in the laminar flow direction and were collected into outlet #2. Most blood cells demonstrated positive DEP attraction to the electrode edges and moved toward outlet #1. Figure 7.8 shows images of the cell separation in the microsystem. The separation efficiency was measured by counting the cancer cells passing through each outlet. With the first experimental condition,

88.30 ± 1.54 % of the cancer cells traveled in the laminar flow direction and were collected into outlet #2, while about 95 % of blood cells were deflected from the original flow direction and collected into outlet #1. With the second experimental condition, 90.20 ± 1.17 % of the cancer cells traveled in the laminar flow direction and were collected into outlet #2, while about 89 % of blood cells were deflected from the original flow direction and collected into outlet #1.

The measured crossover frequencies of the cancer cells in the media with different conductivities were lower than those of the blood cells. Therefore, it was expected that during the separation experiments at the frequency higher than the crossover frequencies of the head / neck cancer cells and blood cells, the cancer cells would be more affected by positive DEP force and deflected into outlet #1, while blood cells would be collected into outlet #2. However, it was found that the lateral displacement of the head / neck cancer cells was smaller than that of blood cells when the cells were flowing continuously in the laminar flow. One possible explanation of these results is that the volumetric mass density of head / neck cancer cells is lower than that of blood cells so that when the cells are flowing in the suspending media, the cancer cells stay higher than the blood cells. To verify this assumption, the relative velocity of cancer cells and blood cells flowing in the laminar flow without any external electric signal was monitored, and it was observed that the cancer cells flew much faster than the blood cells.

The continuous flow dielectrophoretic microseparation system has successfully demonstrated the ability to separate the cancer cells from human whole

blood cells in continuous fashion and can be used as the downstream separation system for further sub-classification of different cell types.

CHAPTER 8

FUTURE MICROSYSTEM DEVELOPMENT

8.1 Introduction

The complete and permanent removal of cancerous tumors from patients with no or little damage to the healthy parts of the body is the ultimate goal of cancer therapies. When diagnosed with cancer, patients usually go through a series of cancer treatments, including surgery, chemotherapy, and radiation therapy. Chemotherapy is a method of treating a disease by killing target cells using chemicals. Most chemotherapeutic drugs target fast dividing cells like cancerous cells, but the effectiveness of chemotherapy is often limited by its toxicity, or damage to normal tissues like cells in hair follicles, the blood, and the digestive tract. This damage often leads to hair loss, gastrointestinal distress, depression of the immune system, and even liver / kidney damage.

Radiation therapy uses ionizing radiation to control cancerous tumors by damaging the DNA of cells. Since oxygen is a potent radiosensitizer that increases the effectiveness of radiation therapy, the major limitation of radiation therapy is cellular access to oxygen, tumors that are in low-oxygen areas do not respond as well to radiation. Surgery can easily remove a lump of cancer cells, but does nothing to limit metastasis, and can't capture circulating tumor cells, which can allow the cancer to spread. Therefore, in the treatment of cancer, removing circulating tumor cells from whole blood can be advantageous. As stated earlier in Chapter 1, detecting CTCs in blood can be used as an early detection methodology for cancer and

determining the level of CTCs in blood can be helpful in characterizing genetic and immunophenotypic changes with tumor progression.

However, it is quite challenging to identify and remove only malignant tumor cells from peripheral blood without disturbing normal blood cells. First, cancerous cells are constantly shed into the blood stream while the primary tumor cells are still active. Therefore, for successful cancer treatment, it is also required to remove malignant tumor cells while doing a whole blood CTC removal process. Secondly, since normal blood cells should be returned back to the peripheral blood and perform their assigned roles after the separation process, chemical modification or molecular tagging methods of target cancerous cells, which would damage or disturb blood cells from their original function, cannot be used in this application. Another major challenge in separating out target cancerous cells in blood arises from the fact that human whole blood is heterogeneous mixture of diverse blood cells and 98% of blood cells are RBCs whose cell density is around 5×10^6 cells / μL while the cell density of CTCs in peripheral blood ranges from 0-1 cells per milliliter, which is extremely low compared to that of RBCs.

In Chapter 3, the magnetophoretic microfluidic system was presented along with its design, fabrication and characterization for RBCs removal from a human whole blood sample. The six-stage cascade paramagnetic mode magnetophoretic separation system removed RBCs successfully in continuous fashion without chemical modification or molecular tagging of the blood sample. In Chapter 6 and 7, the dielectrophoretic microsystem has demonstrated its ability to switch a massive blood cells stream from one outlet to the other and to separate different types of cells

based on their native dielectric properties in continuous flow. Malignant head / neck cancer cells were characterized for their dielectric properties and shown to have quite different dielectrophoretic crossover frequencies from those of normal blood cells.

Based on the characterization results of the presented magnetophoretic and dielectrophoretic separation systems, a magnetophoresis system cascaded with a dielectrophoresis system could potentially enable efficient and novel separation of target rare cells from human whole blood. Continuous flow magnetophoresis could be used in stage one as an enrichment device for separating most RBCs from a human whole blood sample, concentrating target rare cells and other nucleated blood cells. In stage two, integrated continuous flow dielectrophoresis could be used as an isolation device for separating target rare cells out from other nucleated cells and residual RBCs.

In addition to the development of a cascade magnetophoresis – dielectrophoresis separation system, there is a need to develop an approach that utilizes whole blood as opposed to diluted blood samples. The ability to process whole blood would open the door for use of the cascade system in point-of-care applications. The key to processing whole blood through the cascade system is to design the first stage (magnetophoretic separator) for whole blood separations, remembering that the second stage, the dielectrophoretic separation stage, is only used to classify the nucleated cells from the sample with the red blood cells removed by the first stage. So, if the first stage could process and remove virtually all the RBCs, then the second stage would need only to process a much smaller number of cells as already demonstrated through the work detailed in Chapter 6 and 7.

Therefore, future microsystem development would be focused on the development of a magnetophoretic separation system capable of processing whole blood. Towards this end, another magnetophoresis with forty separation stages has been designed and will be presented in the following sections.

8.2 Combined Magnetophoretic / Dielectrophoretic Separation System

Figure 8.1 illustrates the principle operation of the microsystem combining the two separation approaches. The microsystem consists of two sample introduction inlets, two magnetophoretic and dielectrophoretic separation stages, two outlets for RBCs, one outlet for cancerous cells, and one outlet for normal nucleated cells. Blood samples spiked with malignant tumor cells enter the microsystem through two inlets, the cells in the sample pass through a six-stage para magnetic mode magnetophoretic stage to remove most of the RBCs from the sample. RBCs or magnetic cells experience an attractive magnetophoretic force and move toward a center microchannel, while other nucleated cells remain in side microchannels. The removed RBCs are collected into the center outlet encircled by the microfluidic channel containing the enriched nucleated cells which are directed into a dielectrophoretic separation stage. In the dielectrophoretic separation stage, malignant tumor cells and other nucleated cells experience different DEP forces depending on their native dielectric properties, sizes and density. This leads to the separation and collection of malignant tumor cells from other nucleated cells into the inner outlet on the right side of the dielectrophoretic stage, while normal nucleated blood cells flow into the outer outlet. The overall design was configured in a way

such that the entire device can be placed on a small glass slide the size of a human hand.

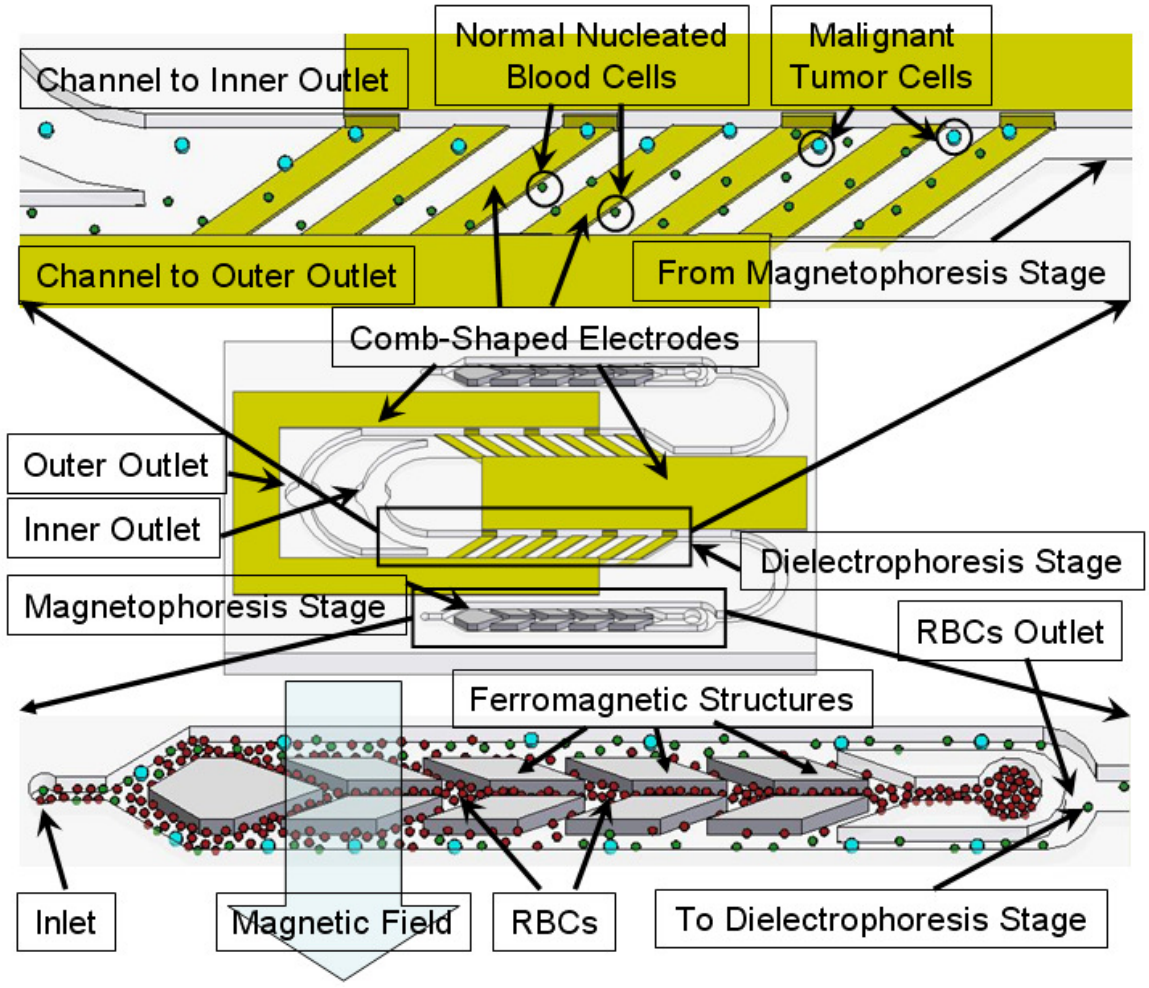

Figure 8.1. The operation principle of the combined continuous flow microseparator.

The fabrication of the combined continuous flow microseparator requires three photolithography steps. Three mask layers for the microfluidic channels, electroplated ferromagnetic structures, and comb-shaped electrodes are shown in Figure 8.2. In the design of the microsystem, there are two mirror-imaged

magnetophoretic and dielectrophoretic separation chambers placed on one glass slides to maximize the throughput.

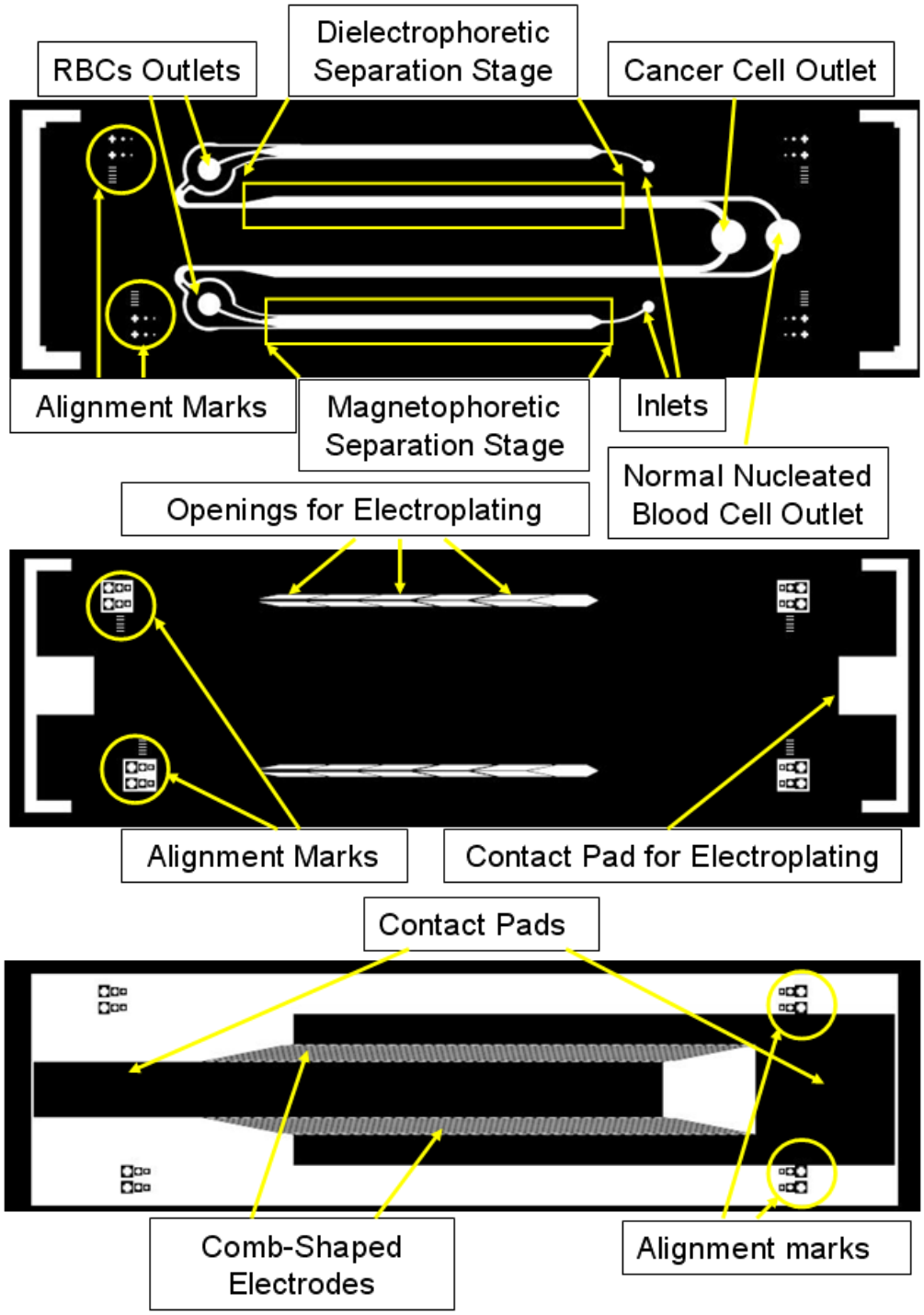

Figure 8.2. Mask designs for microfluidic channel (top), electroplated ferromagnetic structures (center), and comb-shaped electrodes (bottom).

8.3 Magnetophoretic System for Whole Blood Processing

Figure 8.3 shows the overview and operation principle of the 40 stage magnetophoresis separation system design. The 40 stage design should allow for processing of samples with a much denser population of suspended cells by providing a much greater number of collection channels for unwanted RBCs. The design of the ferromagnetic structures were modified to more efficiently attract RBCs from the main blood sample stream and release the RBCs easily into the subsequent RBC collection channels using the dragging force of laminar flow.

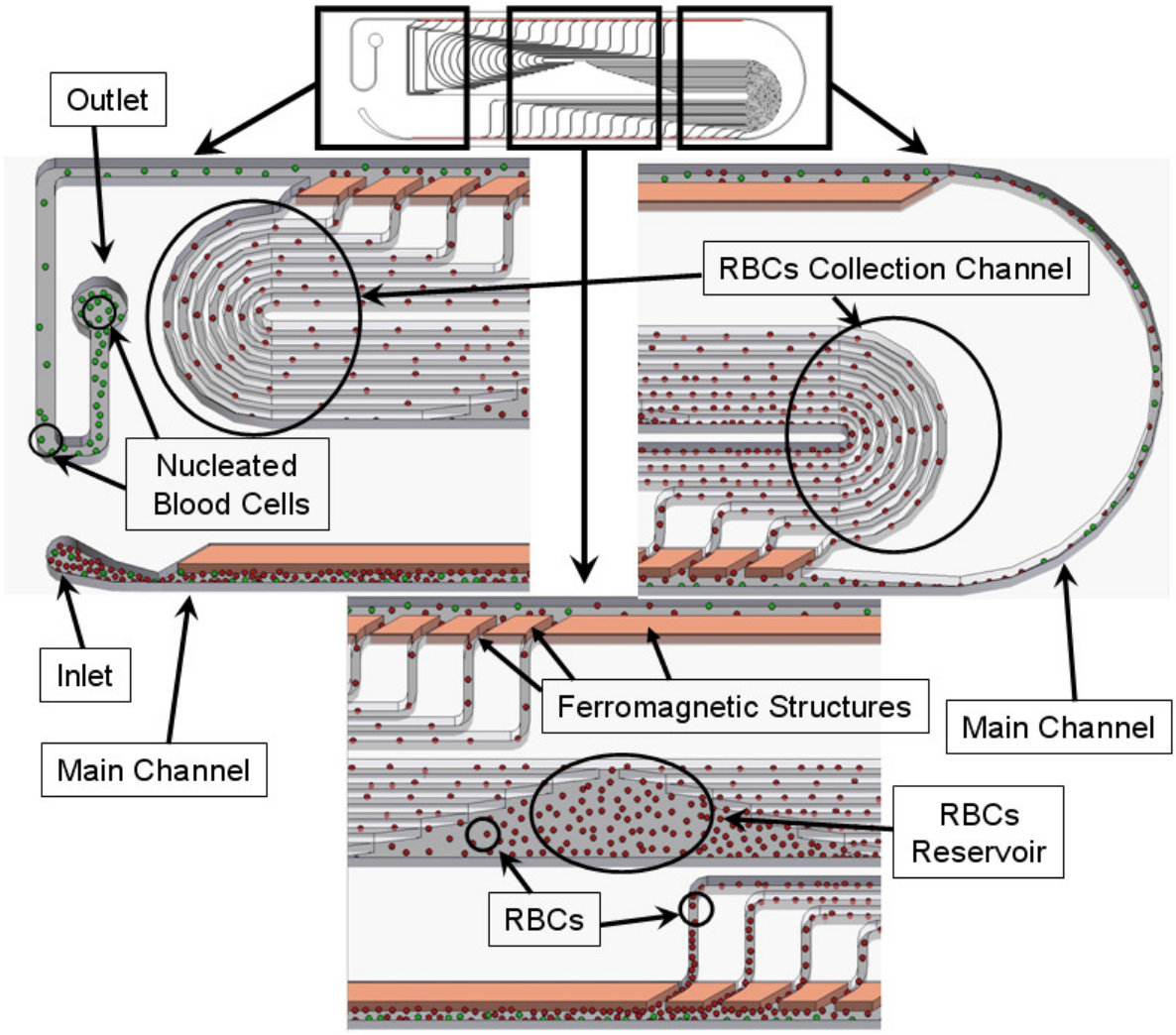

Figure 8.3. Design overview and operational principle of the multiple stage magnetophoresis microsystem.

The design of the microfluidic channels was revised so that the RBC collection channels from each separation stage remain separated until reaching the outlet waste reservoir. The operation principle is similar to that of the previously presented blood cell separator. The RBCs are moved towards the ferromagnetic structures by an attractive magnetophoretic force, while other nucleated cells stay in the main channel. The length of the first separation stag is designed to be much longer to provide enough trapping-time. By combining forty separation stages in a cascade mode, the RBC level in the main channel will be reduced stage by stage and only nucleated cells will be collected in the outlet. The two mask layers for the microfluidic channels and electroplated ferromagnetic structures are shown in Figure 8.4.

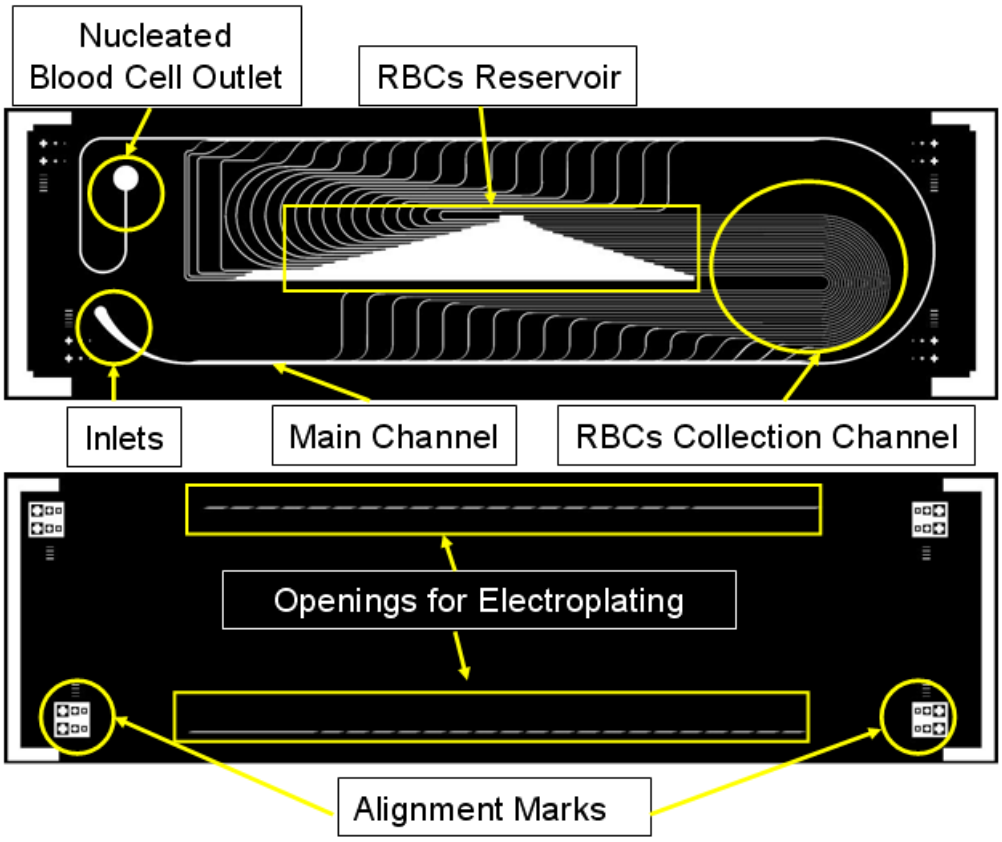

Figure 8.4. Mask designs for microfluidic channel (top) and electroplated ferromagnetic structures (bottom).

8.4 Microsystem Fabrication and Interface / Packaging

The microfluidic interface for the combined continuous flow microseparator consists of two inlet ports. The big center opening in the interface shown in the top figure of Figure 8.5 is to provide an opening for the two outlets for malignant tumor cells and normal nucleated blood cells, while offering additional bonding areas between the interface and the glass chip. Similarly to the previously described interfaces, each port has two rubber O-rings inserted and the interface has a "[" shaped edge to give spaces for the system package tip holder (Figure 8.5).

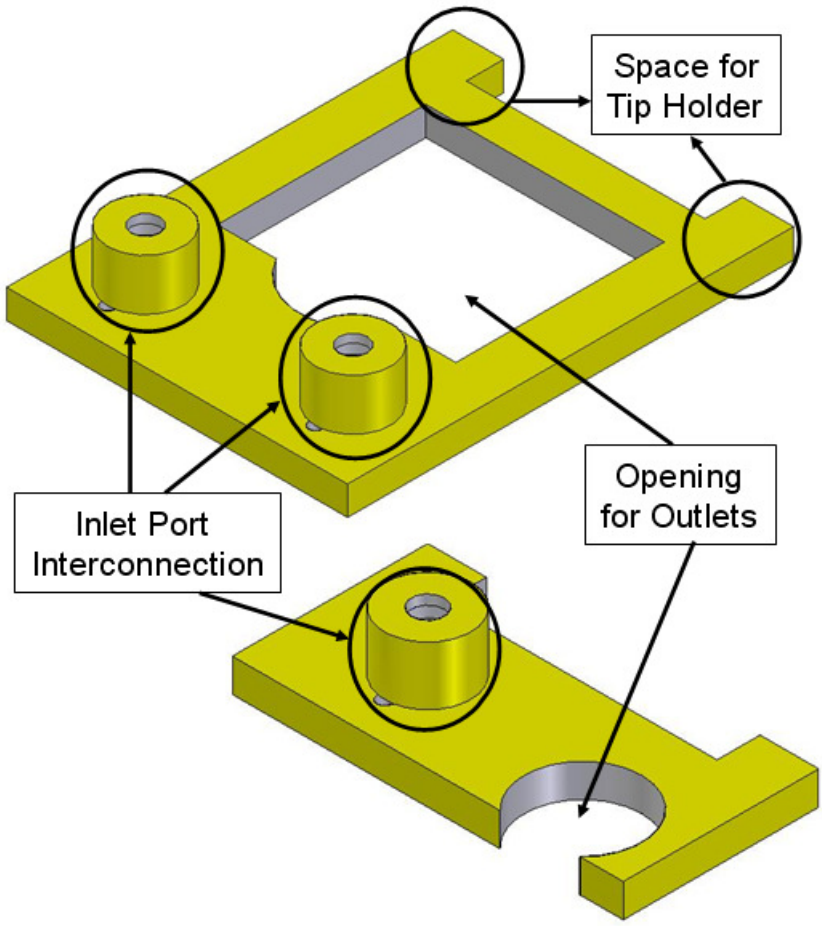

Figure 8.5. Microfluidic interface design: combined microseparator (top) and multiple stage magnetophoresis system (bottom).

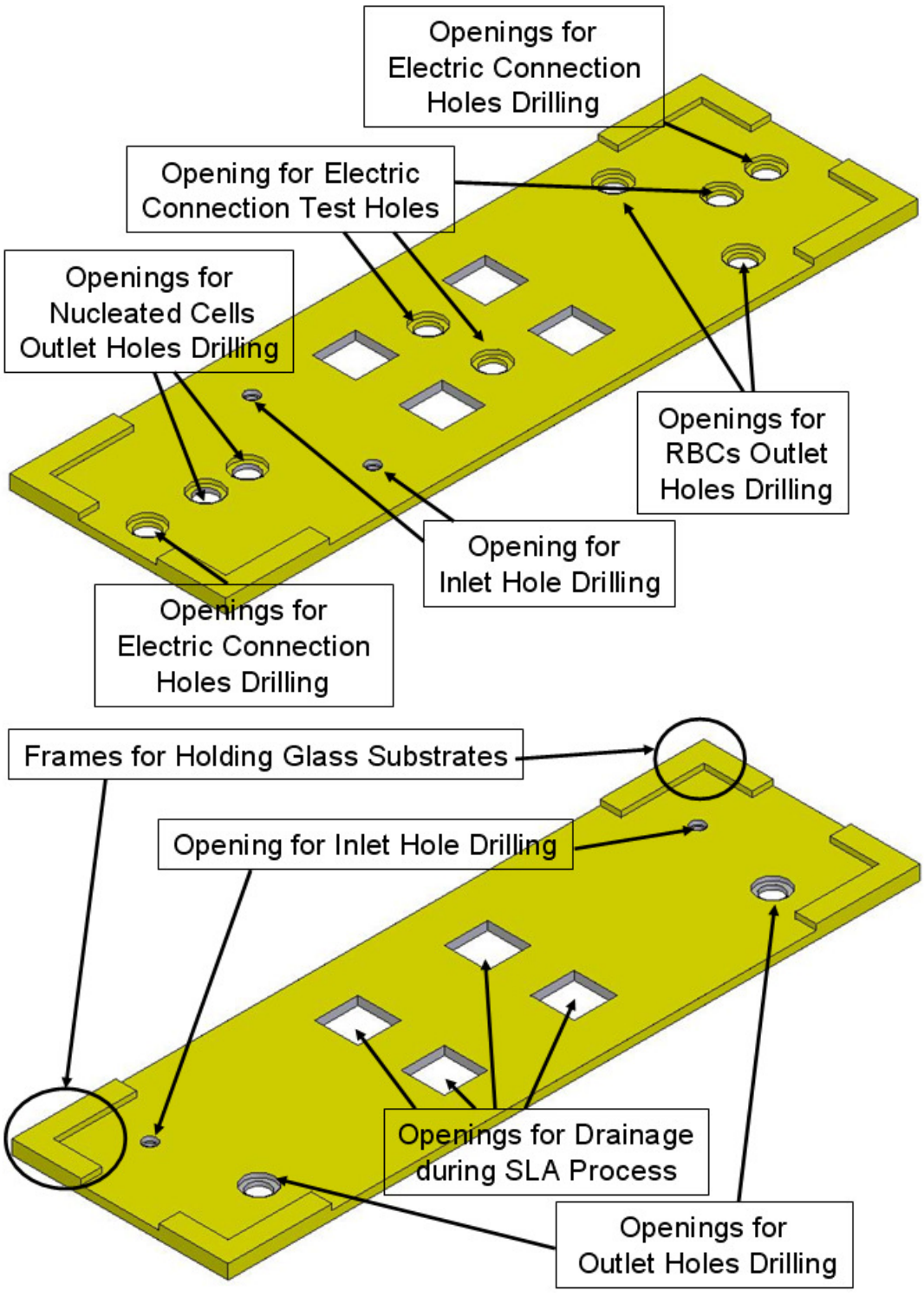

Figure 8.6. The drilling guide for combined microsystem (top) and multiple magnetophoresis system (bottom).

The system packaging presented in Chapter 4 is used for both the combined microseparator and the new multi-stage magnetophoresis system. The drilling guide design for correct positioning of the inlet / outlet ports and electrical connection / test holes in the top glass substrate is shown in Figure 8.6.

The combined microsystem is composed of microfluidic channels, ferromagnetic separation structures, comb-shape planar electrodes, inlet / outlet and electric connection holes, and microfluidic interfaces. The overall fabrication process of the microseparator is more complicated than those of previously presented microsystems since it has both magnetophoresis and dielectrophoresis components. The fabrication process consists of wet etching of the glass substrate for microfluidic channels, electroplating of ferromagnetic separation structures, patterning of comb-shaped planar electrodes, glass-to-glass bonding, glass-to-plastic bonding of the microfluidic interfaces, and electric wire bonding to the microsystem. The overall fabrication process is shown in Figure 8.7.

Layers of sputtered Cr / Au are used as protective layers along with patterned photoresist during a hydrofluoric acid wet etching process to create 50 μm deep microfluidic channels as previously described in Chapter 3, 4, 6, and 7. After removing the residual photoresist and metal masking layers, the glass slide with the microchannels is cleaned in a piranha solution (Figure 8.7(a)). Then Ti / Cu / Cr electroplating seed layers are sputtered and a mold for the ferromagnetic structures in the magnetophoretic separation stage is made with another photolithography step using thick photoresist. The softbake process of thick photoresist is carried out identically to the softbake described in Chapter 3 and 4. Ni / Fe permalloy

ferromagnetic structures are electroplated as tall as 50 μm tall as described in Chapter 4 (Figure 8.7(b)).

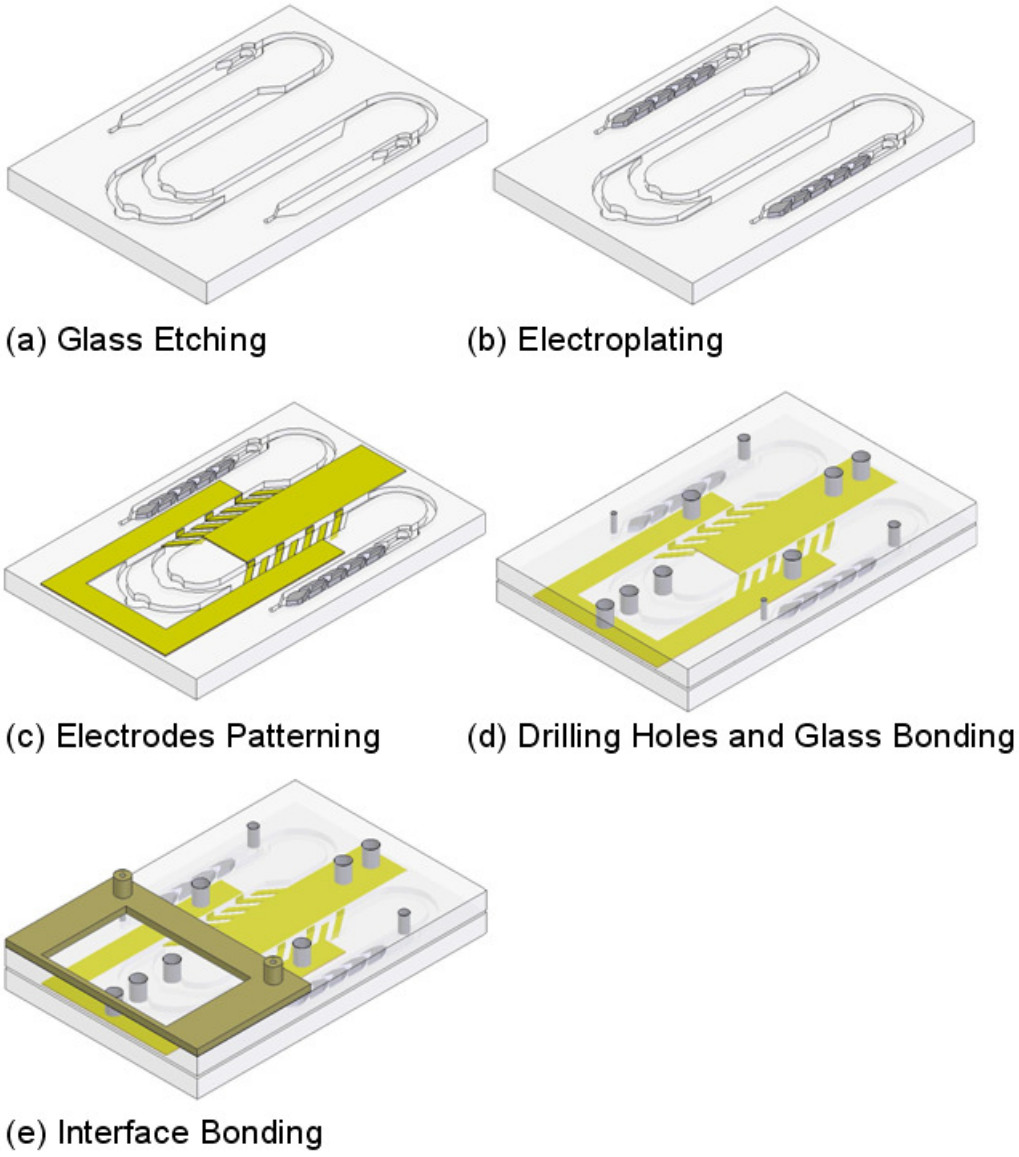

Figure 8.7. The fabrication process of the combined microsystem.

After removing the thick photoresist molds and seed metal layers, another Cr / Au layers for planar electrodes are sputtered with a DC sputterer on the front-side surface of the etched glass substrate. Then, a thick photoresist is used to pattern a comb-shape electrode as described in Chapter 6 and 7 (Figure 8.7©).

The inlet / outlet holes and electric connection / test holes are drilled using 1.0 mm / 2.0 mm diamond drill bits in a blank glass slide using an SLA-fabricated drilling guide. The drilled top glass slide is aligned and bonded to the microfluidic channel defined bottom glass slide by introducing UV curable adhesive as described in previous chapters (Figure 8.7(d)). A microfluidic interface is bonded to the microseparator by repeating the UV curable adhesive bonding process (Figure 8.7(e)). Finally, two wires are connected to each contact pad through the electrical connection holes using conductive silver paste as described in Chapter 7. The electrical connection is tested by measuring the resistance between the wire end and an electric connection test hole.

Although most of the fabrication steps are similar to that of previously developed microsystem, there are several problems expected in the fabrication process. The first one is the problem in the patterning of comb-shaped electrodes. In the development of previous MAP and DEP microsystem, an Au layer was etched with iodine-based gold etchant. However, during a preliminary fabrication, electroplated NiFe structures were damaged or weakened in the gold etchant. Therefore, new etchant or etching method for the patterning of the electrodes must be considered. Another possible problem is the drilling process for various holes. The drilling process was done with a conventional bench top drill press machine. However, the number of holes in the microseparator was almost doubled from the previous microsystem, and this increases the possibility of the glass slide shatter in the glass drilling. A drill with higher rotational speeds may be required.

The overview of fabrication process of the multiple magnetophoresis system is shown in Figure 8.8. Each fabrication step is identical to that of the previously presented microsystem in Chapter 4.

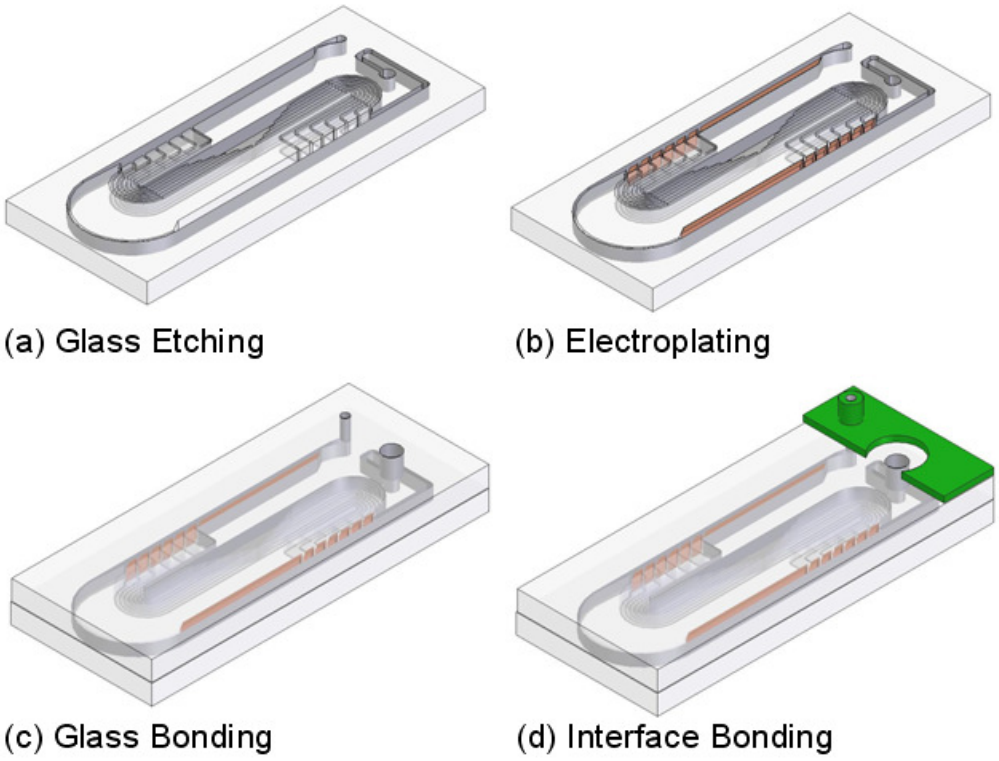

Figure 8.8. The fabrication process of the multiple magnetophoresis microsystem.

Pictures of the microchannel with electroplating molds are shown in Figure 8.9. Before the electroplating process, a Cr layer is removed to expose the Cu layer underneath by submerging the device in a 50 % hydrochloric acid solution. Because of the small size of each mold, additional care is needed to prevent bubbles in the mold cavity. Pictures of the electroplated structures on a device before bonding are shown in Figure 8.10. An oblique channel between two electroplated structures is shown connected to a RBCs collection channel.

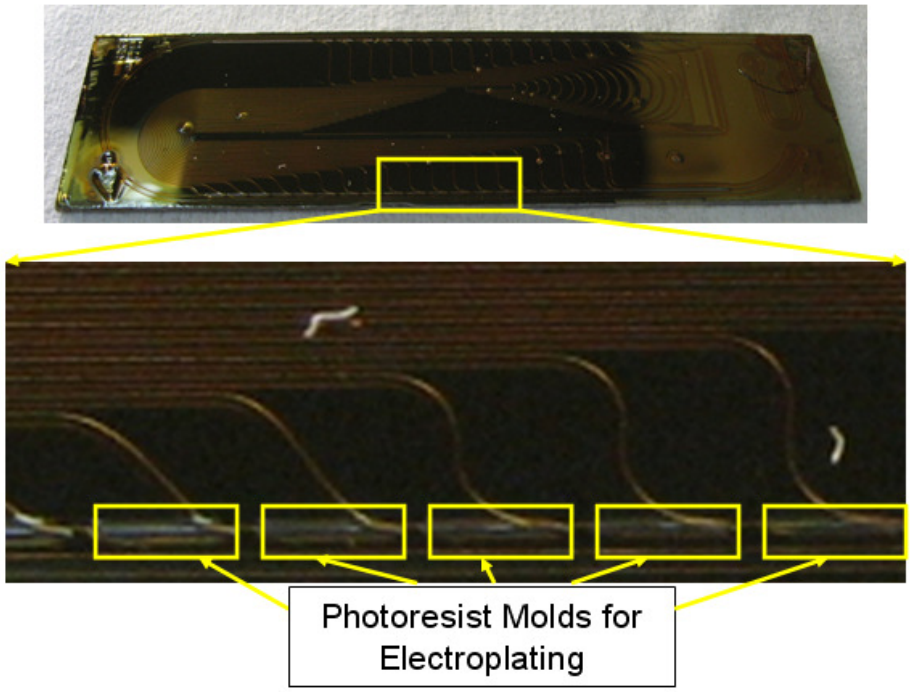

Figure 8.9. The picture of the electroplating molds for the multiple magnetophoresis microsystem.

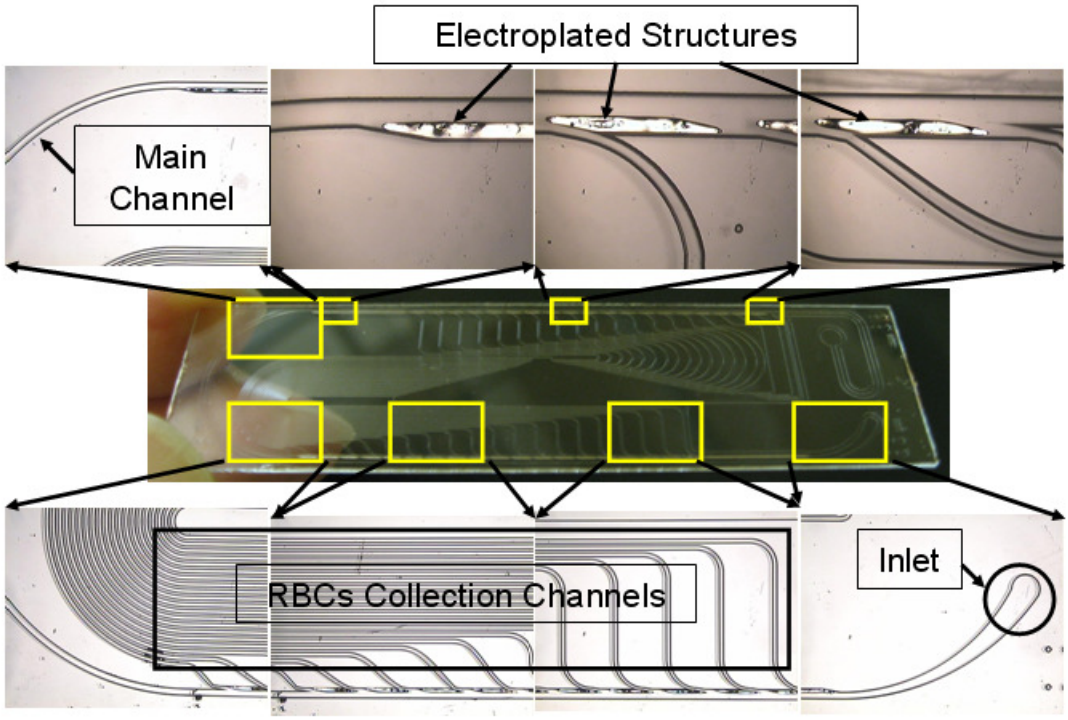

Figure 8.10. The microfluidic channel with electroplated ferromagnetic structures before the bonding process.

For the glass-to-glass bonding process, UV curable adhesive bonding was tried first. However, because of the device's complex microfluidic channels, the introduced adhesive blocked one or more microchannel and the bonding process was unsuccessful. A bonding process using PDMS as described in Chapter 4 was also tried without an adequate result. Finally, a thermal glass fusion bonding process was carried out. It gave a better result compared to those with UV adhesive and PDMS bonding, but an area of the main channel shown in the top-left image in Figure 8.10 and areas at the edge of a glass slide were always blocked or narrowed by fused glass material (Figure 8.11).

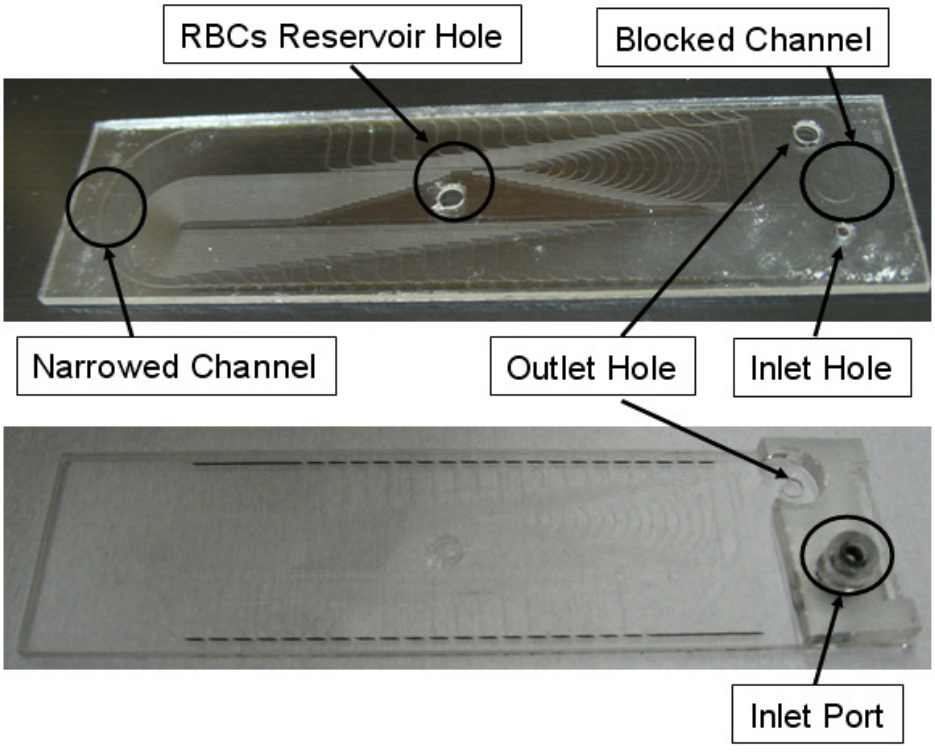

Figure 8.11. The picture of the microsystem after glass-to-glass bonding (top) and glass-to-plastic bonding of an interface.

8.5 Experimental Methods

The integrated microfluidic system could be tested with a whole blood sample spiked with malignant tumor cells. Human venous blood could be collected into evacuated glass tubes, containing EDTA as an anticoagulant. 212LN head / neck cancer cells could be used as malignant tumor cells. The malignant tumor cells could be cultured in DMEM / F12 medium (1:1) supplemented with 10 % FBS at 37 °C in a humidified atmosphere with 5 % CO_2 as described in the previous chapters. The cells could be detached with Cellstripper™ solution following wash / aspiration / incubation procedures and collected by centrifugation. SYTO-13 fluorescent dye could be used to identify the tagged cancerous cells during experiments. For the fluorescent tagging, the collected cancer cells could be incubated for additional 2 hours with SYTO-13 fluorescent dye in an incubator. The tagged cancer cells could be filtered through a cell strainer with a 20 μm mesh size before re-suspending in the prepared blood samples.

Before introducing the sample, the microseparator could be treated similarly with a surfactant solution to reduce the adhesion of cells on the microfluidic channel surface during the experiments. The microsystem could be assembled into the SLA system packaging presented in Chapter 4 and the attached wires could be connected to a function generator. Two 500 μL gas tight glass syringe could be used to load the blood sample spiked with the tumor cells. A syringe pump capable of pumping two syringes at the same flow rate could be used.

The rare cell isolation of the integrated microsystem is characterized in two ways. First, the number of the separated cancer cells is compared to that of the introduced

ones to provide rare cell recovery efficiency. This could be done by counting the fluorescent tumor cells in each outlet using video motion capture. Second, the number of normal blood cells in each collection outlet is measured to determine the rare cell concentration efficiency. The number of blood cells could be counted using a Coulter Cell Counter.

The multiple magnetophoresis system could be tested with an identical experimental setup to that demonstrated in Chapter 3 for the six-stage PMMS system.

CHAPTER 9

CONCLUSIONS AND FUTURE WORK

9.1 Summary

The objective of my research was to develop microsystem based separation technologies for whole cell cancer analysis using human whole blood as the input sample. Two different approaches have been demonstrated; one based on a miniaturized cascade magnetophoresis system and a second based on dielectrophoresis, both enable efficient and novel separation of targeted rare cells from human whole blood. Both systems can be fabricated using MEMS technologies combined with plastic fabrication techniques. Several versions of the magnetophoresis and dielectrophoresis microsystems were designed, fabricated, packaged, and characterized for different applications. Also the design of a magnetophoresis and dielectrophoresis integrated continuous flow microseparator was presented.

Each microsystem consisted of microfluidic channels, inlet / outlet ports, ferromagnetic structures and / or comb-shaped electrodes, a microfluidic interface, and system packaging. For the operation of each microsystem, a blood or tumor cell sample was loaded in a gas-tight glass syringe and introduced into a device through Teflon ^{TM} tubing and an SLA-based interface. In the magnetophoresis system, the RBCs or the magnetic cells in the sample experienced a strong magnetophoretic force under a non-uniform magnetic field created by external permanent magnets and electroplated ferromagnetic structures. This allowed the RBCs to be separated from

the nucleated blood cells or the tagged cells to be separated from the non-magnetic cells. In the dielectrophoresis system, cells with different dielectric properties experienced either positive or negative dielectrophoretic force under a non-uniform electric field created by an external AC signal and comb-shaped electrodes and moved from their original positions in a laminar flow pattern to different positions. Several applications for magnetophoresis and dielectrophoresis were demonstrated.

The first magnetophoresis microsystem, the six-stage cascade paramagnetic mode magnetophoretic separation system, was designed and has successfully shown high throughput RBC separation from a human whole blood sample. The overall design was based on the previously developed magnetophoresis system and in order to optimize the separation throughput and efficiency, several design changes were made with theoretical consideration and calculations. The new design increased the throughput of the magnetophoresis system more than four times over the previous magnetophoretic separation system. However, the design changes caused several unexpected fabrication problems and required additional efforts. The increase in the depth of the microchannel design required an extra stirring process in the middle of the glass wet-etching process. Also, it created a curing issue because much thicker photoresist layer was required for electroplating molds. The larger area of the electroplated ferromagnetic structures made an electroplating process much longer and brought about problems such as unevenness in the height between the electroplated structures. Bubble creation in the photoresist molds during the electroplating process was another issue that needed to be addressed. The drilling of several holes in a glass slide created another challenge and a drilling guide was used

with a drilling machine to solve the issue. The thermal bonding of two glass slides was a major problem as it had broken lots of devices in their final fabrication process, and alternative approach using UV curable adhesive for glass-to-glass bonding was developed. The bonding of interface to the glass slide was not huge problem, but it was modified for better results. All the aforementioned problems in the fabrication of the microsystem had been solved one by one through trial and error over time. The design of the system packaging was modified several times to ensure better experimental conditions. Later, while doing the experiments, it was found that in order to observe cell movements better, the inlet and outlet holes should have been placed further away from the main separation chamber, thus the overall design was updated.

The second magnetophoresis microsystem was developed for the isolation of malignant cancer cells from benign tumor cells and has successfully separated malignant tumor cells tagged with magnetic nanoparticles based on their surface expression level of a specific protein from benign tumor cells. The design of the second magnetophoresis system was revised from that of the first one to address the specific problems in this application. The size of the microchannel, the shape of ferromagnetic structures, and the number of separation stages were adjusted. Since the magnetic nanoparticle tagged cells showed much higher magnetophoretic force than RBCs, for the comparable magnetophoretic force to be applied to the tagged cells, the magnetic field intensity needed to be adjusted. The design of the system packaging was changed so that the relative position of permanent magnets to the microsystem, thus the magnetic field intensity on the microsystem could be adjusted.

Techniques learned during fabrication of the first magnetophoresis system were applied to fabrication of the second, and there were no major issues in the development of the new magnetophoresis system. A new bonding method using PDMS as a gapping and bonding layer was tried for the case when the ferromagnetic structures were over-electroplated. Head / neck cancer cells were cultured and detached from the culture plate later for the experiments. Unwanted cell cluster often caused a microchannel blockage and a cell strainer was used to pre-filter the cancer cell sample.

Both dielectrophoresis systems were developed side by side. One dielectrophoresis system tested its switching and separation capability based on the native dielectric properties of different cell types, while the other investigated the frequency response of different cell types by measuring their crossover frequencies in a medium with different conductivity. One major problem in the fabrication process of the dielectrophoresis system was the electrode disconnection at the edge of the microchannel. Also, the unique design of sheath flow introduction channel, encircling the sample inlet hole, created an issue in the bonding process using UV curable adhesive. Initially, the quality of silver paste used to bond wires to contact the pads caused much higher electrical resistance between a wire end and an electrical connection test hole. Even after overcoming the fabrication problems, there were issues in the experiments such as the electrolysis of water at a low frequency below 1 kHz, resulting in damage to the electrodes. In addition, the conductivity of the fluid in the separation chamber varied depending on the flow condition of the sheath fluid, making separation of target cells complicated because their crossover frequencies

changed accordingly. After all the efforts to solve the problems, the dielectrophoresis systems successfully demonstrated their switching and separating capabilities.

9.2 Future Work

The developed magnetophoresis systems have demonstrated improved throughput in the removal of RBC from a human whole blood sample and its application to the separation of tagged cancer cells based on their surface expression level of a specific protein. In an effort to improve the throughput of RBC removal, another magnetophoresis with 40 separation stages was proposed. The microsystem and its interface were designed and the fabrication process was successful except the glass-to-glass bonding process. The bonding process of the proposed microsystem is challenging because of it much complicated microfluidic channel design and resulting higher possibility of channel blockage during the bonding process. For future work, the microsystem will be fabricated with a bonding process and tested with an undiluted or less diluted human blood sample.

The dielectrophoresis microsystem has successfully shown the ability to switch a blood stream between two outlets and to separate WBCs from a human whole blood sample. Based on the experimental results for the dielectrophoresis response of different blood cell types and head / neck cancer cells, the experiments separating cancer cells from normal nucleated blood cells was carried out successfully. Han et al. (REF #67) have reported that they separated WBCs from a whole blood sample in a high conductive medium, using a difference in the magnitude of negative dielectrophoretic forces between various cell types. For future

work, the microsystem will be further investigated with respect to its application to a high conductive medium.

The magnetophoresis and dielectrophoresis integrated system has been proposed and designed. The system could be fabricated considering the possible problems previously stated and could be tested for the separation of malignant tumor cells from a human blood sample. The results will probably suggest an update in the design of the microsystem as well as the experimental protocol. An alternative flexible material for a device substrate could be sought to investigate its practical applications for the continuous removal of malignant cells from the human body.

APPENDIX A

Six Stage Cascade Paramagnetic Mode Magnetophoretic Separation System Fabrication Process. (Bottom Substrate)

1. Begin with a bare Schott Borofloat glass
   SB-1, 75.0 mm × 20.0 mm × 0.7 mm

2. Informal Cleaning Process
   Submerge in H_2SO_4:H_2O_2 (1:1) for 10 min
   Rinse with DI water 6 times
   Submerge in HF (50:1) for 30 sec
   Rinse with DI water 6 times

3. Cr / Au Sputtering (Front and Back sides)
   Equipment: Unifilm Sputter
   Cr nominal deposition rate: 600 Å/min
   Au nominal deposition rate: 800 Å/min
   Cr target thickness: 500 Å
   Au target thickness: 2000 Å

4. 1st Lithography for Microchannel (Shipley 1813 positive)
   Equipment: OAI Mask Aligner
   Spin @ 5000 rpm, 1500 rpm/sec ramp, 30 sec
   Softbake in Oven @ 115 °C for 60 sec
   Expose with H line (405 nm)
      UV intensity: ~ 9 mW/cm^2
      Target exposure energy: 150 mJ/cm^2
      Expose time: ~ 17 sec
   Develop with MF 319
      Develop time: ~20 sec

Rinse with DI water 6 times

Paint Back side and perimeter edges

Cotton swab soaked with Shipley 1813

Hardbake in Oven @ 120 °C for 5 min

5. Au / Cr Etching

Au etchant: Potassium Iodide 100 g/L and Iodine 25 g/L

Submerge in Au etchant for 1~2 min

Inspect front side Cr layer

Rinse with DI water 6 times

Submerge in Cr etchant (CR-7) for 1~2 min

Inspect back side Cr layer

Rinse with DI water 6 times

6. Glass Etching for Microchannel

Etching solution for etching two glass slides

HF (49 %): 130 mL

DI water: 130 mL

HNO_3: 40 mL

Submerge the glass slide for 50 min

Carefully Rinse with DI water

Submerge the glass slide for additional 20 min

Target depth: 100 μm

Rinse with DI water 6 times

7. Photoresist Removal

Submerge in hot acetone for 10 min

Rinse with DI water 6 times

Submerge in H_2SO_4:H_2O_2 (1:1) for 10 min

Let both sides exposed to the solution

Rinse with DI water 6 times

8. Au / Cr Etching

   Submerge in Au etchant for 1~2 min

   Rinse with DI water 6 times

   Submerge in Cr etchant for 1~2 min

   Rinse with DI water 6 times

9. Bottom Glass Cleaning

   Submerge in H_2SO_4:H_2O_2 (1:1) for 10 min

   Rinse with DI water 6 times

   Submerge in HF (50:1) for 30 sec

   Rinse with DI water 6 times

10. Ti / Cu / Cr Seed Layer Sputtering (Front Side)

    Equipment: Unifilm Sputter

    Ti nominal deposition rate: 300 Å/min

    Ti target thickness: 250 Å

    Cu nominal deposition rate: 800 Å/min

    Cu target thickness: 1200 Å

    Cr nominal deposition rate: 600 Å/min

    Cr target thickness: 1000 Å

11. 2nd Lithography for Ferromagnetic Structures (AZ 9260 positive)

    Equipment: MA-6 Mask Aligner

    Spin @ 300 rpm, 500 rpm/sec ramp, 35 sec

    Photoresist Stabilization

        15 min in an open air

        15 min in a sealed container

    Softbake on Hot plate @ 110 °C for 20 min

        Cool down in air for 30 min

    Expose with H line (405 nm: CI2)

UV intensity: ~ 18 mW/cm^2

Target exposure energy: 3800 mJ/cm^2

Expose time: ~ 200 sec

Develop with AZ 400K: DI (1:2.5)

Develop time: ~10 min

Rinse with DI water 6 times

12. Shielding Perimeter Edges

Paint with cotton swab soaked with Shipley 1813

13. Cr Etching

Cr etchant: HCl: DI (1:1)

Submerge the device and catalyze by using an Al foil

Rinse with DI water

14. NiFe Electroplating

Electroplating Bath

Nickel Sulfate ($NiSO_4$ $6H_2O$): 200 g/L

Ferrous Sulfate ($FeSO_4$ $7H_2O$): 8 g/L

Nickel Chloride ($NiCl_2$ 6 H_2O): 5 g/L

Boric Acid (H_3BO_3): 25 g/L

Saccharin ($C_7H_5NO_3S$): 3 g/L

Nickel anode, pH: 4, Temp: 20~25 °C

Current: 20 mA

Process time: ~ 10 hrs

Switch contact side after 5, 5, 10, 10, 15, 15, 30, 30, 60, 60, 90, 90, 90, and 90 min

Cover the submerged contact with blue tape.

15. PR Removal

Submerge in hot acetone for 5 min

Rinse with DI water 6 times

Submerge in hot acetone for 5 min

Rinse with DI water 6 times

16. Mechanically Peel off the NiFe electroplated on the perimeter edges

17. Ti / Cu / Cr Etching

Cr etchant: HCl: DI (1:1)

Submerge and catalyze by using an Al foil

Rinse with DI water 6 times

Cu etchant: Cupric Sulfate in Ammonium Hydroxide

Submerge in Cu etchant for 1 min

Rinse with DI water 6 times

Ti etchant: HF (10:1)

Submerge in Ti etchant for 5 sec

Rinse with DI water 6 times

18. Glass Surface Cleaning

Submerge in HF (50:1) for 30 sec

Rinse with DI water 6 times

APPENDIX B

The Dielectrophoresis Separation System Fabrication Process. (Bottom Substrate)

1. Begin with a bare Schott Borofloat glass
   SB-1, 75.0 mm × 20.0 mm × 0.7 mm

2. Informal Cleaning Process
   Submerge in H_2SO_4:H_2O_2 (1:1) for 10 min
   Rinse with DI water 6 times
   Submerge in HF (50:1) for 30 sec
   Rinse with DI water 6 times

3. Cr / Au Sputtering (Front and Back sides)
   Equipment: Unifilm Sputter
   Cr nominal deposition rate: 600 Å/min
   Au nominal deposition rate: 800 Å/min
   Cr target thickness: 500 Å
   Au target thickness: 2000 Å

4. 1st Lithography for Microchannel (Shipley 1813 positive)
   Equipment: OAI Mask Aligner
   Spin @ 5000 rpm, 1500 rpm/sec ramp, 30 sec
   Softbake in Oven @ 115 °C for 60 sec
   Expose with H line (405 nm)
      UV intensity: ~ 9 mW/cm^2
      Target exposure energy: 150 mJ/cm^2
      Expose time: ~ 17 sec
   Develop with MF 319
      Develop time: ~20 sec

Rinse with DI water 6 times

Paint Back side and perimeter edges

Cotton swab soaked with Shipley 1813

Hardbake in Oven @ 120 °C for 5 min

5. Au / Cr Etching

Au etchant: Potassium Iodide 100 g/L and Iodine 25 g/L

Submerge in Au etchant for 1~2 min

Inspect front side Cr layer

Rinse with DI water 6 times

Submerge in Cr etchant (CR-7) for 1~2 min

Inspect back side Cr layer

Rinse with DI water 6 times

6. Glass Etching for Microchannel

Etching solution for etching two glass slides

HF (49 %): 130 mL

DI water: 130 mL

HNO_3: 40 mL

Submerge the glass slide for 28 min

Rinse with DI water 6 times

7. Photoresist Removal

Submerge in hot acetone for 10 min

Rinse with DI water 6 times

Submerge in H_2SO_4:H_2O_2 (1:1) for 10 min

Let both sides exposed to the solution

Rinse with DI water 6 times

8. Au / Cr Etching

Submerge in Au etchant for 1~2 min

Rinse with DI water 6 times

Submerge in Cr etchant for 1~2 min

Rinse with DI water 6 times

9. Bottom Glass Cleaning

Submerge in H_2SO_4:H_2O_2 (1:1) for 10 min

Rinse with DI water 6 times

Submerge in HF (50:1) for 30 sec

Rinse with DI water 6 times

10. Cr / Au Sputtering (Front sides

Equipment: Unifilm Sputter

Cr nominal deposition rate: 600 Å/min

Au nominal deposition rate: 800 Å/min

Cr target thickness: 500 Å

Au target thickness: 2500 Å

11. 2nd Lithography for Ferromagnetic Structures (AZ 9260 positive)

Equipment: MA-6 Mask Aligner

Spin @ 300 rpm, 500 rpm/sec ramp, 35 sec

Photoresist Stabilization

15 min in an open air

15 min in a sealed container

Softbake on Hot plate @ 110 °C for 20 min

Cool down in air for 30 min

Expose with H line (405 nm: CI2)

UV intensity: ~ 18 mW/cm^2

Target exposure energy: 3800 mJ/cm^2

Expose time: ~ 200 sec

Develop with AZ 400K: DI (1:2.5)

Develop time: ~10 min

Rinse with DI water 6 times

12. Au / Cr Etching

Submerge in Au etchant for 1~2 min

Rinse with DI water 6 times

Submerge in Cr etchant for 1~2 min

Rinse with DI water 6 times

13. PR Removal

Submerge in hot acetone for 5 min

Rinse with DI water 6 times

Submerge in hot acetone for 5 min

Rinse with DI water 6 times

REFERENCES

[1] M. Heron, D. L. Hoyert, S. L. Murphy, J. Xu, K. D. Kochanek, and B. Tejada-Vera**, "**Deaths: Final Data for 2006**,"** *National Vital Statistics Reports,* vol. 57, No. 14, April 2009.

[2] American Cancer Society, *Cancer Prevention & Early Detection Facts & Figures 2009*. Atlanta, GA: American Cancer Society, 2009.

[3] American Cancer Society, *Cancer Statistics 2009 Presentation.* Atlanta, GA: American Cancer Society, 2009.

[4] M. J. Horner, L. A. G. Ries, M. Krapcho, N. Neyman, R. Aminou, N. Howlader, S. F. Altekruse, E. J. Feuer, L. Huang, A. Mariotto, B. A. Miller, D. R. Lewis, M. P. Eisner, D. G. Stinchcomb, and B. K. Edwards. *SEER Cancer Statistics Review, 1975-2006*, National Cancer Institute. http://seer.cancer.gov/csr/1975_2006/, based on November 2008 SEER data submission, posted to the SEER web site, 2009.

[5] "Screening and Testing to Detect Cancer," http://www.cancer.gov/cancertopics/screening, Oct. 20, 2009.

[6] D. W. Fairbairn, P. L. Olive, and K. L. Oneill, "THE COMET ASSAY - A COMPREHENSIVE REVIEW," *Mutation Research-Reviews in Genetic Toxicology,* vol. 339, pp. 37-59, Feb 1995.

[7] M. Hollstein, D. Sidransky, B. Vogelstein, and C. C. Harris, "P53 MUTATIONS IN HUMAN CANCERS," *Science,* vol. 253, pp. 49-53, Jul 1991.

[8] B. T. Kurien and R. H. Scofield, "Protein blotting: a review," *Journal of Immunological Methods,* vol. 274, pp. 1-15, Mar 2003.

[9] E. Stockert, E. Jager, Y. T. Chen, M. J. Scanlan, I. Gout, J. Karbach, M. Arand, A. Knuth, and L. J. Old, "A survey of the humoral immune response of cancer patients to a panel of human tumor antigens," *Journal of Experimental Medicine,* vol. 187, pp. 1349-1354, Apr 1998.

[10] T. J. McDonnell, P. Troncoso, S. M. Brisbay, C. Logothetis, L. W. K. Chung, J. T. Hsieh, S. M. Tu, and M. L. Campbell, "EXPRESSION OF THE PROTOONCOGENE BCL-2 IN THE PROSTATE AND ITS ASSOCIATION WITH EMERGENCE OF ANDROGEN-INDEPENDENT PROSTATE-CANCER," *Cancer Research,* vol. 52, pp. 6940-6944, Dec 1992.

[11] H. J. Issaq, T. D. Veenstra, T. P. Conrads, and D. Felschow, "The SELDI-TOF MS approach to proteomics: Protein profiling and biomarker identification," *Biochemical and Biophysical Research Communications,* vol. 292, pp. 587-592, Apr 2002.

[12] J. Villanueva, J. Philip, D. Entenberg, C. A. Chaparro, M. K. Tanwar, E. C. Holland, and P. Tempst, "Serum peptide profiling by magnetic particle-assisted, automated sample processing and MALDI-TOF mass spectrometry," *Analytical Chemistry,* vol. 76, pp. 1560-1570, Mar 2004.

[13] G. MacBeath, "Protein microarrays and proteomics," *Nature Genetics,* vol. 32, pp. 526-532, Dec 2002.

[14] S. Spisak, Z. Tulassay, B. Molnar, and A. Guttman, "Protein microchips in biomedicine and biomarker discovery," *Electrophoresis,* vol. 28, pp. 4261-4273, Dec 2007.

[15] N. Ramalingam, H. B. Liu, C. C. Dai, Y. Jiang, H. Wang, Q. H. Wang, K. M. Hui, and H. Q. Gong, "Real-time PCR array chip with capillary-driven sample loading and reactor sealing for point-of-care applications," *Biomedical Microdevices,* vol. 11, pp. 1007-1020, Oct 2009.

[16] C. S. Zhang and D. Xing, "Miniaturized PCR chips for nucleic acid amplification and analysis: latest advances and future trends," *Nucleic Acids Research,* vol. 35, pp. 4223-4237, 2007.

[17] M. Geear, R. R. A. Syms, S. Wright, and A. S. Holmes, "Monolithic MEMS quadrupole mass spectrometers by deep silicon etching," *Journal of Microelectromechanical Systems,* vol. 14, pp. 1156-1166, Oct 2005.

[18] N. Sillon and R. Baptist, "Micromachined mass spectrometer," *Sensors and Actuators B: Chemical*, vol. 83, pp. 129-137, 2002.

[19] P. Arenkov, A. Kukhtin, A. Gemmell, S. Voloshchuk, V. Chupeeva, and A. Mirzabekov, "Protein microchips: Use for immunoassay and enzymatic reactions," *Analytical Biochemistry,* vol. 278, pp. 123-131, Feb 2000.

[20] H. Zhu, M. Bilgin, R. Bangham, D. Hall, A. Casamayor, P. Bertone, N. Lan, R. Jansen, S. Bidlingmaier, T. Houfek, T. Mitchell, P. Miller, R. A. Dean, M. Gerstein, and M. Snyder, "Global analysis of protein activities using proteome chips," *Science,* vol. 293, pp. 2101-2105, Sep 2001.

[21] D. K. Chatterjee, K. Sitaraman, C. Baptista, J. Hartley, T. M. Hill, and D. J. Munroe, "Protein Microarray On-Demand: A Novel Protein Microarray System," *Plos One,* vol. 3, p. 5, Sep 2008.

[22] G. MacBeath, "Protein microarrays and proteomics," *Nature Genetics,* vol. 32, pp. 526-532, Dec 2002.

[23] W. J. Allard, J. Matera, M. C. Miller, M. Repollet, M. C. Connelly, C. Rao, A. G. J. Tibbe, J. W. Uhr, and L. Terstappen, "Tumor cells circulate in the peripheral blood of all major carcinomas but not in healthy subjects or patients with nonmalignant diseases," *Clinical Cancer Research,* vol. 10, pp. 6897-6904, Oct 2004.

[24] W. A. Bonner, R. G. Sweet, H. R. Hulett, and Herzenbe.La, "FLUORESCENCE ACTIVATED CELL SORTING," *Review of Scientific Instruments,* vol. 43, pp. 404-&, 1972.

[25] L. A. Herzenberg, D. Parks, B. Sahaf, O. Perez, M. Roederer, and L. A. Herzenberg, "The history and future of the fluorescence activated cell sorter and flow cytometry: A view from Stanford," *Clinical Chemistry,* vol. 48, pp. 1819-1827, Oct 2002.

[26] A. Y. Fu, C. Spence, A. Scherer, F. H. Arnold, and S. R. Quake, "A microfabricated fluorescence-activated cell sorter," *Nature Biotechnology,* vol. 17, pp. 1109-1111, Nov 1999.

[27] S. Sergent-Tanguy, C. Chagneau, I. Neveu, and P. Naveilhan, "Fluorescent activated cell sorting (FACS): a rapid and reliable method to estimate the number of neurons in a mixed population," *Journal of Neuroscience Methods,* vol. 129, pp. 73-79, Oct 2003.

[28] Y. Ito and K. Shinomiya, "A new continuous-flow cell separation method based on cell density: Principle, apparatus, and preliminary application to separation of human buffy coat," *Journal of Clinical Apheresis,* vol. 16, pp. 186-191, 2001.

[29] H. Shiono and Y. Ito, "Novel method for continuous cell separation by density gradient centrifugation: Evaluation of a miniature separation column," *Preparative Biochemistry & Biotechnology,* vol. 33, pp. 87-100, 2003.

[30] A. V. Quirk and J. R. Woodrow, "TANGENTIAL FLOW FILTRATION - A NEW METHOD FOR THE SEPARATION OF BACTERIAL ENZYMES FROM CELL DEBRIS," *Biotechnology Letters,* vol. 5, pp. 277-282, 1983.

[31] J. Fluitman, "Microsystems technology: Objectives," *Sensors and Actuators a-Physical,* vol. 56, pp. 151-166, Aug 1996.

[32] C. C. Liu and Z. H. Jin, "Applications of microfabrication and micromachining techniques to biotechnology," *Trends in Biotechnology,* vol. 15, pp. 213-216, Jun 1997.

[33] D. V. McAllister, M. G. Allen, and M. R. Prausnitz, "Microfabricated microneedles for gene and drug delivery," *Annual Review of Biomedical Engineering,* vol. 2, pp. 289-313, 2000.

[34] J. Voldman, M. L. Gray, and M. A. Schmidt, "Microfabrication in biology and medicine," *Annual Review of Biomedical Engineering,* vol. 1, pp. 401-425, 1999.

[35] J. El-Ali, P. K. Sorger, and K. F. Jensen, "Cells on chips," *Nature,* vol. 442, pp. 403-411, Jul 2006.

[36] N. Pamme, "Continuous flow separations in microfluidic devices," *Lab on a Chip,* vol. 7, pp. 1644-1659, 2007.

[37] C. D. Chin, V. Linder, and S. K. Sia, "Lab-on-a-chip devices for global health: Past studies and future opportunities," *Lab on a Chip,* vol. 7, pp. 41-57, 2007

[38] P. Yager, T. Edwards, E. Fu, K. Helton, K. Nelson, M. R. Tam, and B. H. Weigl, "Microfluidic diagnostic technologies for global public health," *Nature,* vol. 442, pp. 412-418, Jul 2006.

[39] A. J. Tudos, G. A. J. Besselink, and R. B. M. Schasfoort, "Trends in miniaturized total analysis systems for point-of-care testing in clinical chemistry," *Lab on a Chip,* vol. 1, pp. 83-95, 2001.

[40] H. Mohamed, L. D. McCurdy, D. H. Szarowski, S. Duva, J. N. Turner, and M. Caggana, "Development of a rare cell fractionation device: Application for cancer detection," *Ieee Transactions on Nanobioscience,* vol. 3, pp. 251-256, Dec 2004.

[41] S. Choi, S. Song, C. Choi, and J. K. Park, "Continuous blood cell separation by hydrophoretic filtration," *Lab on a Chip,* vol. 7, pp. 1532-1538, 2007.

[42] S. Vankrunkelsven, D. Clicq, K. Pappaert, W. Ranson, C. De Tandt, H. Ottevaere, H. Thienpont, G. V. Baron, and G. Desmet, "A novel microstep device for the size separation of cells," *Electrophoresis,* vol. 25, pp. 1714-1722, Jun 2004.

[43] M. Yamada and M. Seki, "Microfluidic particle sorter employing flow splitting and recombining," *Analytical Chemistry,* vol. 78, pp. 1357-1362, Feb 2006.

[44] J. J. Hawkes and W. T. Coakley, "Force field particle filter, combining ultrasound standing waves and laminar flow," *Sensors and Actuators B-Chemical,* vol. 75, pp. 213-222, May 2001.

[45] T. Laurell, F. Petersson, and A. Nilsson, "Chip integrated strategies for acoustic separation and manipulation of cells and particles," *Chemical Society Reviews,* vol. 36, pp. 492-506, 2007.

[46] A. Nilsson, F. Petersson, H. Jonsson, and T. Laurell, "Acoustic control of suspended particles in micro fluidic chips," *Lab on a Chip,* vol. 4, pp. 131-135, 2004.

[47] F. Petersson, A. Nilsson, C. Holm, H. Jonsson, and T. Laurell, "Continuous separation of lipid particles from erythrocytes by means of laminar flow and acoustic standing wave forces," *Lab on a Chip,* vol. 5, pp. 20-22, 2005.

[48] F. Petersson, L. Aberg, A. M. Sward-Nilsson, and T. Laurell, "Free flow acoustophoresis: Microfluidic-based mode of particle and cell separation," *Analytical Chemistry,* vol. 79, pp. 5117-5123, Jul 2007.

[49] K. Dholakia, M. P. MacDonald, P. Zemanek, and T. Cizmar, "Cellular and colloidal separation using optical forces," in *Laser Manipulation of Cells and Tissues*. vol. 82, 2007, pp. 467-495.

[50] M. P. MacDonald, S. Neale, L. Paterson, A. Richies, K. Dholakia, and G. C. Spalding, "Cell cytometry with a light touch: Sorting microscopic matter with an optical lattice," *Journal of Biological Regulators and Homeostatic Agents,* vol. 18, pp. 200-205, Apr-Jun 2004.

[51] Y. Y. Sun, X. C. Yuan, L. S. Ong, J. Bu, S. W. Zhu, and R. Liu, "Large-scale optical traps on a chip for optical sorting," *Applied Physics Letters,* vol. 90, Jan 2007.

[52] M. Ozkan, M. Wang, C. Ozkan, R. Flynn, A. Birkbeck, and S. Esener, "Optical manipulation of objects and biological cells in microfluidic devices," *Biomedical Microdevices,* vol. 5, pp. 61-67, Mar 2003.

[53] Y. H. Lin and G. B. Lee, "Optically induced flow cytometry for continuous microparticle counting and sorting," *Biosensors & Bioelectronics,* vol. 24, pp. 572-578, Dec 2008.

[54] M. M. Wang, E. Tu, D. E. Raymond, J. M. Yang, H. C. Zhang, N. Hagen, B. Dees, E. M. Mercer, A. H. Forster, I. Kariv, P. J. Marchand, and W. F. Butler, "Microfluidic sorting of mammalian cells by optical force switching," *Nature Biotechnology,* vol. 23, pp. 83-87, Jan 2005.

[55] M. P. MacDonald, G. C. Spalding, and K. Dholakia, "Microfluidic sorting in an optical lattice," *Nature,* vol. 426, pp. 421-424, Nov 2003.

[56] R. W. Applegate, J. Squier, T. Vestad, J. Oakey, and D. W. M. Marr, "Optical trapping, manipulation, and sorting of cells and colloids in microfluidic systems with diode laser bars," *Optics Express,* vol. 12, pp. 4390-4398, Sep 2004.

[57] A. F. Ngomsik, A. Bee, M. Draye, G. Cote, and V. Cabuil, "Magnetic nano- and microparticles for metal removal and environmental applications: a review," *Comptes Rendus Chimie,* vol. 8, pp. 963-970, Jun-Jul 2005.

[58] M. Sarikaya, T. Abbasov, and M. Erdemoglu, "Some aspects of magnetic filtration theory for removal of fine particles from aqueous suspensions," *Journal of Dispersion Science and Technology,* vol. 27, pp. 193-198, 2006.

[59] Richard Gerber and Robert R. Birss *High Gradient Magnetic Separation.*

[60] A. Ditsch, J. Yin, P. E. Laibinis, D. I. C. Wang, and T. A. Hatton, "Ion-exchange purification of proteins using magnetic nanoclusters," *Biotechnology Progress,* vol. 22, pp. 1153-1162, Aug 2006.

[61] G. D. Moeser, K. A. Roach, W. H. Green, P. E. Laibinis, and T. A. Hatton, "Water-based magnetic fluids as extractants for synthetic organic compounds," *Industrial & Engineering Chemistry Research,* vol. 41, pp. 4739-4749, Sep 2002.

[62] T. E. Thomas, S. J. R. Abraham, A. J. Otter, E. W. Blackmore, and P. M. Lansdorp, "HIGH-GRADIENT MAGNETIC SEPARATION OF CELLS ON THE BASIS OF EXPRESSION LEVELS OF CELL-SURFACE ANTIGENS," *Journal of Immunological Methods,* vol. 154, pp. 245-252, Oct 1992.

[63] A. J. Richards, O. S. Roath, R. J. S. Smith, and J. H. P. Watson, "The mechanisms of high gradient magnetic separation of human blood and bone marrow," *Ieee Transactions on Magnetics,* vol. 32, pp. 459-470, Mar 1996.

[64] B. B. Yellen, Z. G. Forbes, D. S. Halverson, G. Fridman, K. A. Barbee, M. Chorny, R. Levy, and G. Friedman, "Targeted drug delivery to magnetic implants for therapeutic applications," *Journal of Magnetism and Magnetic Materials,* vol. 293, pp. 647-654, May 2005.

[65] H. T. Chen, A. D. Ebner, A. J. Rosengart, M. D. Kaminski, and J. A. Ritter, "Analysis of magnetic drug carrier particle capture by a magnetizable intravascular stent: 1. Parametric study with single wire correlation," *Journal of Magnetism and Magnetic Materials,* vol. 284, pp. 181-194, Dec 2004.

[66] J. A. Ritter, A. D. Ebner, K. D. Daniel, and K. L. Stewart, "Application of high gradient magnetic separation principles to magnetic drug targeting,"

Journal of Magnetism and Magnetic Materials, vol. 280, pp. 184-201, Sep 2004.

[67] D. L. Siegel, T. Y. Chang, S. L. Russell, and V. Y. Bunya, "Isolation of cell surface-specific human monoclonal antibodies using phage display and magnetically-activated cell sorting: applications in immunohematology," *Journal of Immunological Methods,* vol. 206, pp. 73-85, Aug 1997.

[68] D. J. Richel, H. E. Johnsen, J. Canon, T. Guillaume, M. R. Schaafsma, C. Schenkeveld, S. W. Hansen, I. McNiece, A. J. Gringeri, R. Briddell, C. Ewen, R. Davies, J. Freeman, S. Miltenyi, and M. Symann, "Highly purified CD34(+) cells isolated using magnetically activated cell selection provide rapid engraftment following high-dose chemotherapy in breast cancer patients," *Bone Marrow Transplantation,* vol. 25, pp. 243-249, Feb 2000.

[69] H. Abts, M. Emmerich, S. Miltenyi, A. Radbruch, and H. Tesch, "CD20 POSITIVE HUMAN LYMPHOCYTES-B SEPARATED WITH THE MAGNETIC CELL SORTER (MACS) CAN BE INDUCED TO PROLIFERATION AND ANTIBODY SECRETION INVITRO," *Journal of Immunological Methods,* vol. 125, pp. 19-28, Dec 1989.

[70] J. T. Kemshead and J. Ugelstad, "MAGNETIC SEPARATION TECHNIQUES - THEIR APPLICATION TO MEDICINE," *Molecular and Cellular Biochemistry,* vol. 67, pp. 11-18, 1985.

[71] V. M. Martin, C. Siewert, A. Scharl, T. Harms, R. Heinze, S. Ohl, A. Radbruch, S. Miltenyi, and J. Schmitz, "Immunomagnetic enrichment of disseminated epithelial tumor cells from peripheral blood by MACS," *Experimental Hematology,* vol. 26, pp. 252-264, Mar 1998.

[72] S. Miltenyi, W. Muller, W. Weichel, and A. Radbruch, "HIGH-GRADIENT MAGNETIC CELL-SEPARATION WITH MACS," *Cytometry,* vol. 11, pp. 231-238, 1990.

[73] E. Schulze, C. Siewert, M. Herber, J. Schmitz, M. Assenmacher, and S. Miltenyi, "Highly sensitive detection of disseminated tumor cells using MACS technology," *Cytometry,* vol. 46, pp. 193-194, Jun 2001.

[74] C. Siewert, M. Herber, N. Hunzelmann, O. Fodstad, S. Miltenyi, M. Assenmacher, and J. Schmitz, "Rapid enrichment and detection of melanoma cells from PBMC by a new assay combining immunomagnetic cell sorting and immunocytochemical staining," *Journal of Investigative Dermatology,* vol. 113, pp. 512-512, Sep 1999.

[75] M. Takayasu, N. Duske, S. R. Ash, and F. J. Friedlaender, "HGMS STUDIES OF BLOOD-CELL BEHAVIOR IN PLASMA," *Ieee Transactions on Magnetics,* vol. 18, pp. 1520-1522, 1982.

[76] K. H. Han, A. Han, and A. B. Frazier, "Microsystems for isolation and electrophysiological analysis of breast cancer cells from blood," *Biosensors & Bioelectronics,* vol. 21, pp. 1907-1914, Apr 2006.

[77] K. H. Han and A. B. Frazier, "Paramagnetic capture mode magnetophoretic microseparator for blood cells," *Iee Proceedings-Nanobiotechnology,* vol. 153, pp. 67-73, Aug 2006.

[78] M. Zborowski, G. R. Ostera, L. R. Moore, S. Milliron, J. J. Chalmers, and A. N. Schechter, "Red blood cell magnetophoresis," *Biophysical Journal,* vol. 84, pp. 2638-2645, Apr 2003.

[79] M. Takayasu, D. R. Kelland, and J. V. Minervini, "Continuous magnetic separation of blood components from whole blood," *Ieee Transactions on Applied Superconductivity,* vol. 10, pp. 927-930, Mar 2000.

[80] N. Pamme and C. Wilhelm, "Continuous sorting of magnetic cells via on-chip free-flow magnetophoresis," *Lab on a Chip,* vol. 6, pp. 974-980, 2006.

[81] N. Xia, T. P. Hunt, B. T. Mayers, E. Alsberg, G. M. Whitesides, R. M. Westervelt, and D. E. Ingber, "Combined microfluidic-micromagnetic separation of living cells in continuous flow," *Biomedical Microdevices,* vol. 8, pp. 299-308, Dec 2006.

[82] K. H. Han and A. B. Frazier, "Continuous magnetophoretic separation of blood cells in microdevice format," *Journal of Applied Physics,* vol. 96, pp. 5797-5802, Nov 2004.

[83] M. Toner and D. Irimia, "Blood-on-a-chip," *Annual Review of Biomedical Engineering,* vol. 7, pp. 77-103, 2005.

[84] Y. S. Chang, E. di Tomaso, D. M. McDonald, R. Jones, R. K. Jain, and L. L. Munn, "Mosaic blood vessels in tumors: Frequency of cancer cells in contact with flowing blood," *Proceedings of the National Academy of Sciences of the United States of America,* vol. 97, pp. 14608-14613, Dec 2000.

[85] S. Mocellin, U. Keilholz, C. R. Rossi, and D. Nitti, "Circulating tumor cells: the 'leukemic phase' of solid cancers," *Trends in Molecular Medicine,* vol. 12, pp. 130-139, Mar 2006.

[86] K. H. Han and A. B. Frazier, "Diamagnetic capture mode magnetophoretic microseparator for blood cells," *Journal of Microelectromechanical Systems,* vol. 14, pp. 1422-1431, Dec 2005.

[87] K. H. Han and A. B. Frazier, "Reliability aspects of packaging and integration technology for microfluidic systems," *Ieee Transactions on Device and Materials Reliability,* vol. 5, pp. 452-457, Sep 2005.

[88] A. B. Frazier, "Metallic microstructures fabricated using photosensitive polyimide electroplating molds," *Journal of Microelectromechanical Systems,* vol. 2, pp. 87-94, 1993.

[89] D. A. Colling, "INTRINSIC MAGNETIZATION OF FE-NI-MN ALLOYS," *Journal of Applied Physics,* vol. 40, pp. 1379-&, 1969.

[90] R. Marhaba, P. Klingbeil, T. Nuebel, I. Nazarenko, M. W. Buechler, and M. Zoeller, "CD44 and EpCAM: Cancer-Initiating Cell Markers," *Current Molecular Medicine,* vol. 8, pp. 784-804, Dec 2008.

[91] L. J. Harper, K. Piper, J. Common, F. Fortune, and I. C. Mackenzie, "Stem cell patterns in cell lines derived from head and neck squamous cell carcinoma," *Journal of Oral Pathology & Medicine,* vol. 36, pp. 594-603, Nov 2007.

[92] C. Brakebusch and R. Fassler, "beta 1 integrin function in vivo: Adhesion, migration and more," *Cancer and Metastasis Reviews,* vol. 24, pp. 403-411, Sep 2005.

[93] M. D. Basson, "An intracellular signal pathway that regulates cancer cell adhesion in response to extracellular forces," *Cancer Research,* vol. 68, pp. 2-4, Jan 2008.

[94] H. A. Pohl, *Dielectrophoresis*. New York: Cambridge University Press, 1978.

[95] H. A. Pohl, "SOME EFFECTS OF NONUNIFORM FIELDS ON DIELECTRICS," *Journal of Applied Physics,* vol. 29, pp. 1182-1188, 1958.

[96] P. R. C. Gascoyne and J. Vykoukal, "Particle separation by dielectrophoresis," *Electrophoresis,* vol. 23, pp. 1973-1983, Jul 2002.

[97] H. A. Pohl and I. Hawk, "SEPARATION OF LIVING AND DEAD CELLS BY DIELECTROPHORESIS," *Science,* vol. 152, pp. 647-&, 1966.

[98] F. F. Becker, X. B. Wang, Y. Huang, R. Pethig, J. Vykoukal, and P. R. C. Gascoyne, "SEPARATION OF HUMAN BREAST-CANCER CELLS FROM BLOOD BY DIFFERENTIAL DIELECTRIC AFFINITY," *Proceedings of*

the National Academy of Sciences of the United States of America, vol. 92, pp. 860-864, Jan 1995.

[99] J. S. Crane and H. A. Pohl, "A STUDY OF LIVING AND DEAD YEAST CELLS USING DIELECTROPHORESIS," *Journal of the Electrochemical Society,* vol. 115, pp. 584-&, 1968.

[100] G. H. Markx, M. S. Talary, and R. Pethig, "SEPARATION OF VIABLE AND NONVIABLE YEAST USING DIELECTROPHORESIS," *Journal of Biotechnology,* vol. 32, pp. 29-37, Jan 1994.

[101] C. H. Tai, S. K. Hsiung, C. Y. Chen, M. L. Tsai, and G. B. Lee, "Automatic microfluidic platform for cell separation and nucleus collection," *Biomedical Microdevices,* vol. 9, pp. 533-543, Aug 2007.

[102] M. D. Vahey and J. Voldman, "An equilibrium method for continuous-flow cell sorting using dielectrophoresis," *Analytical Chemistry,* vol. 80, pp. 3135-3143, May 2008.

[103] M. S. Pommer, Y. T. Zhang, N. Keerthi, D. Chen, J. A. Thomson, C. D. Meinhart, and H. T. Soh, "Dielectrophoretic separation of platelets from diluted whole blood in microfluidic channels," *Electrophoresis,* vol. 29, pp. 1213-1218, Mar 2008.

[104] Y. L. Li, C. Dalton, H. J. Crabtree, G. Nilsson, and K. Kaler, "Continuous dielectrophoretic cell separation microfluidic device," *Lab on a Chip,* vol. 7, pp. 239-248, 2007.

[105] I. Doh and Y. H. Cho, "A continuous cell separation chip using hydrodynamic dielectrophoresis (DEP) process," *Sensors and Actuators a-Physical,* vol. 121, pp. 59-65, May 2005.

[106] K. H. Han and A. B. Frazier, "Lateral-driven continuous dielectrophoretic microseparators for blood cells suspended in a highly conductive medium," *Lab on a Chip,* vol. 8, pp. 1079-1086, 2008.